DANMARKS OG GRØNLANDS GEOLOGISKE UNDERSØGELSE RAPPORT 2011/131

Evaluation and interpretation of geophysical data from the Røros and Meråker districts, Norway

Report prepared for Intex Resources ASA

T. M. Rasmussen

(1 DVD included)

GEOLOGICAL SURVEY OF DENMARK AND GREENLAND
MINISTRY OF CLIMATE AND ENERGY

DANMARKS OG GRØNLANDS GEOLOGISKE UNDERSØGELSE RAPPORT 2011/131

Evaluation and interpretation of geophysical data from the Røros and Meråker districts, Norway

Report prepared for Intex Resources ASA

T. M. Rasmussen

(1 DVD included)

Confidential report

Copy No.

Not to be released

GEOLOGICAL SURVEY OF DENMARK AND GREENLAND
MINISTRY OF CLIMATE AND ENERGY

GEUS

Contents

1. Executive summary 4

2. Introduction 5

3. Røros 9

3.1 Data and data quality 9
3.1.1 Airborne magnetic data 9
3.1.2 Aerodat frequency domain EM data 10
3.1.3 Totem 2A VLF 11
3.1.4 Radiometric data 11
3.2 Processing and interpretation 11
3.2.1 Magnetic field data 11
3.2.2 Frequency domain EM 17
3.2.3 Totem 2A VLF 19
3.3 Ground follow-up targets and descriptions 20

4. Meråker 23

4.1 Data and data quality 23
4.1.1 Airborne magnetic data 23
4.1.2 Aerodat frequency domain EM data 23
4.1.3 Totem 2A VLF 23
4.1.4 Radiometric data 23
4.2 Processing and interpretation 24
4.2.1 Magnetic data 24
4.2.2 Frequency domain EM data 31
4.2.3 Totem 2A VLF 33
4.2.4 Self Organised Map analysis of frequency domain EM and magnetic data 37
4.3 Ground follow-up targets and descriptions 40

5. Conclusions and recommendations 43

6. References 44

7. Appendix A – Self Organised Map (SOM) analysis 45

8. Appendix B – Røros data files 47

9. Appendix C –Røros targets 49

10. Appendix D – Meråker data files 123

11. Appendix E – Meråker targets 125

1. Executive summary

Airborne geophysical survey data from the Røros and Meråker districts are presented and analysed with the purpose of outlining areas of interest for hosting Zn and Cu mineralisations.

Target locations/areas for ground follow-up have been identified from visual inspection of the data. Target areas are presented together with the arguments for the choices made. The locations are provided by a centre/peak location and a polygon encompassing the area of interest. Next, prioritising for a ground follow-up has been based on an evaluation of the data. The locations are provided in digital format in an Excel and ArcView SHP shapefile formats. Maps with target locations are provided in digital format.

In total 72 locations are identified for ground follow-up from the Røros survey data and 44 locations are identified from the Meråker survey data.

2. Introduction

This report is produced for Intex Resources ASA. The purpose is analyses of geophysical data from the Røros and Meråker districts in central Norway in relation to potential mineralisations. The mineralisations of particular interest in these two areas are Zn and Cu (see e.g. Grenne *et al.* 1999). Airborne geophysical survey data are available from both areas and include magnetic field recordings, frequency domain EM (Aerodat system), VLF and gamma-spectrometry. Detailed ground geophysical data are available from a number of areas within the Røros district. Assay data from a number of localities exist within the survey area. Geological information about previous mine sites are accessible from the Geological Survey of Norway (NGU) at www.ngu.no.

The data sets utilised for this report contains a huge amount of information, and the interpretations and processing presented in this report is restricted in terms of applied techniques due to time constraints for the project work. Emphasis has been placed on providing an overview of the entire airborne data set simultaneously with an attempt to provide target areas for ground follow-up work. The exploration model is basically a search for good electrical conductor associated with sulphides. The approach used for target definitions builds on various types of data processing combined with visual inspection and evaluation of the data characteristics. The target definitions are based partly on an analysis of correlation between various data types. Modelling of the electromagnetic data with the aim of providing conductivity-depth sections over target areas is not included for this report due to time limitations, but this type of quantitative analysis should be considered for future work.

The report contains a short description of the data with some comments on data quality that needs to be considered, when processing the data. Then follows descriptions of the applied data processing techniques and results are presented as maps and in tables. Targets areas are presented together with the arguments for the particular choices that are made. Coordinates for target areas are provided digitally on the accompanying DVD. Maps are also provided digitally on DVD.

The data from Røros and Meråker are presented separately and no attempt has been made to integrate and synthesise the interpretations from the two areas. Maps of the surface geology for the two survey areas are shown in Figures 1 and 2 respectively. The lengend for the geological maps is shown in Figure 3. The maps in Figures 1 and 2 have been provided digitally by Intex Resources for this report and are based on maps produced by NGU in scale 1:50 000 (see www.ngu.no).

Some of the data have been analysed using a Self Organised Map (SOM) approach (Kohonen, 2001, Fraser *et al.* 2007). SOM is a technique for visualising and analysing multivariable data. Appendix A includes a description of this technique, which is used here as a classification tool.

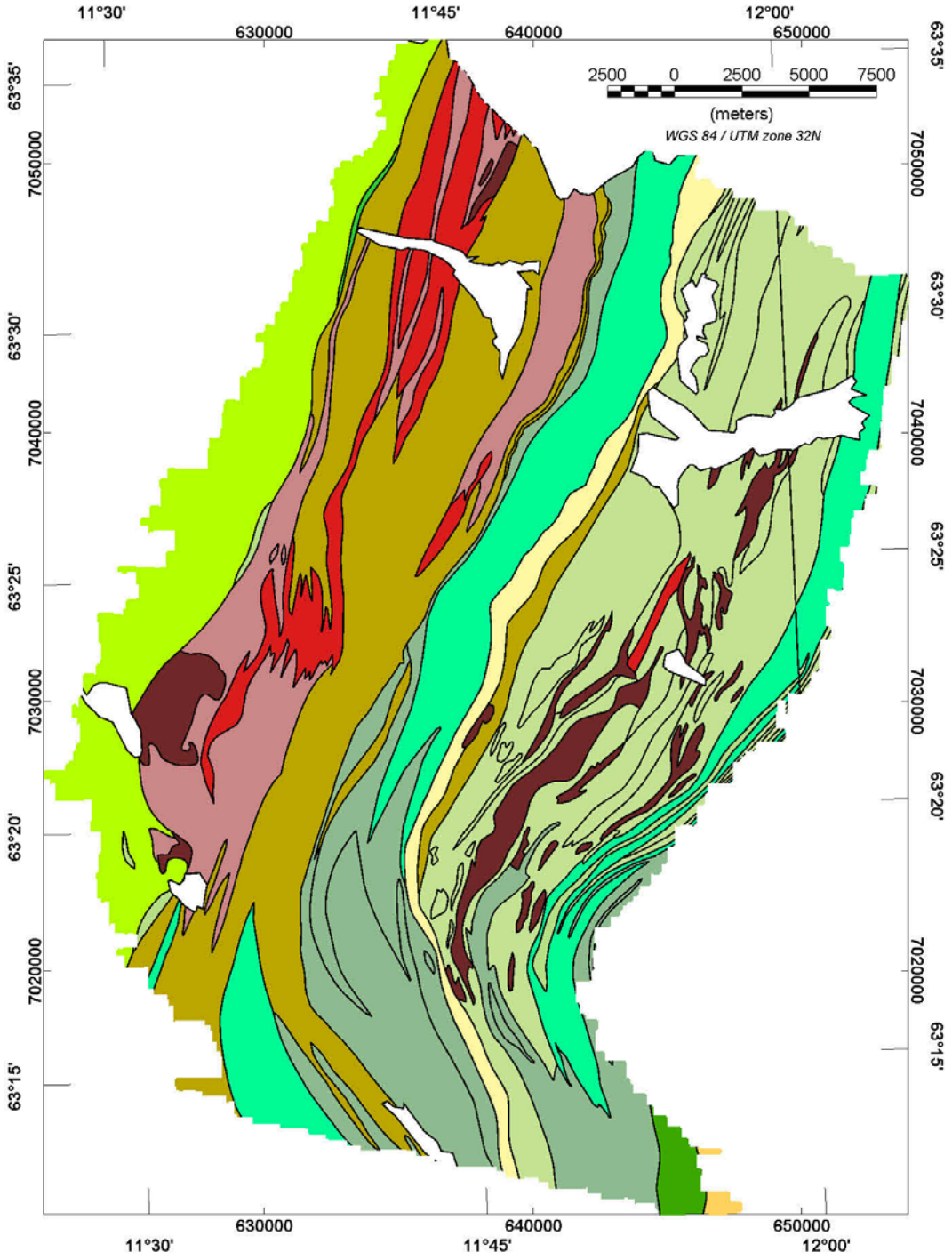


Figure 2. *Geological map of the Meråker survey area. The Legend is displayed in Figure 3.*



Figure 3. *Legend for the geological maps in Figures 2 and 3.*

4. Meråker

4.1 Data and data quality

An assessment of data quality for the Meråker survey has been made by Fugro Airborne surveys and presented in a “report on the re-processing & interpretation of an HEM survey flown by NGU/Aerodat in the Meråker Area, Norway”. The Meråker survey differs slightly from the Røros survey with respect to the configuration of the EM system, but otherwise the system set-up and processing is fairly similar. No auxiliary information such as topography and infrastructure is provided together with this data set. Information about infrastructure used for this report was obtained from Google Earth.

4.1.1 Airborne magnetic data

The magnetic data are considered of high quality although no tie-lines have been available for processing.

4.1.2 Aerodat frequency domain EM data

The Aerodat frequency domain system used for the Meråker survey includes four frequencies for the following receiver-transmitter configurations:

1. 923 Hz vertical coaxial coils
2. 4551Hz vertical coaxial coils
3. 4287 Hz horizontal coplanar coils
4. 33165 Hz horizontal coplanar coils

Fugro Airborne Surveys converted the data into apparent resistivity for each of the four frequencies, and they are provided both as line data and as grids together with the in-phase and quadrature line data.

4.1.3 Totem 2A VLF

This system set-up and processing is similar to the one used for the Røros survey.

Some flight lines have high noise content, and they are easily recognised as striations along the E-W flight line orientation in grid presentations of the data. Power-line noise and responses caused by the high conductivity in power line cables can be seen in the survey data. The sections with excessive noise are in many cases along roads.

4.1.4 Radiometric data

Estimates of potassium, uranium and thorium concentrations are available, but according to the agreement with Intex not used for this report.

4.2 Processing and interpretation

4.2.1 Magnetic data

The total magnetic intensity field data has been decomposed into orthogonal vector component data using the same technique as described above for the Røros survey. Similarly, the magnetic gradient tensor and its rotational invariants are derived from these component data. Figure 17 show the total magnetic field anomaly map and Figures 18-20 show the estimated components of the anomaly field.

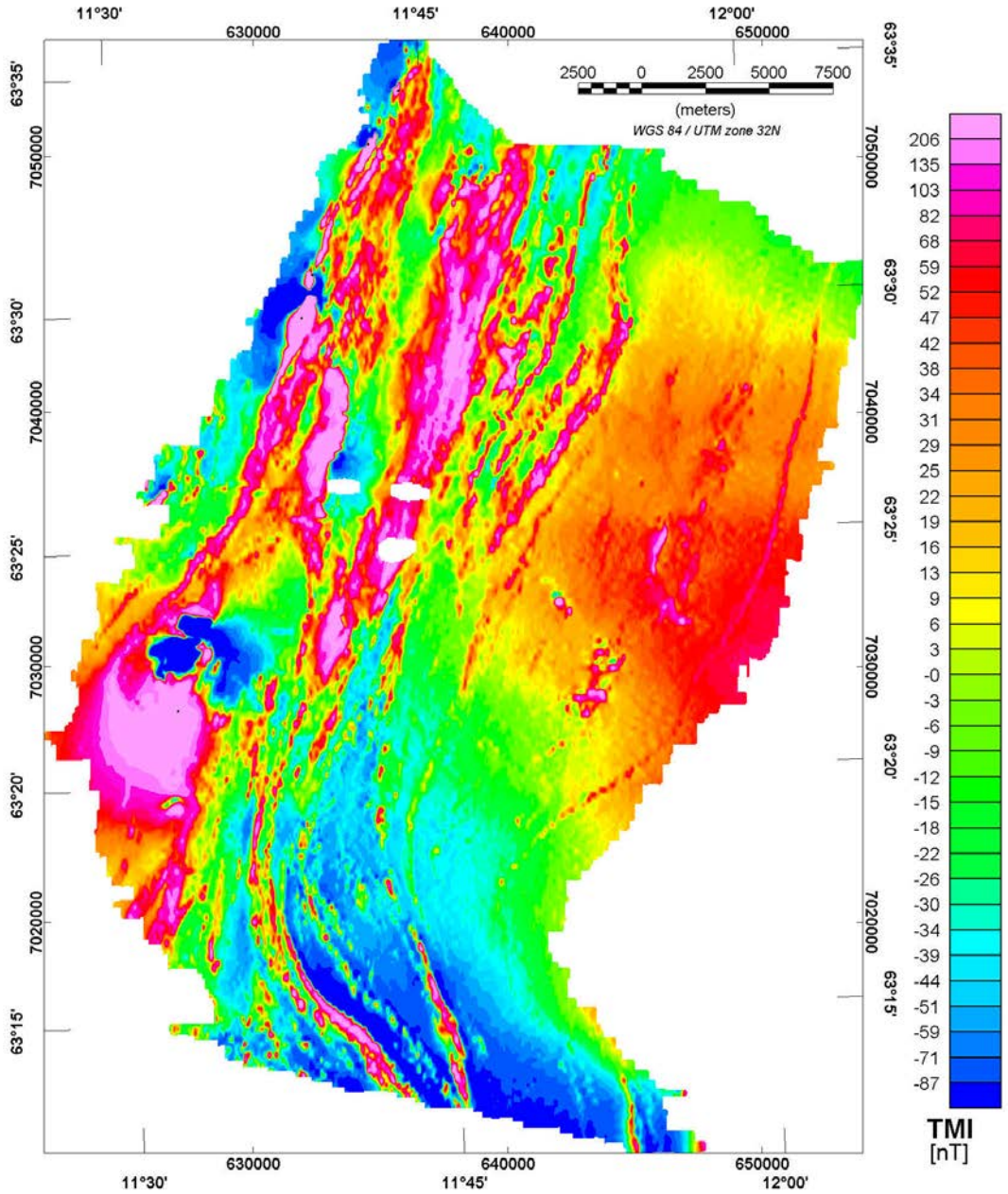


Figure 17. *Magnetic total field anomaly from the Meråker survey*

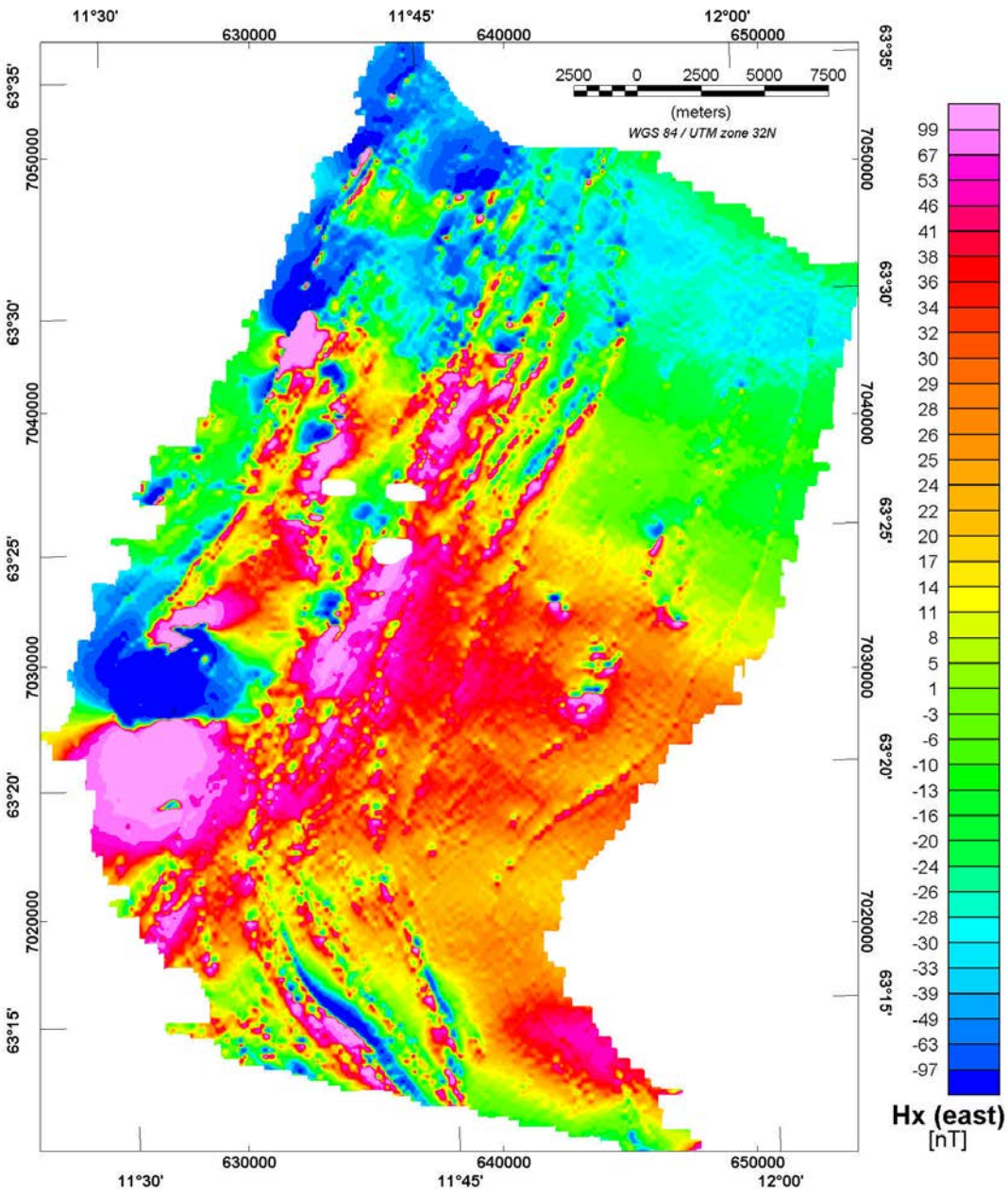


Figure 18. *The calculated north component of the magnetic field anomaly.*

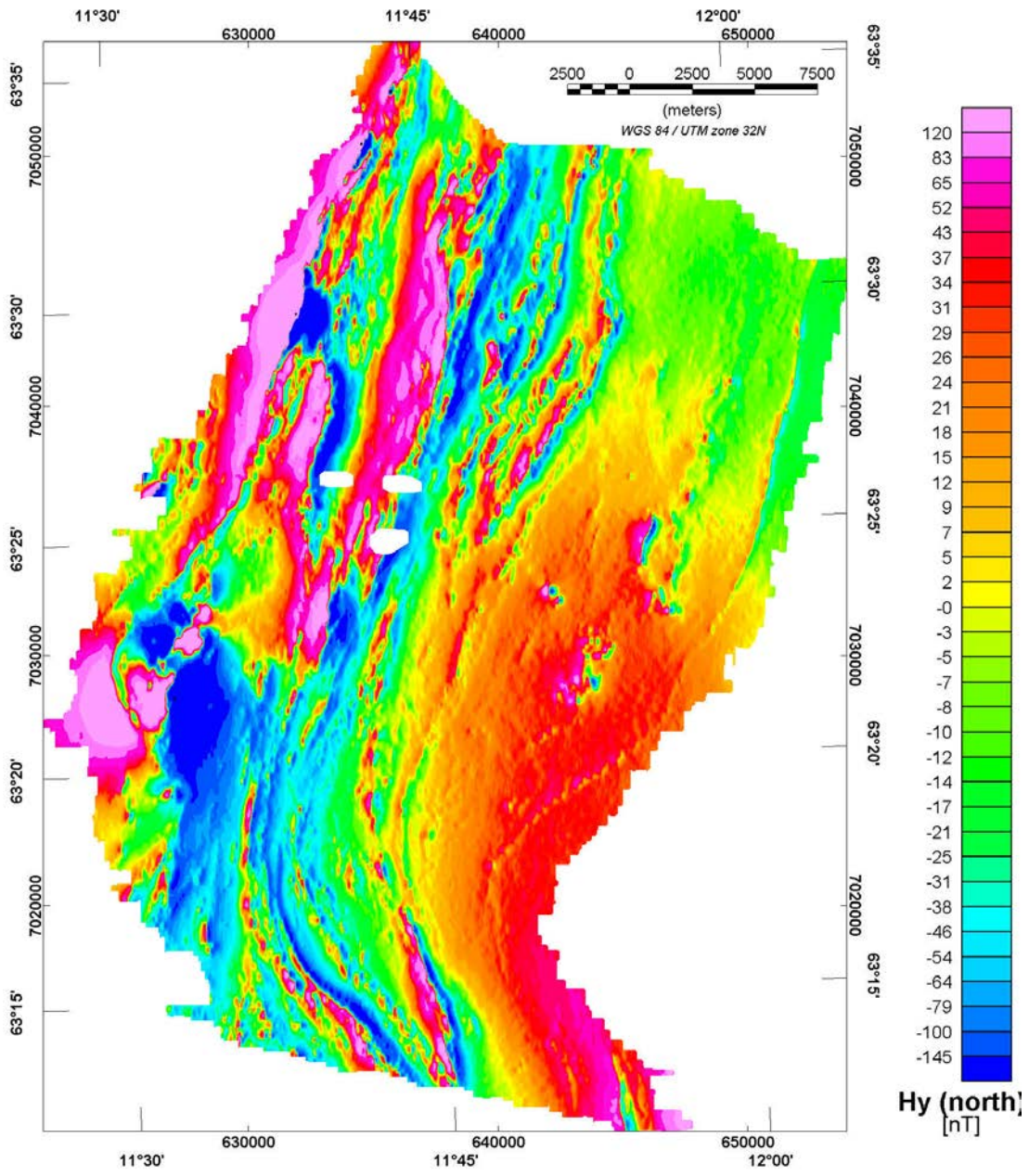


Figure 19. *The calculated east component of the magnetic field anomaly.*

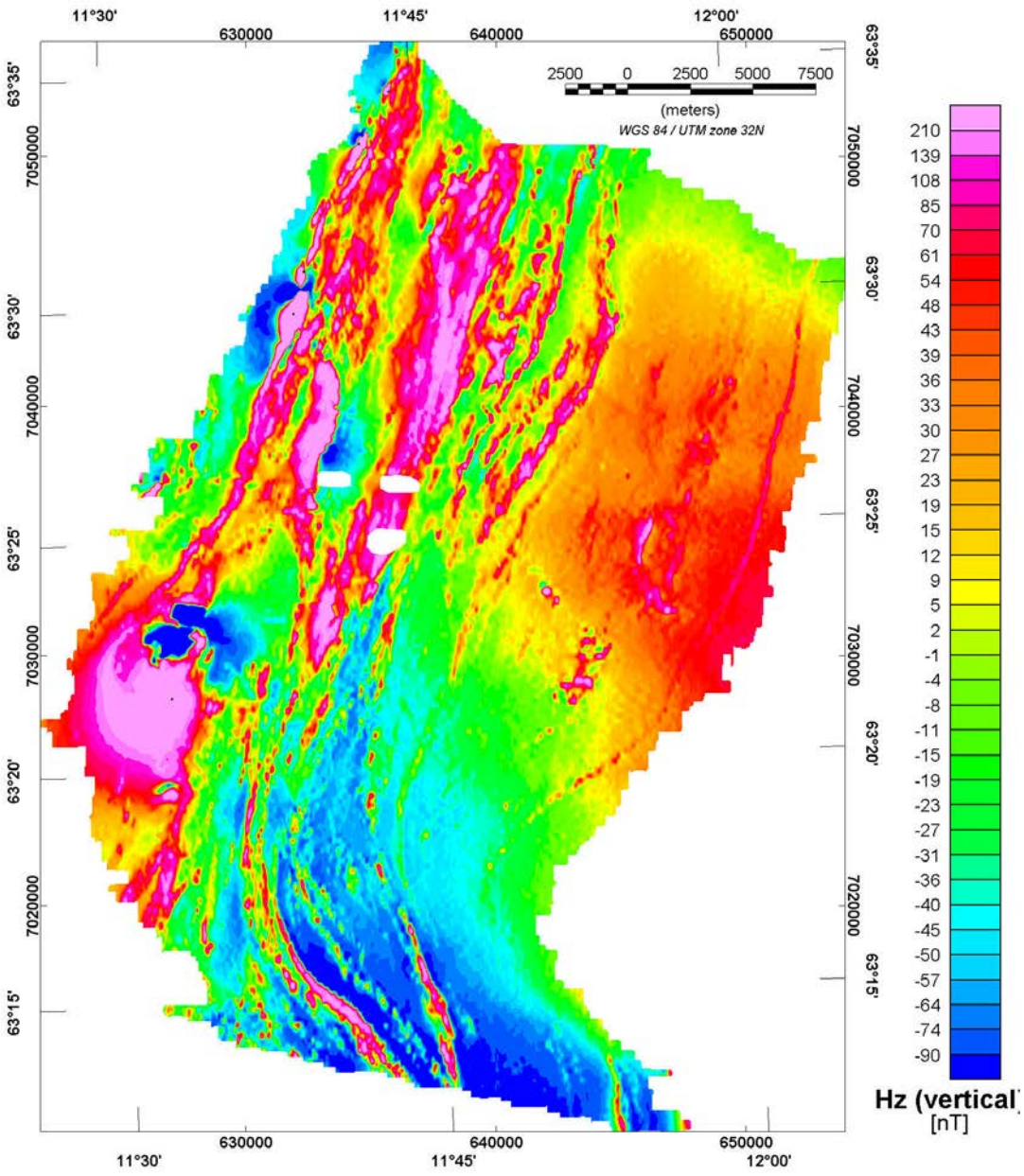


Figure 20. *The calculated vertical component of the magnetic field anomaly.*

A location approximately at WGS84/UTM32N location of 627000 mE, 7030000 mN with evidence of remanent magnetisation is mentioned in the report by Fugro Airborne Surveys. This interpretation is confirmed by the display in Figure 21 of the magnetic declination of the magnetic anomaly field. A few other areas with evidence of strong remanent magnetisation are also evident from the declination and are indicated by ellipses on the map. Centre coordinates are as follows:

- R_1:627040 m, 7028269 m
- R_2: 631905 m, 7043685 m
- R_3: 632315 m, 7045375 m
- R_4: 634517 m, 7050497 m
- R_5: 635695 m, 7052597 m

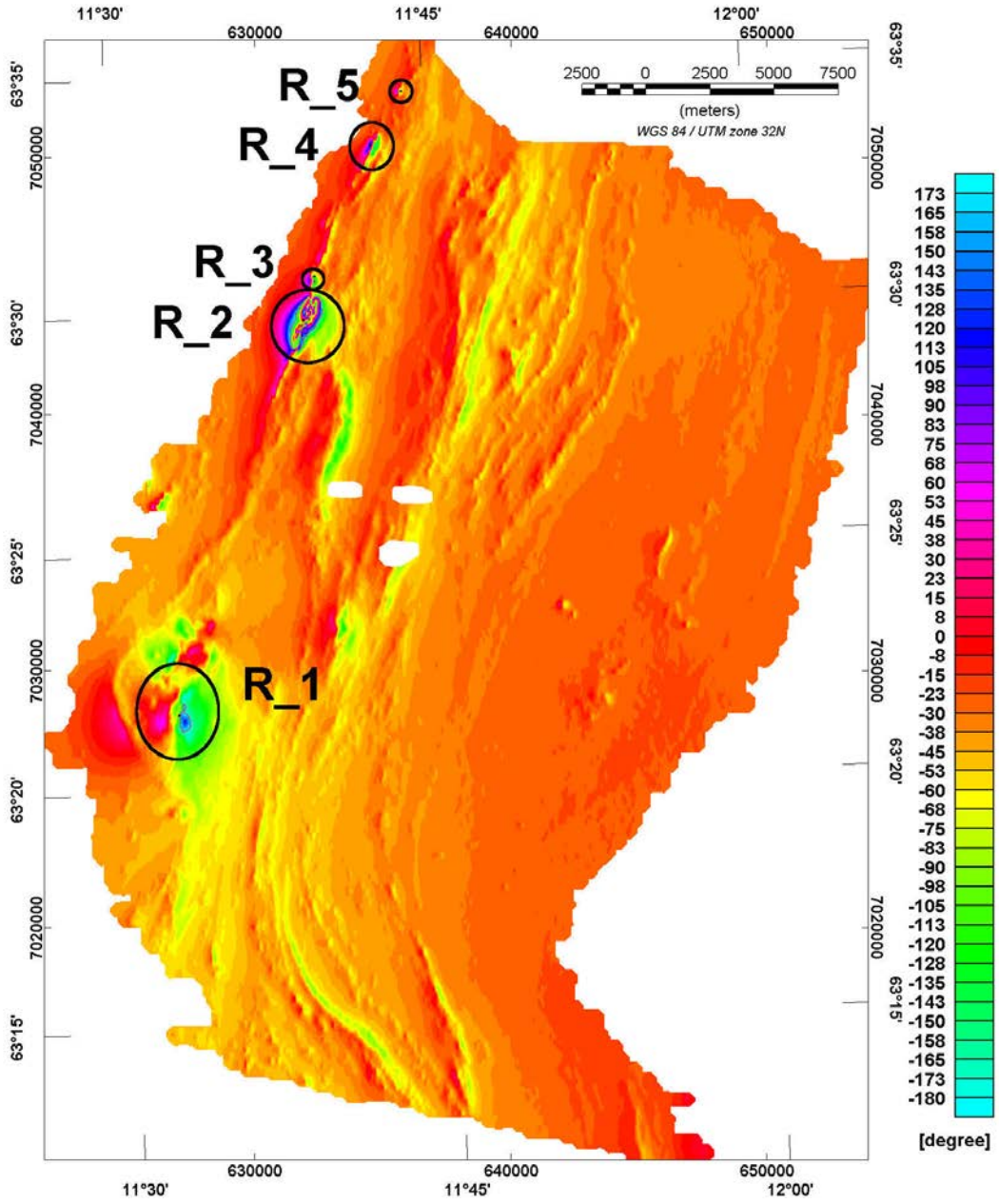


Figure 21. *Declination of magnetic anomaly field. Note that the colour transition from -180 degree to +180 degrees is smooth, which implies that no spurious edges in colours are introduced when the horizontal field vector are close to pointing towards south. Locations with remanent magnetisations are marked.*

The locations with remanent magnetisation should be checked in the field with respect to possible mineralisation associated with these anomalous magnetic field properties.

The horizontal and vertical derivatives used for the gradient tensor invariant calculations are shown in Figure 22 together with the rotational invariants I_1, $\log_{10}(|I_2|)$ and analytic filtered I_1. Superimposed on the map with the horizontal derivative in the east direction of the vertical magnetic component (dHz/dy) are some lineaments defined by locations where anomalies are truncated or broken in terms of magnetic texture continuity. The above men-

tioned centre locations with remanent magnetisations are also superimposed on this map. Locations R_2 and R_3 are seen to be adjacent to these magnetic break lines.

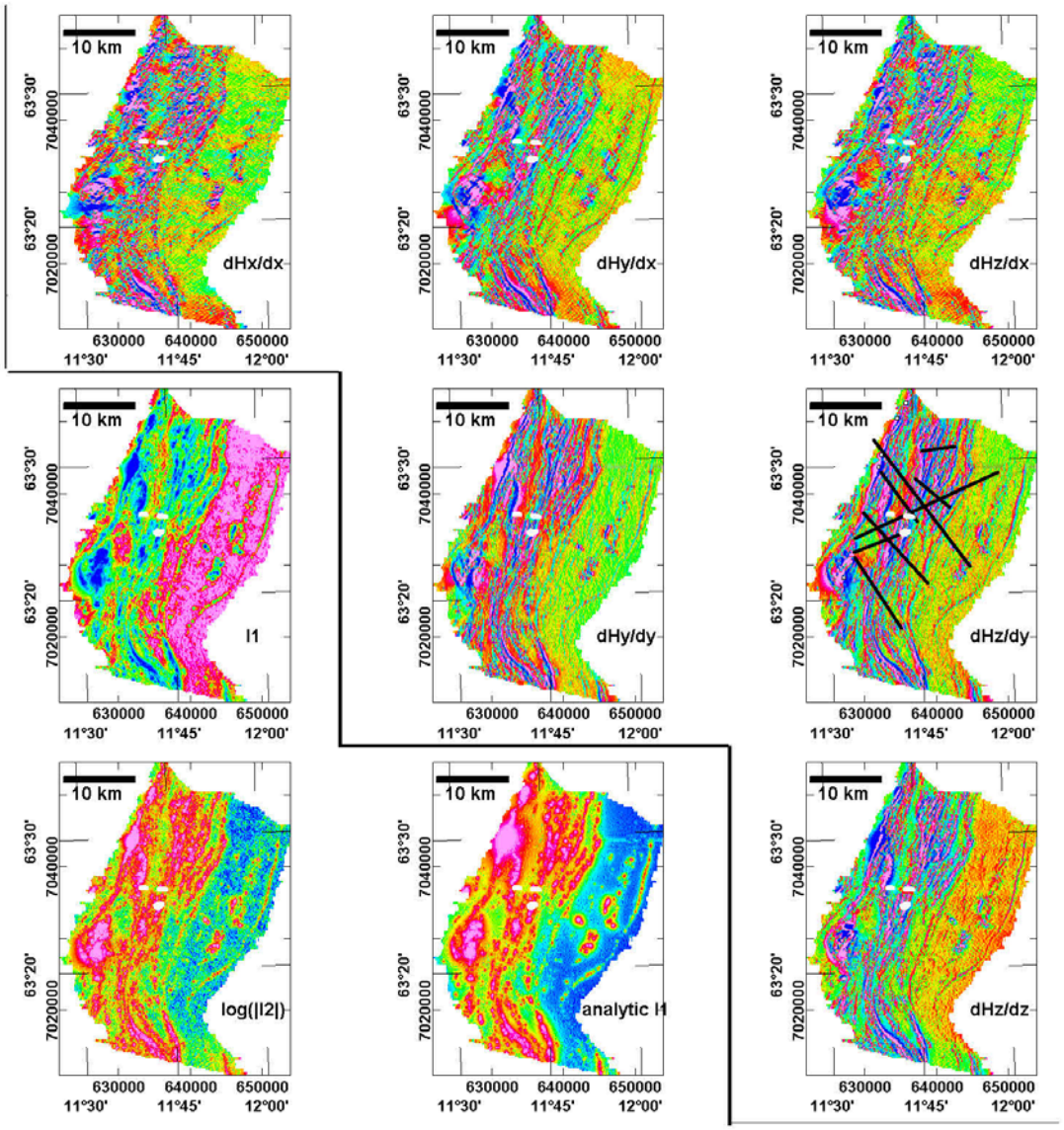


Figure 22. *The upper triangle and diagonal of the magnetic gradient tensor*

$$\begin{Bmatrix} \partial H_x/\partial x & \partial H_y/\partial x & \partial H_z/\partial x \\ - & \partial H_y/\partial y & \partial H_z/\partial y \\ - & - & \partial H_z/\partial z \end{Bmatrix}$$

and the rotational invariants I_1 *and* $\log_{10}|I_2|$ *,and the analytic signal filtered* I_2*.*

The map with the analytic signal filtered invariant I_1 is repeated in Figure 23 at a different scale. Several locations with “point” sources are seen on this map, and they are clearly of interest in terms of a ground follow-up. The lineament adjacent to R_3 displayed in Figure

23 is seen to connect to some isolated anomalies within the eastern part of the map, where the magnetic field intensity in general shows gentle or long wavelength variations. Two abandoned mine sites, Mannfjell (latitude 63.3669) and Lillefjell (latitude 63.2509) are shown on the map.

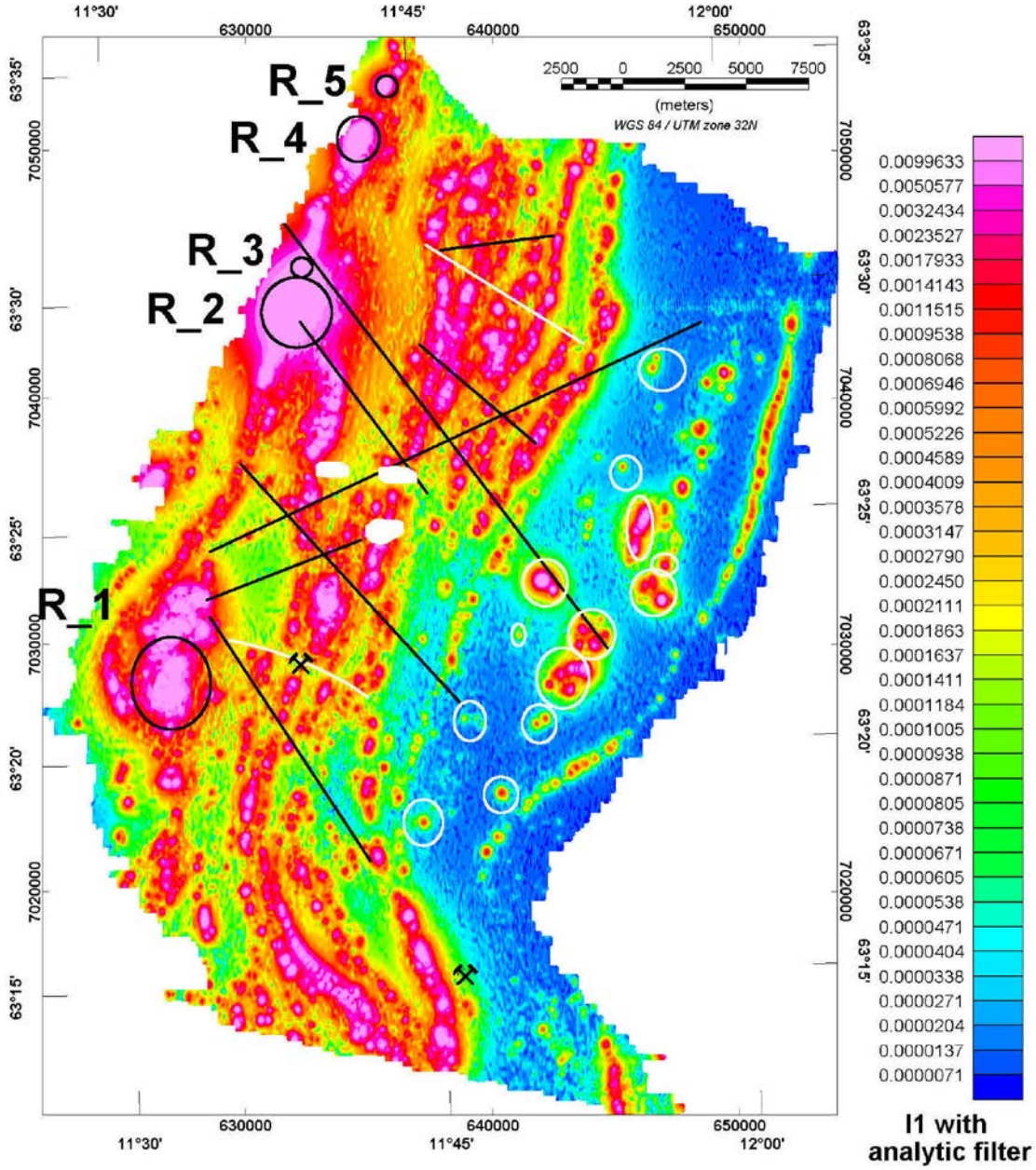


Figure 23. *Analytic signal filtered rotational invariant I_1 with superimposed positions of remanent magnetisations and magnetic break lines (black colour ellipses). Two magnetic break lines (white colour) have been added based on the background image. The locations of two abandoned mines are shown, and it is noticed that one of the previous mines are located on one of the break lines defined by the background image. Some isolated peaks in the image of particular interest for a ground follow-up are encircled.*

The magnetic tilt angle for the Meråker survey is shown in Figure 24. The tilt angle is calculated from the ratio between horizontal and vertical components. The implication of this is

that structures in areas of weak magnetisation are imaged in a similar manner as structures with high magnetisation. The correlation to the structures in the geological map Figure 2 is evident.

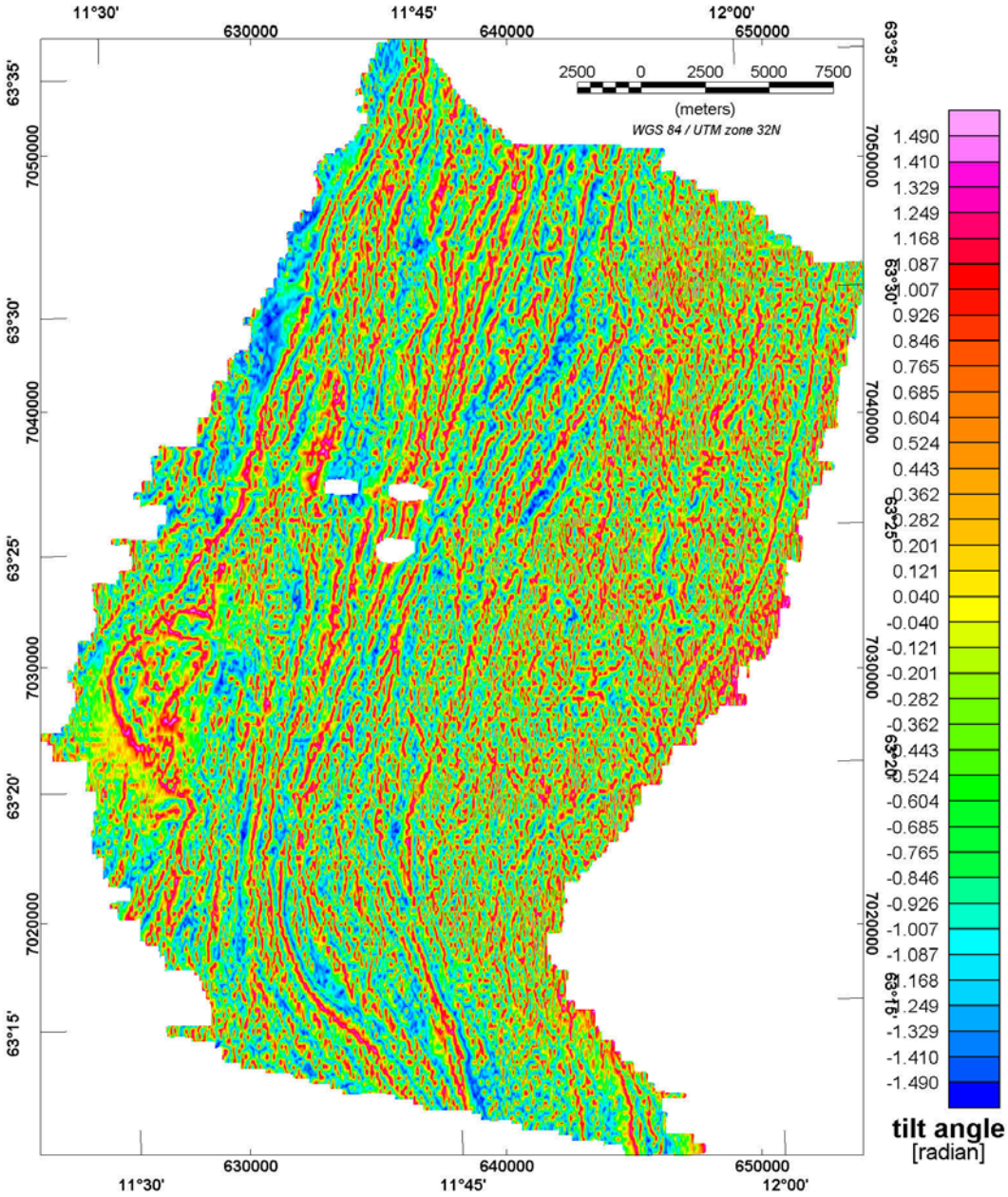


Figure 24. *Magnetic tilt angle for the Meråker survey.*

4.2.2 Frequency domain EM data

The grids with calculated apparent resistivity for each of the four frequencies and the anomaly listing provided by Fugro Airborne Surveys provides a good data set for evaluation of the EM data. No further processing has been done except for a presentation of the apparent resistivities in a ternary image based on the three lowest frequencies. The ternary image is displayed in Figure 25. White colour indicated low resistivities for all three resistivi-

ty values. Conductance estimates at the anomalies tabulated by Fugro Airborne Surveys are superimposed on the ternary image by using proportional sized symbols for value representation. Assay values for Zn (provided by Intex) are also displayed on the map and the locations of two abandoned mines are shown. The highest conductance values are noted in the southern part of the map. The two mine locations are not associated with any significant EM anomalies, but Mannfjell is noted to be in a conductive zone which is seen to bend around the location R_1 with remanent magnetisation.

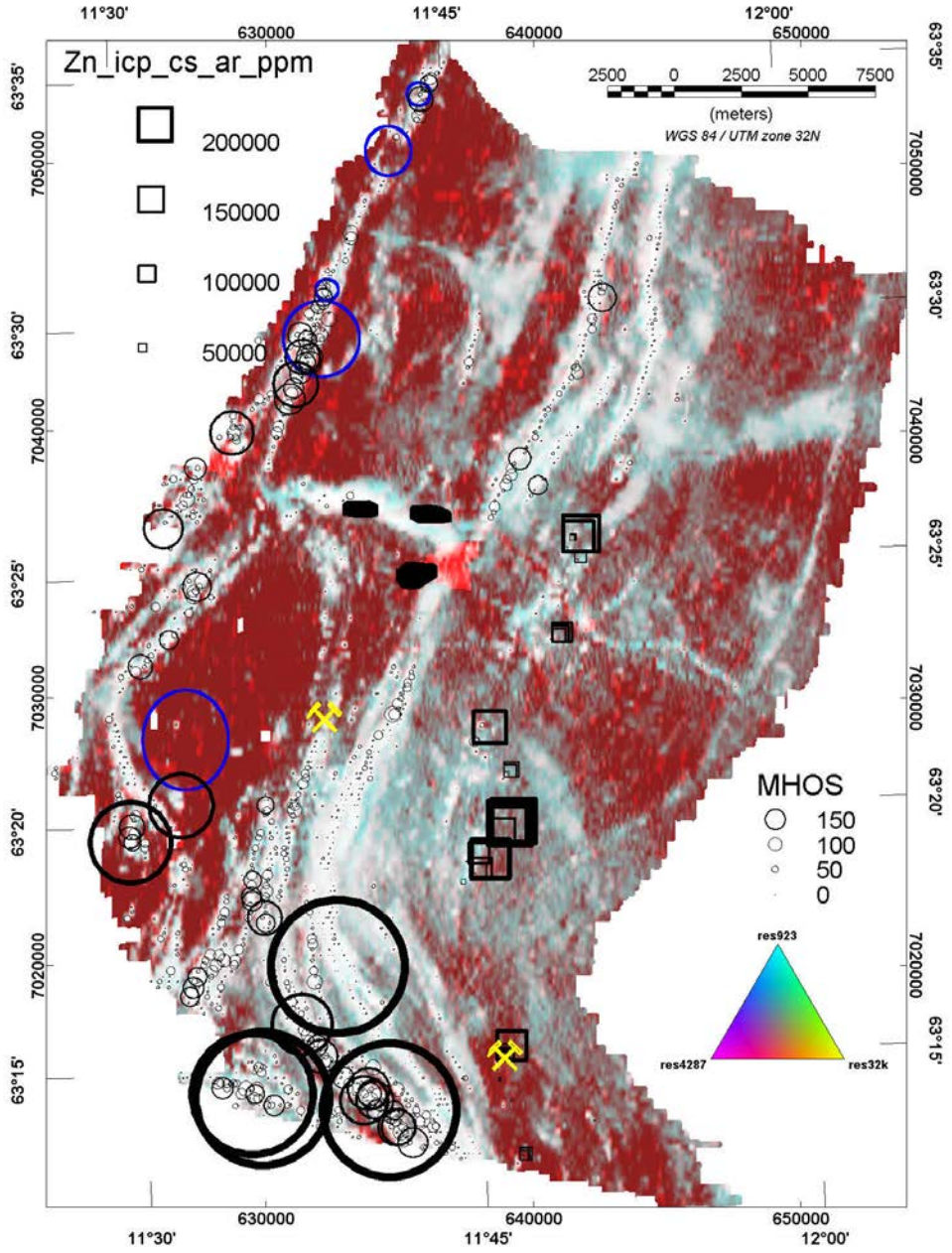


Figure 25. *Ternary image of apparent resistivity data with superimposed symbol showing estimated conductance (black circles centred at sample location) and assay data for Zn (black squares- lower left corner is sample location). The five locations with remanent magnetisation are shown by blue circles. The location of two abandoned mines is also shown.*

4.2.3 Totem 2A VLF

Grids of the VLF data are provided in Figures 26 and 27. In order to search for isolated peaks, the data have also been transformed (Figure 28 and 29) using the analytic signal of the gradient tensor invariant I_1 (irrespective that the gradient tensor technique is developed for magnetic data and has a physical meaning in this case – the transformations used here is purely a matter of enhancing short wavelength features!). The peaks from the tensor are useful when comparing the VLF anomalies with the frequency domain EM anomalies. Conductance values obtained from the frequency domain EM data are superimposed on the maps with VLF data. It is evident that only some of the VLF anomalies are associated with high amplitude frequency domain EM anomalies. This reason for this apparent discrepancy is that the frequency domain EM data are focussed spatially due to the local EM transmitter used for this technique, whereas the VLF responses are generated from a plane-wave excitation and contributions to the anomaly are integrated from a larger area spatially.

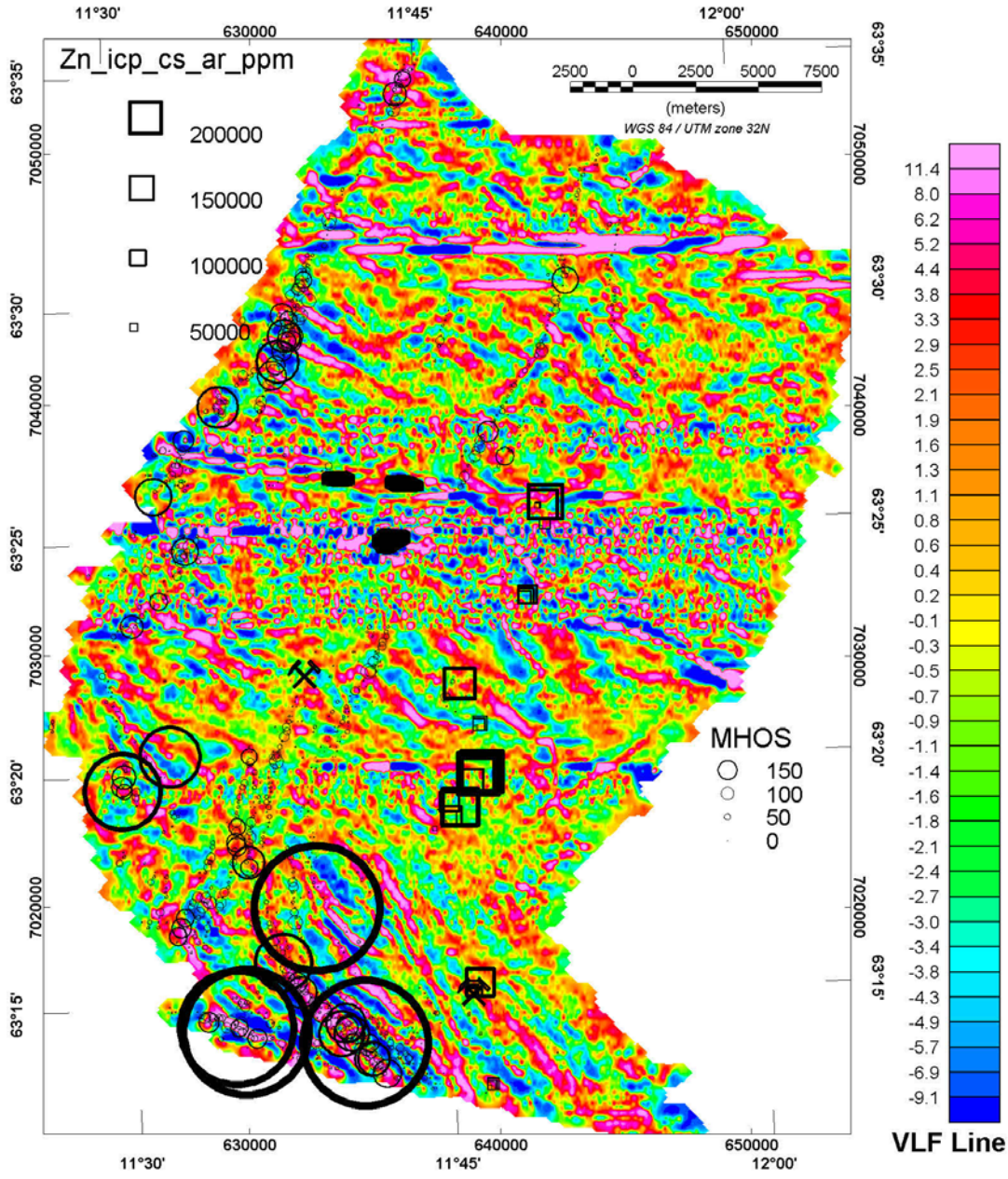


Figure 26. *VLF LINE response with superimposed symbol showing estimated conductance (black circles centred at sample location) from frequency domain EM and assay data for Zn (black squares- lower left corner is sample location).*

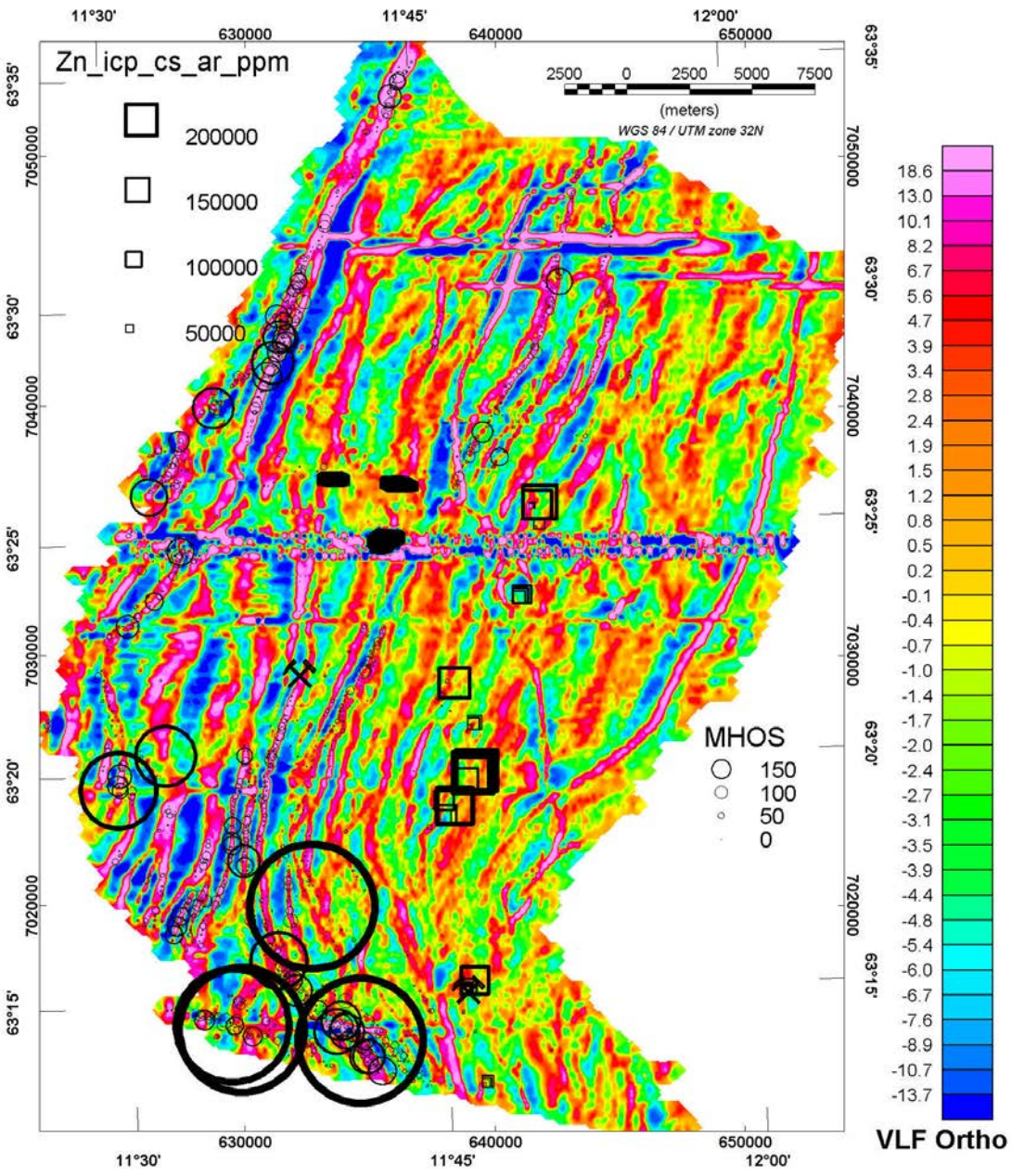


Figure 27. *VLF ORTHO response with superimposed symbol showing estimated conductance (black circles centred at sample location) from frequency domain EM and assay data for Zn (black squares- lower left corner is sample location).*

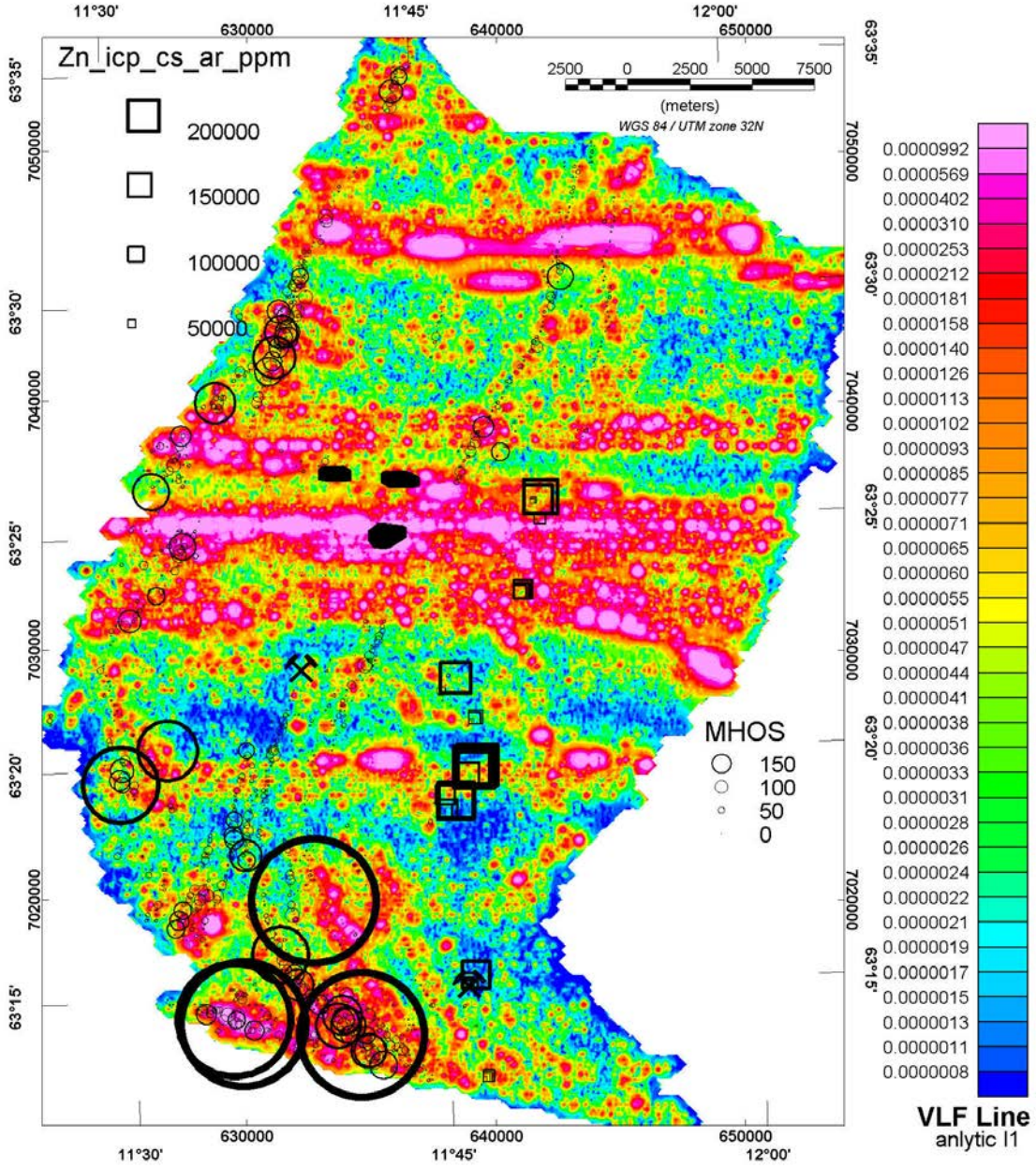


Figure 28. *Analytic signal filtered gradient tensor I1 based on VLF Line response with superimposed symbol showing estimated conductance (black circles centred at sample location) from frequency domain EM and assay data for Zn (black squares- lower left corner is sample location).*

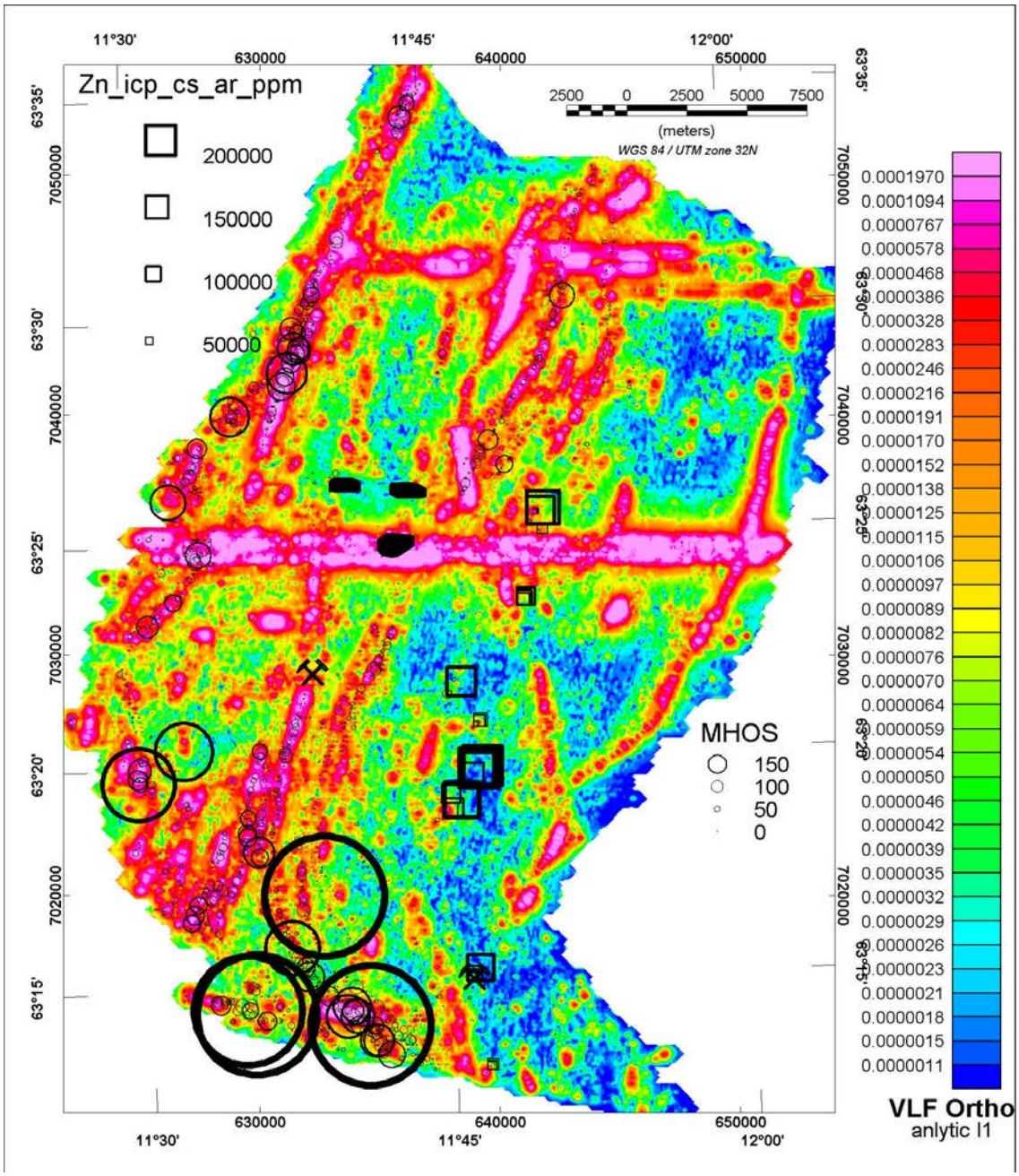


Figure 29. *Analytic signal filtered gradient tensor I1 based on VLF Ortho response with superimposed symbol showing estimated conductance (black circles centred at sample location) from frequency domain EM and assay data for Zn (black squares- lower left corner is sample location).*

4.2.4 Self Organised Map analysis of frequency domain EM and magnetic data

The data in the anomaly listing by Fugro Airborne Surveys were subjected to a SOM analysis with input of in-phase and quadrature data for the four frequencies, the estimated conductance and the observed magnetic field at the location of each EM anomaly. Component maps including the results of a clustering analysis are shown in Figure 30, and the spatial locations of data for the 15 clusters obtained are shown in Figure 31. The component maps clearly show a lack of correlation between high magnetic field values and EM responses.

High magnetic field values are associated with cluster no 10 whereas high conductance values are associated with clusters 13 and 14. Note however that the distribution of clusters has some correlation to the location of magnetic break lines. The significance of this correlation in relation to mineralisation is not clear.

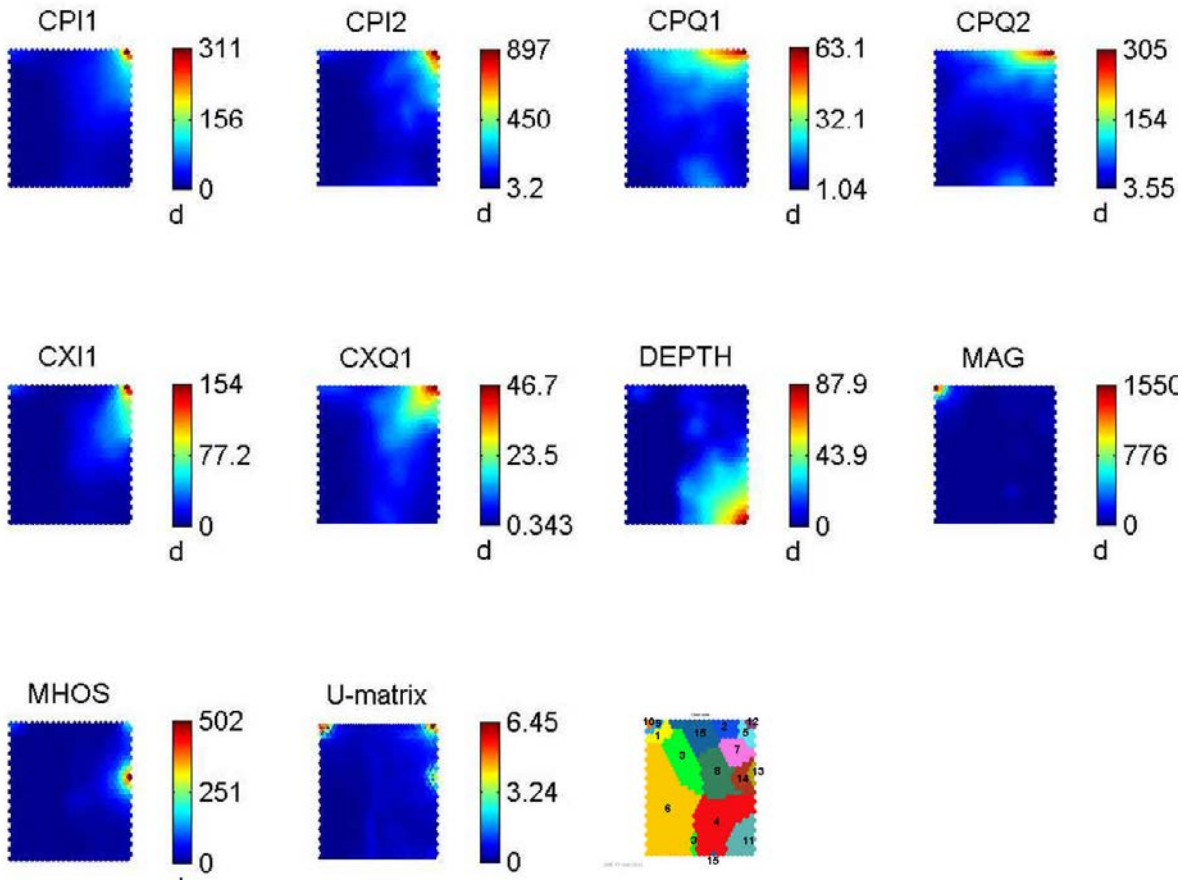


Figure 30. *Component maps in SOM-space and the clusters defined by k-mean clustering of the SOM-data.*

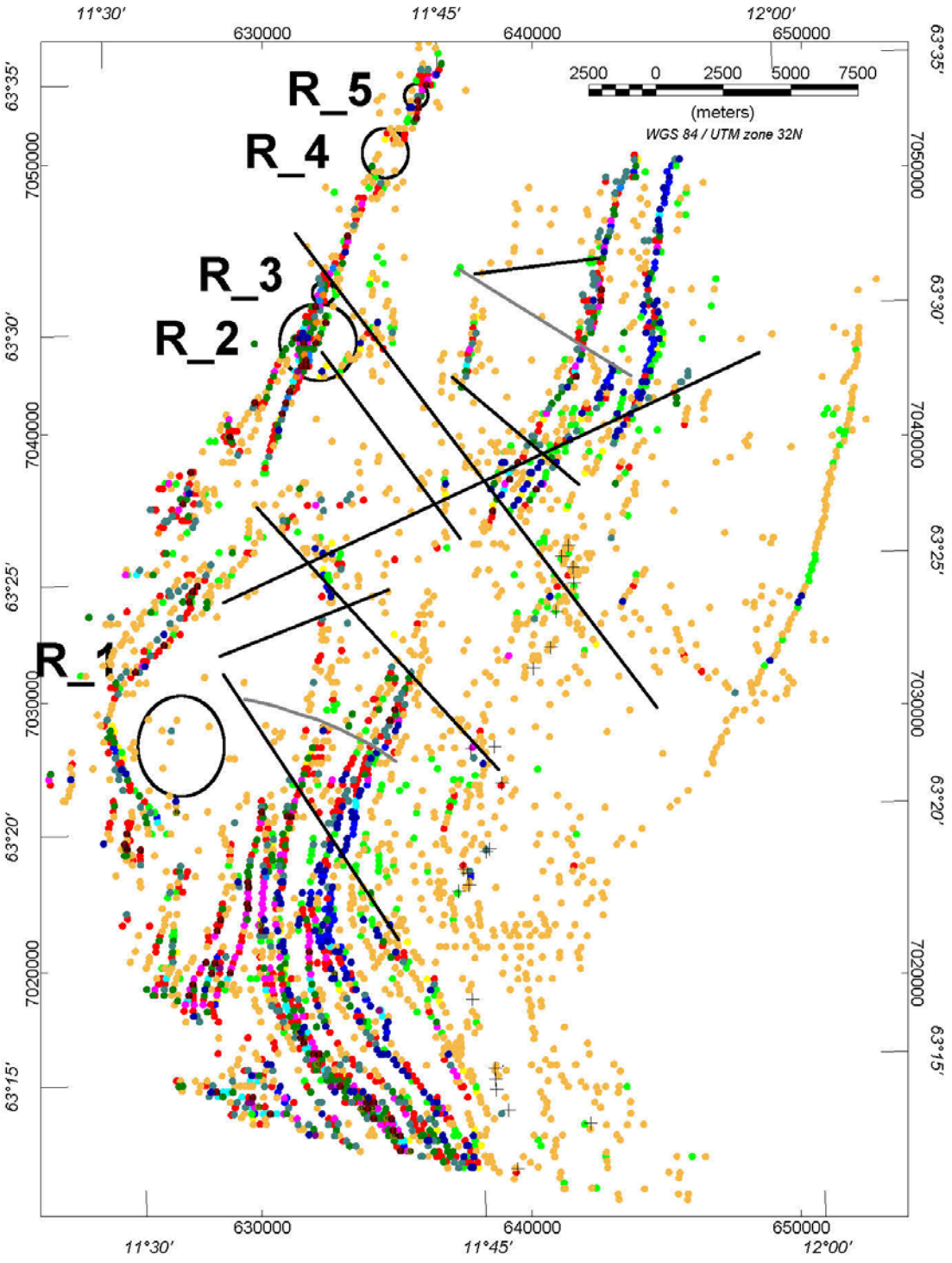


Figure 31. *Distribution of clusters from SOM analysis of frequency domain EM anomaly data and the magnetic field. Clusters of particular interest are no. 13 (olive green colour) and 14 (dark green), which are associated with high conductance values. Locations with assay data are shown by + sign.*

4.3 Ground follow-up targets and descriptions

The locations with high conductance values obtained from the frequency domain EM should be prioritised for a ground follow-up, but the observation that the two previous mines sites are not associated with any significant EM anomalies indicates that locations with intermediate conductance values should not be neglected. Locations with coincidence of high VLF response and frequency domain EM anomalies should be prioritised.

Three types of magnetic features are of particular interest:

- the five locations with remanent magnetisation
- locations of magnetic break lines - in particular if associated with any adjacent EM anomalies
- isolated peaks - in particular if associated with any adjacent EM anomalies

The SOM analysis of data from the locations with EM anomalies indicated a general lack of coincidence/correlation between EM anomalies and magnetic anomalies (both high and low), but any spatial relations regarding adjacency is not revealed by this analysis.

A large number of locations/areas have been identified from visual inspection of the presented data. The locations are provided in digital format in an Excel format and in shapefile format. The locations are provided by a centre location and a polygon encompassing the area of interest. Prioritising (1 [highest] – 5 [lowest]) has been done based on an evaluation of the maps shown above. A map of target locations is provided in digitial format. Figure 32 shows target location with priority index, and Figure 33 shows target locations with target numbering.

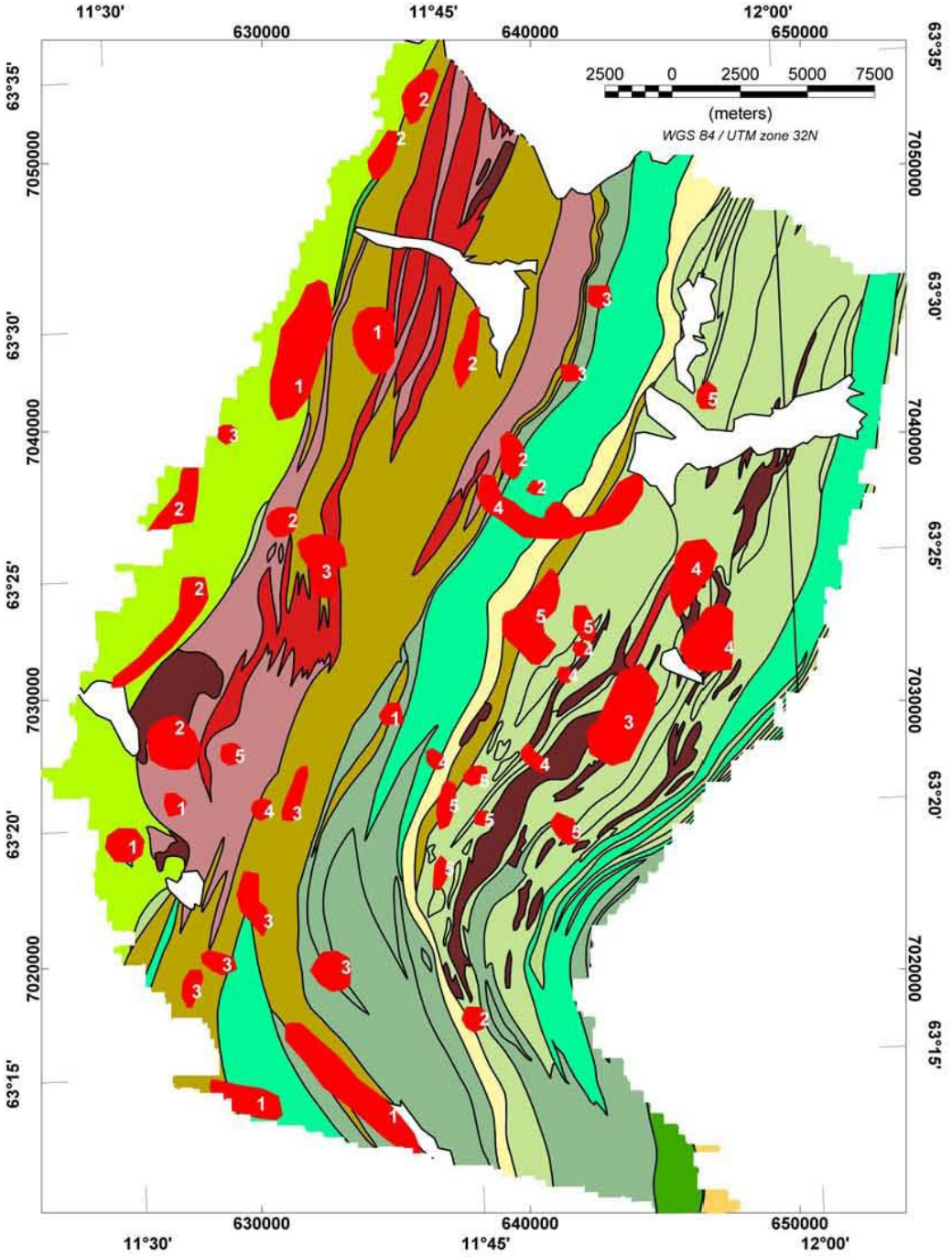


Figure 32. *Target areas (filled red polygons) superimposed on the geological map of the Meråker district. Legend for the map is shown in Figure 3.Target priority number in the range 1-5 is indicated. Priority 1 is highest.*

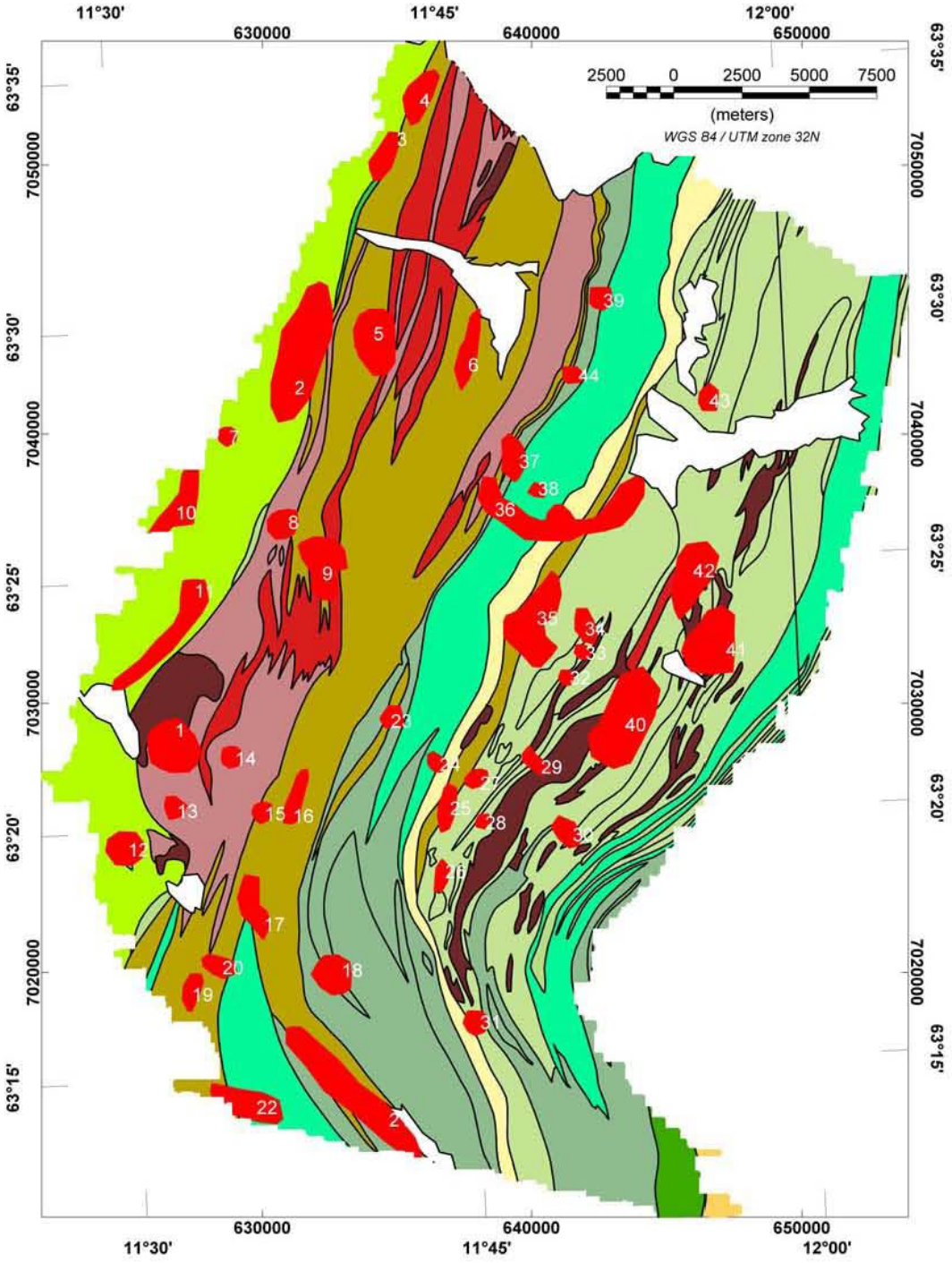


Figure 33. *Target areas (filled red polygons) superimposed on the geological map of the Meråker district. Legend for the map is shown in Figure 3.Target numbering is superimposed.*

5. Conclusions and recommendations

The airborne geophysical data from the Røros and Meråker districts analyzed are in general of good quality and contain valuable information for a general understanding of the geology. A high degree of correlation to mapped geological units is observed. Targets areas for a ground follow-up in a search for mineralisations can be identified from both magnetic and electromagnetic data.

Quantitative modeling of the electromagnetic data has not been done for this report, but should be considered for further work. In particular, insight from modeling of data from locations with known and mapped mineralisations is expected to be useful for a more refined prioritizing of targets. An integrated interpretation in which geochemical data is included may further improve the prioritizing of target areas. The self organizing map analysis presented in this report is considered a feasible approach for data integration.

6. References

Grenne, T., Ihlen, P. M. & Vokes, F. M., 1999: Scandinavian Caledonide Metallogeny in a plate tectonic perspective. Mineralium Deposita **34**, 422-471.

Fraser, S.J. & Dickson, B.L., 2007: A New Method for Data Integration and Integrated Data. Interpretation: Self-Organising Maps. In "Proceedings of Exploration 07: Fifth Decennial International Conference on Mineral Exploration" edited by B. Milkereit, 2007, p. 907-910.

Huang, H. & Fraser, D.C. 2000: Airborne resistivity and susceptibility mapping in magnetically polarizable areas. Geophysics, 65, NO. 2, p. 502–511.

Kohonen, T, 2001: Self-Organizing Maps. Third Extended Edition, Springer Series in Information Sciences, Vol. 30, Springer, Berlin, Heidelberg, New York, 2001.

Pedersen, L.B., Qian, W., Dynesius, L., and Zhang, P., 1994. An Airborne Tensor VLF System.From Concept to Realisation. Geoph. Prosp., **42**, 863-883.

Pedersen, L.B. & Rasmussen, T.M., 1990. The gradient tensor of potential field anomalies. Geophysics, 55, 1558-1566.

Pedersen, L.B., Rasmussen, T.M. & Dyrelius, D., 1989. Construction of component maps from aeromagnetic total field anomaly maps. Geophys. Prosp., 38, 795-804.

7. Appendix A – Self Organised Map (SOM) analysis

Three data types, d1, d2 and d3, are analysed in the example with synthetic data. The data values and geographic locations are shown (Fig. 34abc) for each data type using a colour code presentation for each data point value. The values are in the range from 1–16. In short the data fall in four sub ranges:

- Very low (VL) – blue colour
- Low (L) – light blue and green colours
- Intermediate (I) – orange colour
- High (H) – purple colour

A listing of the three data types in terms of sub ranges reveals the following combinations from south (1) to north (4) when inspecting the three data types in Fig 30abc:

1. VL-L-L
2. VL-I-L
3. L-L-L
4. VL-L-H

The listing above give four different combinations of data and it is clear immediately that the data define four groups. In this simple synthetic example with only a few types of data, it is straightforward to distinguish the four groups. However, an analysis by visual inspection becomes much more difficult when both more data types and more complex data distributions are added. The SOM is useful in these complicated cases. The basic principles are described below.

The SOM processing finds an approximation to the data by mapping the input data into another data set with fewer data than the initial amount of data. This approximation referred to as the best matching units (BMU) has the same amount of data types (same dimensionality) as the input data. The BMU's are presented in the SOM which is a two-dimensional map, and referred as the SOM-space (see Fig. 34 lowermost panels). The SOM is discretized in a pre-selected number of rows and columns (matrix-representation). Thus, the original multi-dimensional data are mapped into a new data space with only two-dimensions and fewer data. In the synthetic example, the number of rows and columns are 21 and 16 respectively. The number of cells or elements defines the data reduction applied to the initial data. In this synthetic case, a reduction from 998 initial data to 21x16=336 data is used. Each BMU is associated with a cell in the matrix or SOM-space, and they are ordered in the matrix such that similar BMU's are adjacent to each other in the two-dimensional map. Although the SOM is two-dimensional, the multidimensionality of the input data is retained by the dimensionality of BMU. Each of the input data has a BMU to which the data are most similar to. Several input data may be associated with the same BMU, in which case the SOM presentation may be viewed as a classification of the input data. An example of a link between initial data and a BMU is indicated in Figure 34, where six data points are represented by one BMU in the matrix. Some BMU's may not have any of the initial data associated to it. The matrix presentation is utilised in two ways:

- U-matrix presentation: similarity between adjacent BMU's
- Component presentation: relationship between components for subsets (i.e. data associated with one or several cells in the matrix) of the data

The U-matrix describes the deviation for a particular cell to the surrounding cells by using a colour scale representation of the "distance" between the associated BMU's. The component presentation simply shows the value of the BMU at each cell and for each component.

The BMU's may be analysed further with respect to clustering of data. A standard k-mean clustering procedure is used. The result for the synthetic data example is that the data cluster into four distinct groups, as displayed in Figure 34d. Thus, a data reduction or simplification from 998 initial data to 4 is obtained.

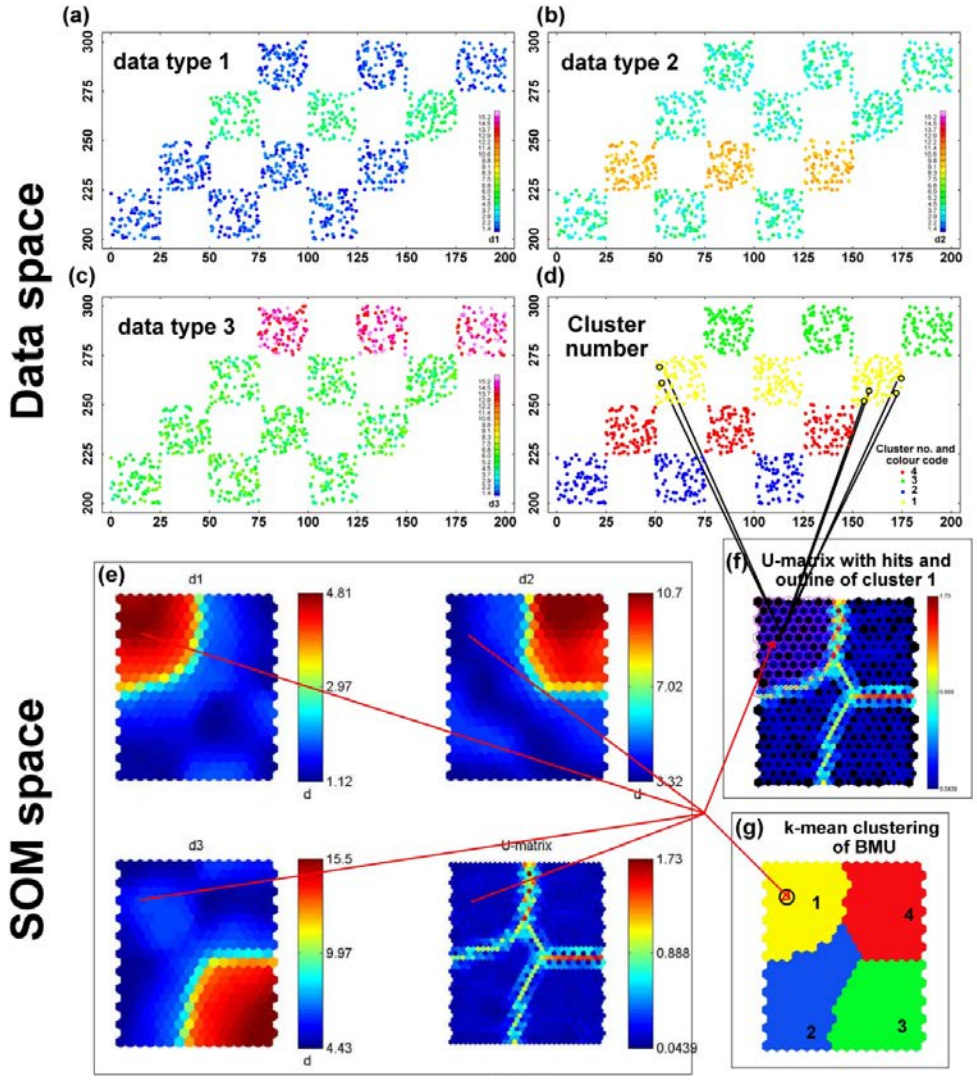
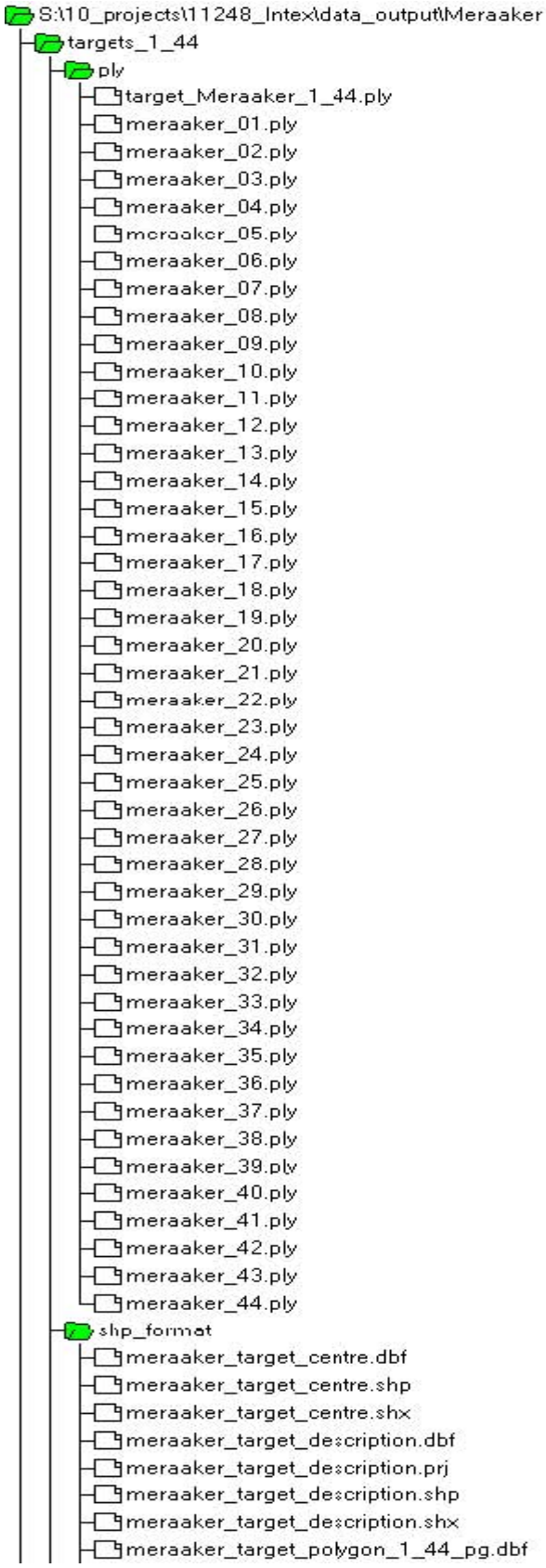


Figure 34. *SOM-presentation of synthetic data consisting of 998 locations with 3 data types at each position: (a) values of data type d1 at each geographic location; (b) values of data type d2; (c) values of data type d3; (d) results of k-mean cluster analysis displayed in a geographic map ; (e) components in SOM-space; (f) U-matrix representation of BMU with colour code showing distance to neighbouring cells; (g) k-mean clusters of BMU's in SOM-space. An example of link between data space and SOM-space is indicated by the lines pointing to one of the cells in the matrix representation.*

10. Appendix D – Meråker data files



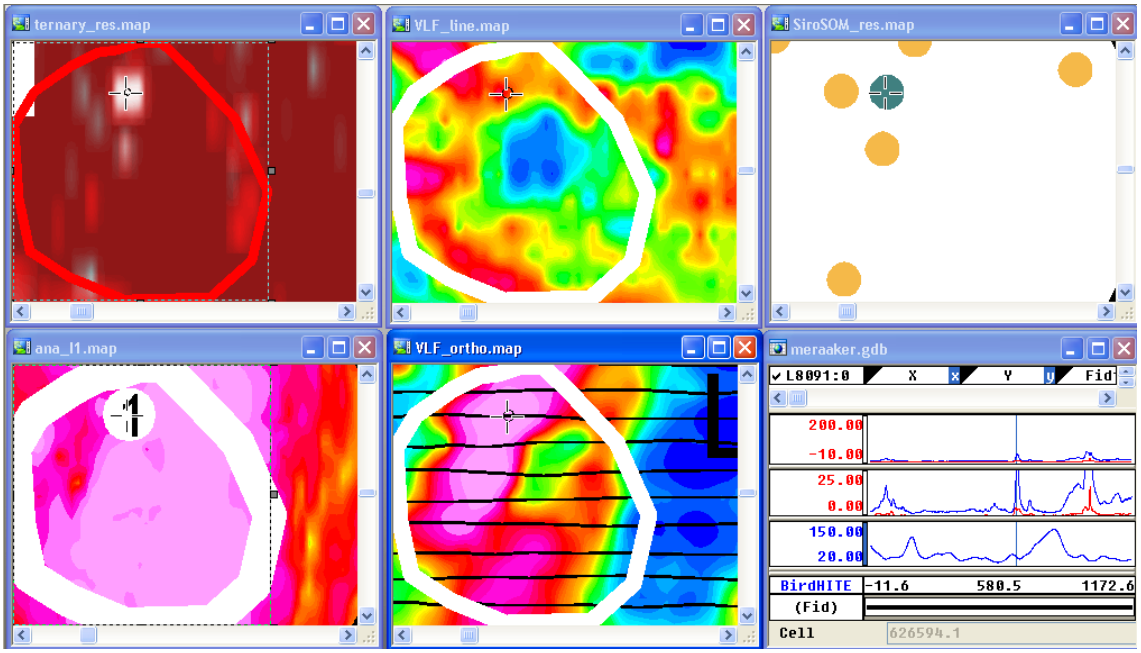

meraaker_target_polygon_1_44_pg.prj
meraaker_target_polygon_1_44_pg.shp
meraaker_target_polygon_1_44_pg.shp.GeosoftMeta
meraaker_target_polygon_1_44_pg.shx
xls
Meraaker_target_description.xls
gdb
meraaker_target_center.gdb
meraaker_target_center.gdb.xml
meraaker_target_description.gdb
meraaker_target_description.gdb.xml
kmz
Meraaker_target_center.kmz
Meraaker_target_polygon.kmz
Meraaker_Oasis_tree_viewer
Geology
BergartflateN250_Rørås_Mer.MID
BergartflateN250_Rørås_Mer.MIF
BergartflateN250_Rørås_Mer.MIF.GeosoftMeta
NGU Bergartsflate_Legend_Rørås.MID
NGU Bergartsflate_Legend_Rørås.MIF
NGU Bergartsflate_Legend_Rørås.MIF.GeosoftMeta
ana_l1.map
ana_l1.map.xml
decest_grader.map
decest_grader.map.xml
meraaker.gdb
meraaker.gdb.xml
meraaker_target_center.gdb
meraaker_target_center.gdb.xml
meraaker_target_description.gdb
meraaker_target_description.gdb.xml
SiroSOM_res.map
SiroSOM_res.map.xml
targets.gpf
ternary_res.map
ternary_res.map.xml
ternary_res_figure.map
ternary_res_figure.map.xml
VLF_line.map
VLF_line.map.xml
VLF_ortho.map
VLF_ortho.map.xml
meraaker.gd~
meraaker_target_center.gd~
meraaker_target_description.gd~
geology.map
geology.map.xml
BergartflateN250_Rørås_Mer.gdb
BergartflateN250_Rørås_Mer.gd~
BergartflateN250_Rørås_Mer.gdb.xml
meraaker_selma.o0
targets_1_44.zip

11. Appendix E – Meråker targets

This appendix includes screen dumps (Figures 108–151) from displays of the frequency domain EM ternary image, grids of VLF anomalies (VLT.map & VOT.map) , grids of analytic signal filtered versions of magnetic gradient tensor invariant I_1 (ana_I1.map). A separate window shows profile data (meraker.gdb), where a fixed range for ordinate values is used for the 923 Hz vertical coaxial coils 4287 Hz horizontal coplanar coils. The SOM clustering results of EM anomalies are shown in a separate window.

Target areas are shown by polygons and the target number is displayed on the ana_I1.map. Coordinates for target positions are shown by white dots and by the + cursor position. The corresponding position in the window for meraker.gdb is shown by a square box. Coordinates are provides digitally on the enclosed DVD together with the target description and priority number in the range from 1 to 5. A priority of 1 is highest priority. Locations with Zn-assay data are shown by proportional size square boxes, where the lower left corner corresponds to the sample location.

(a)



(b)

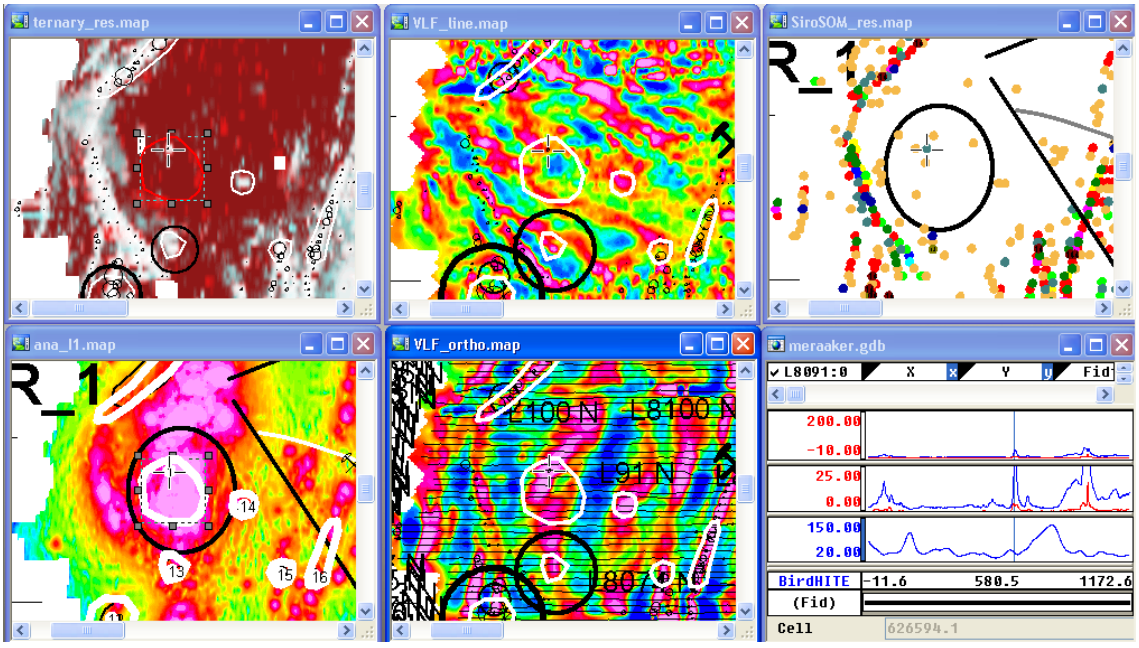
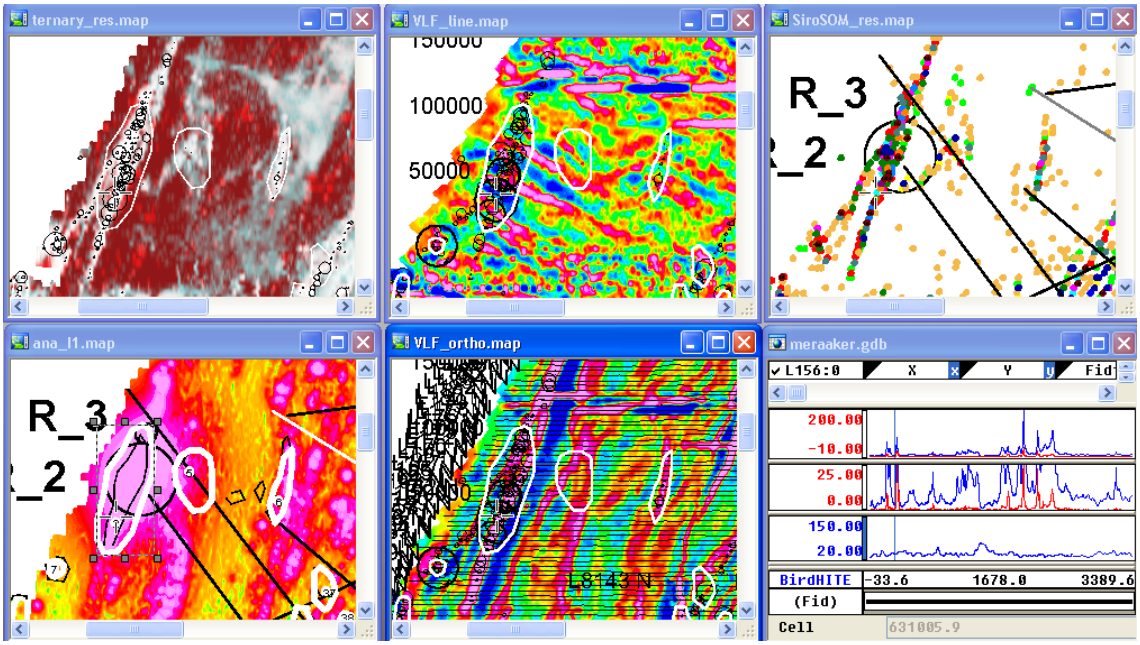


Figure 108. *Meråker target 01; low conductance; variable VLF; strong magnetic anomaly (remanent); priority 2*

(a)



(b)

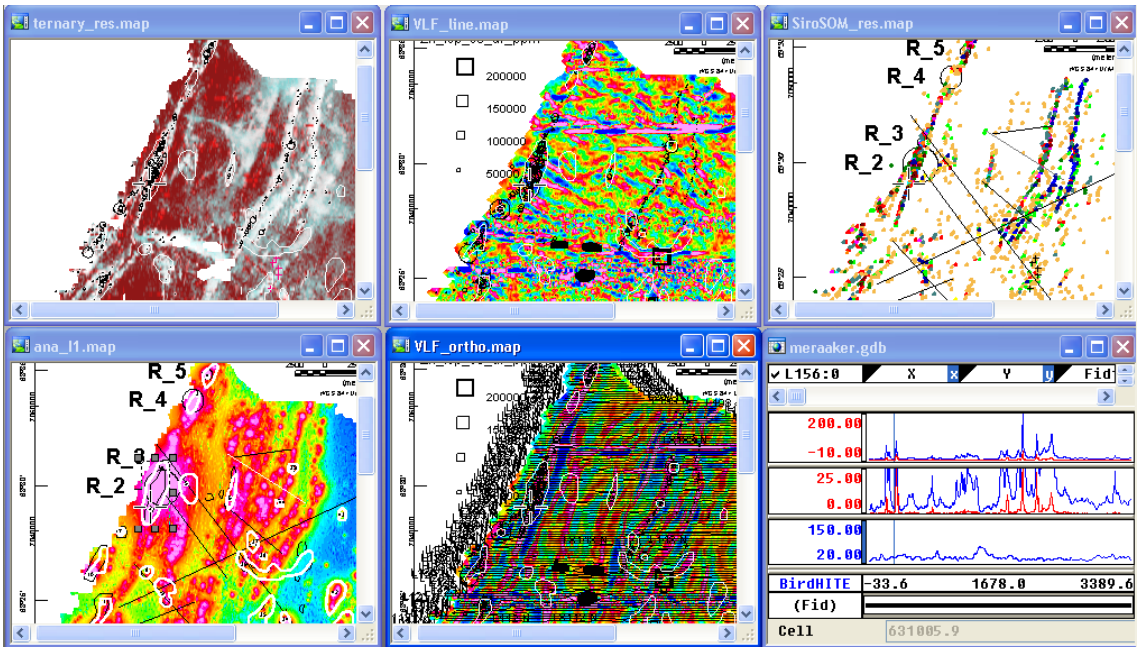
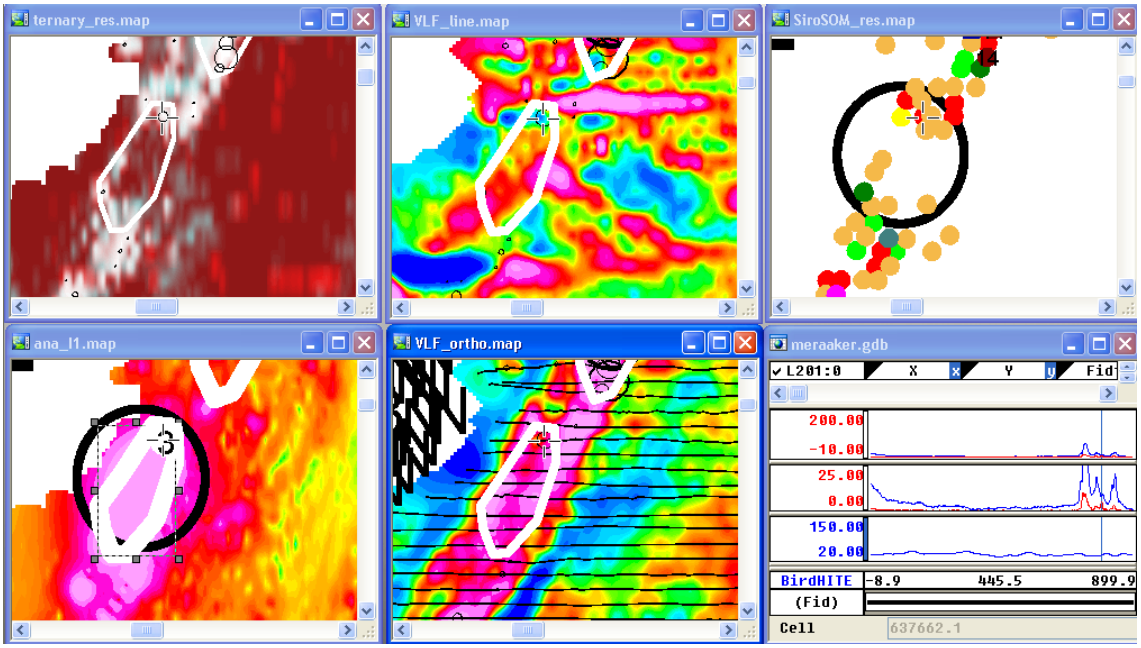


Figure 109. *Meråker target 02; medium conductance; large VLF; strong magnetic anomaly (remanent); priority 1*

(a)



(b)

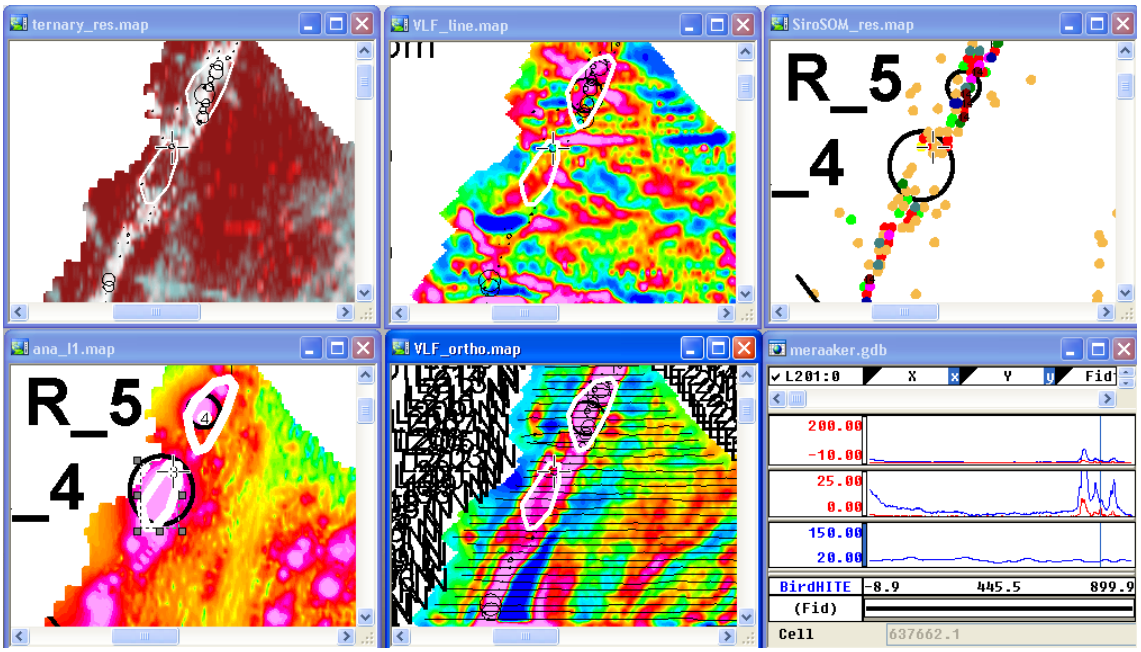
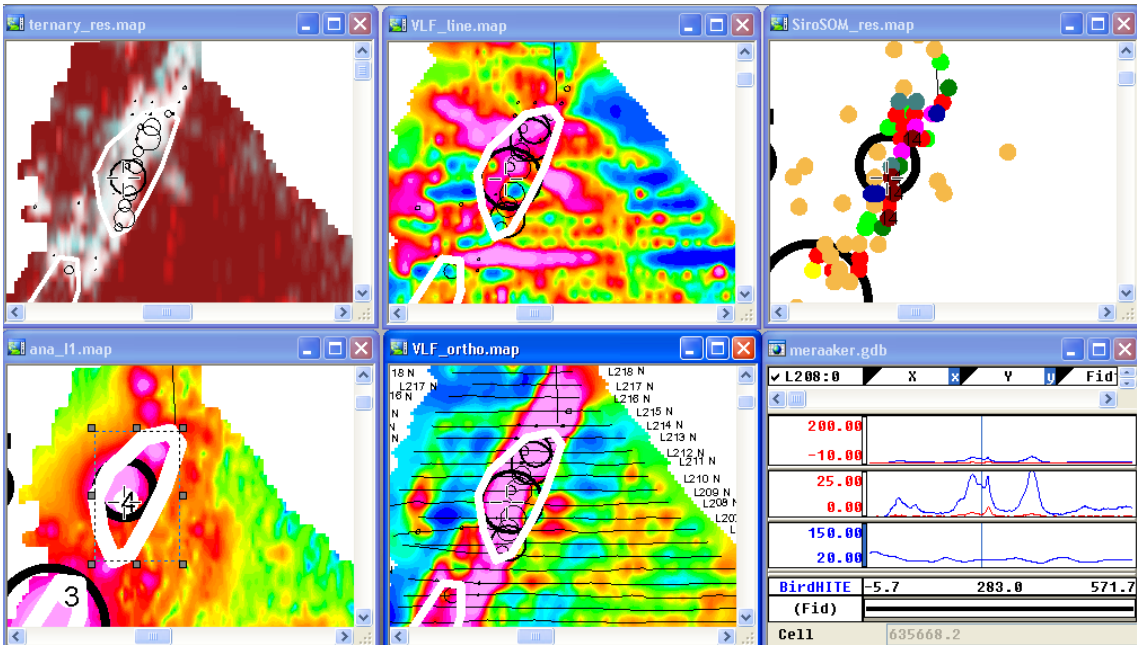


Figure 110. *Meråker target 03; low to medium conductance; medium VLF; strong magnetic anomaly (remanent); priority 2*

(a)



(b)

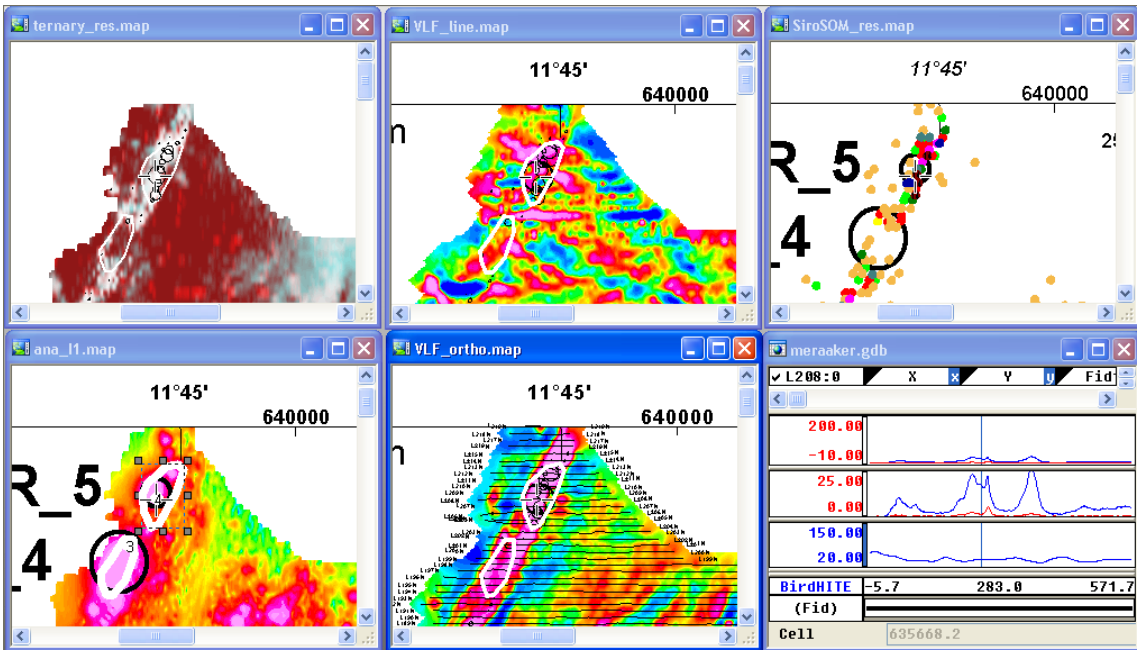
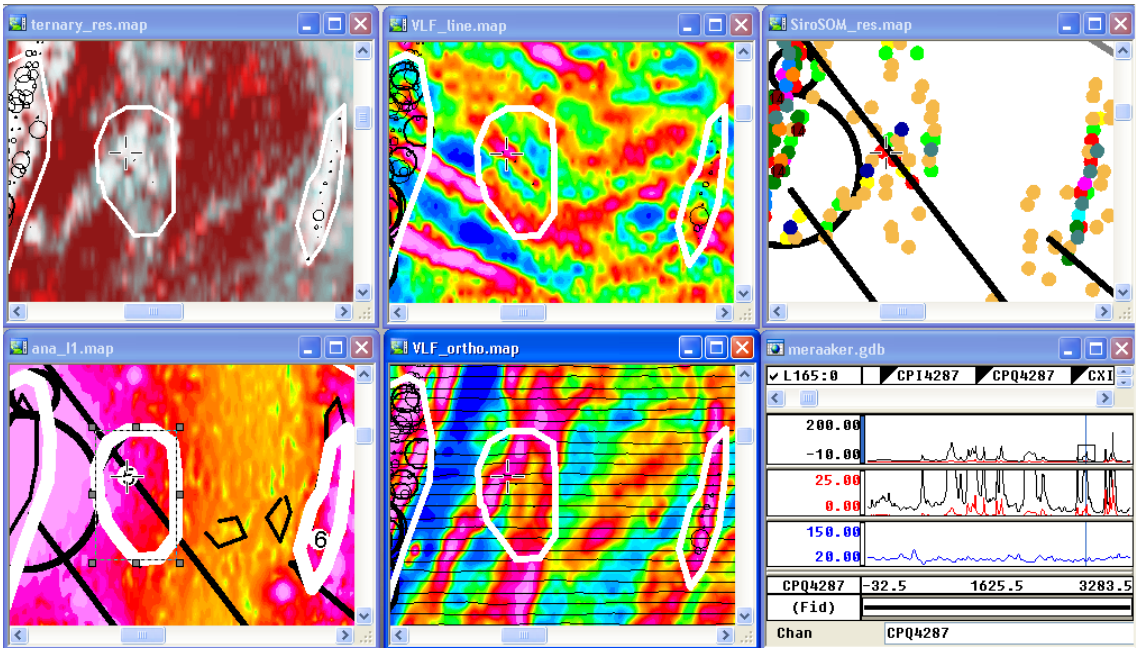


Figure 111. *Meråker target 04; medium conductance; medium to large VLF; strong magnetic anomaly (remanent); priority 2*

(a)



(b)

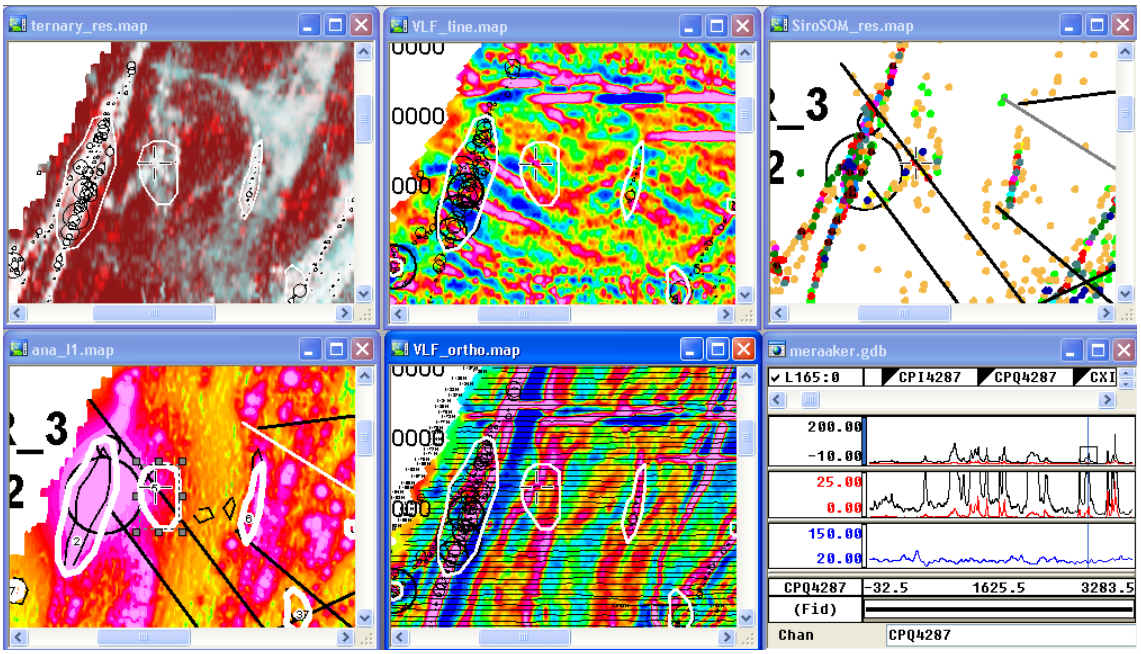
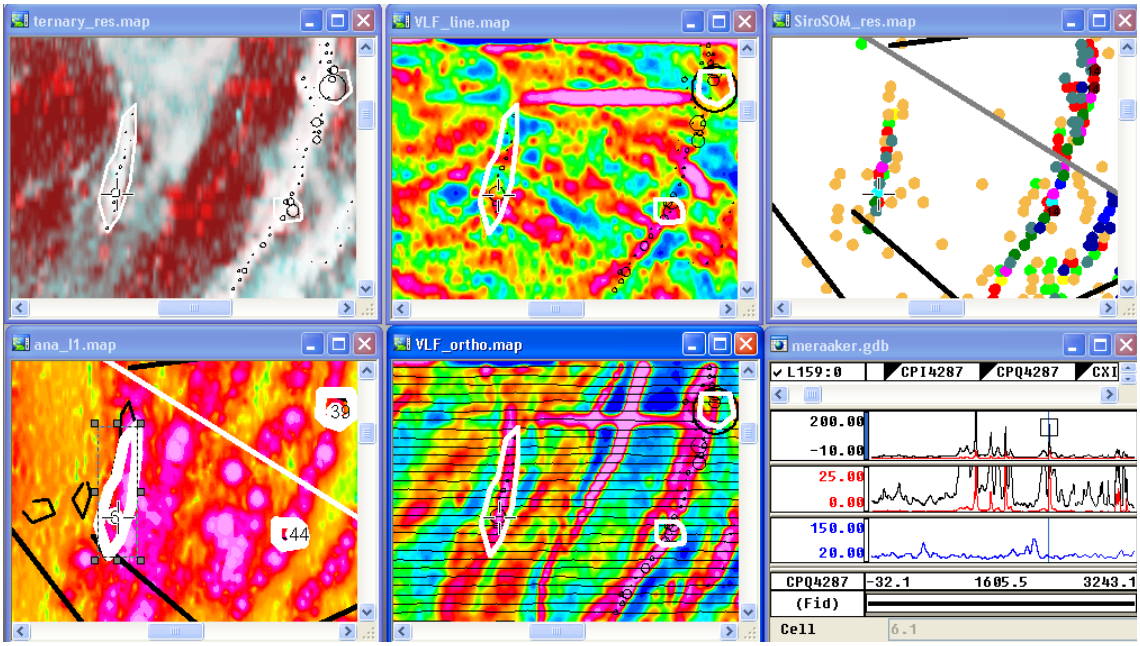


Figure 112. *Meråker target 05; large number of weak EM anaomalies; medium to strong VLF; on magnetic break line; priority 1*

(a)



(b)

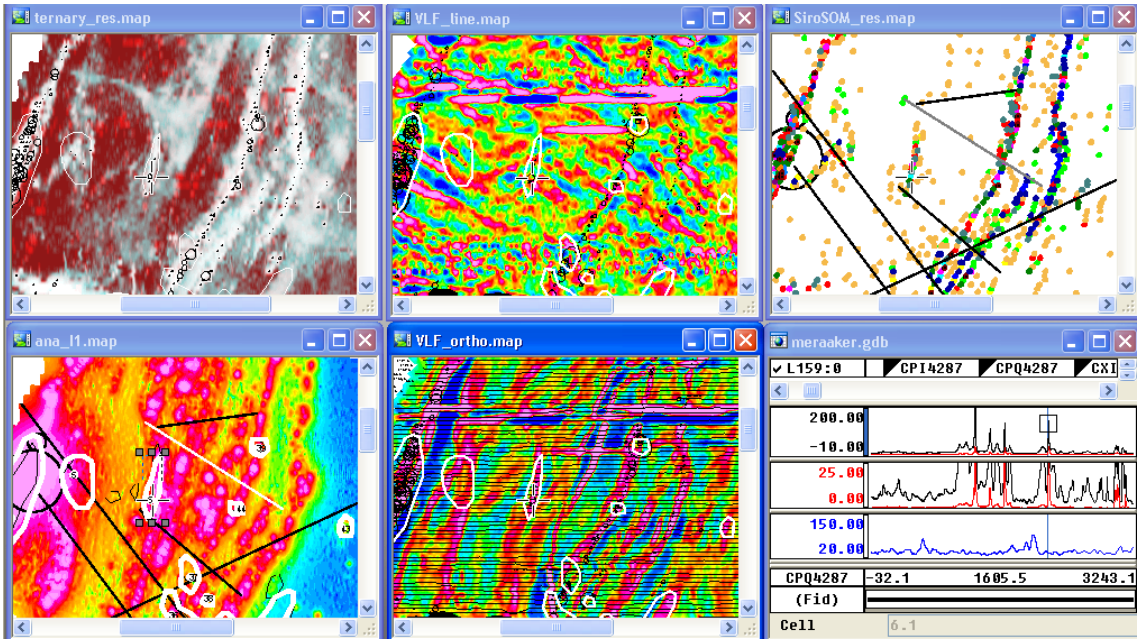
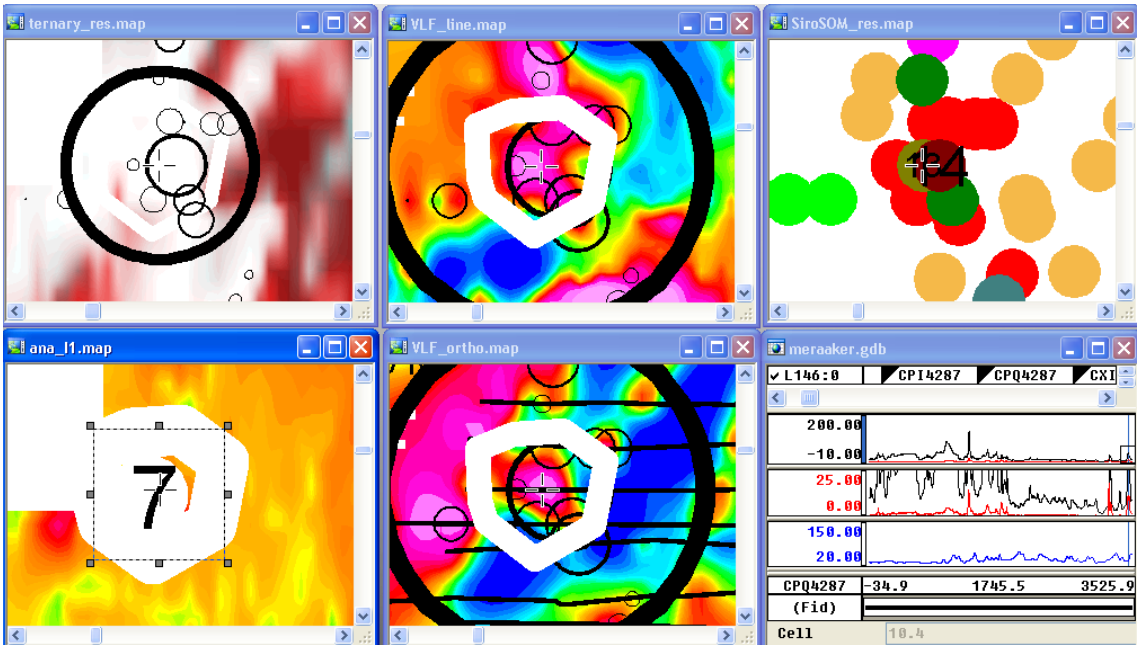


Figure 113. *Meråker target 06; narrow large EM; variable VLF; close to magnetic break line; priority 2*

(a)



(b)

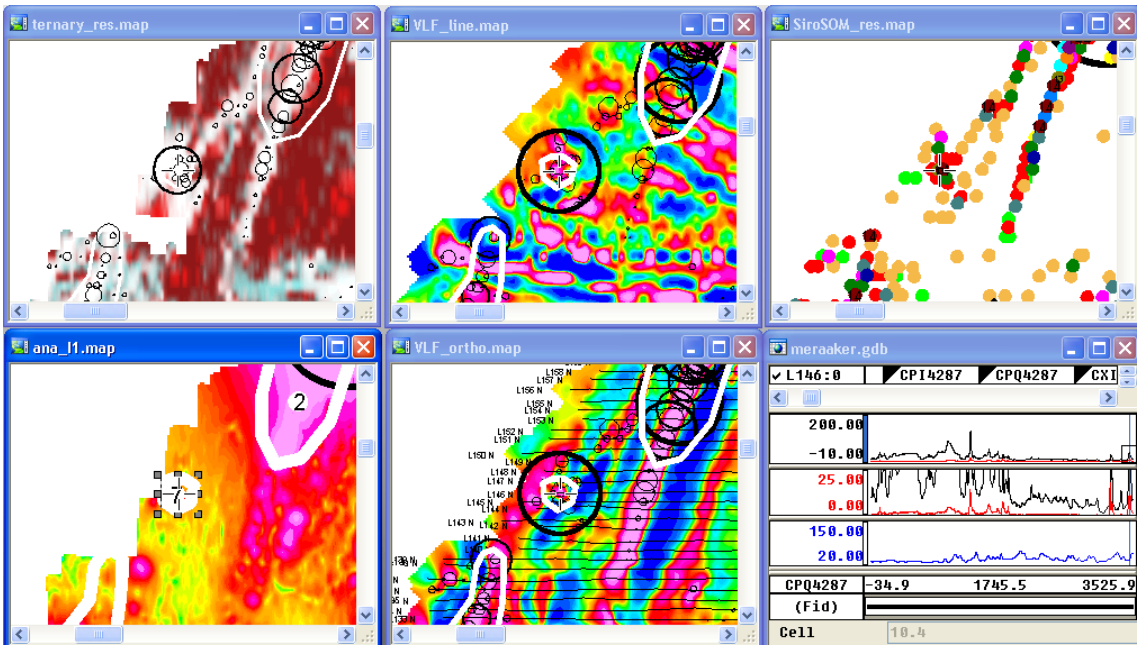
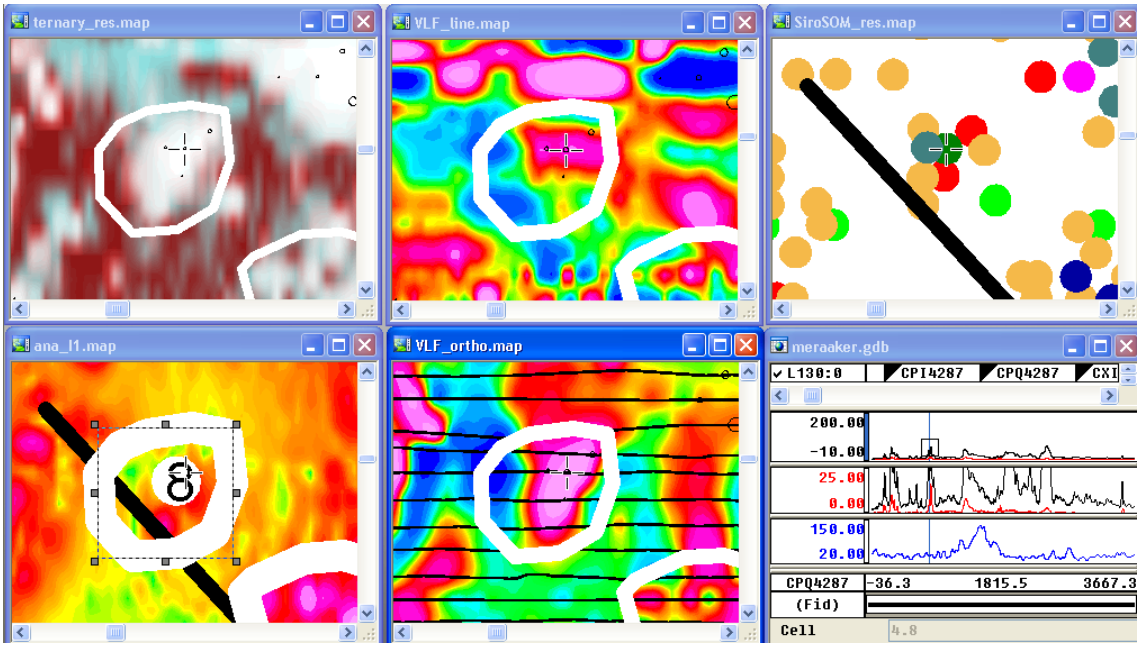


Figure 114. *Meråker target 07; medium to high conductance; medium VLF; low magnetic area; priority 3*

(a)



(b)

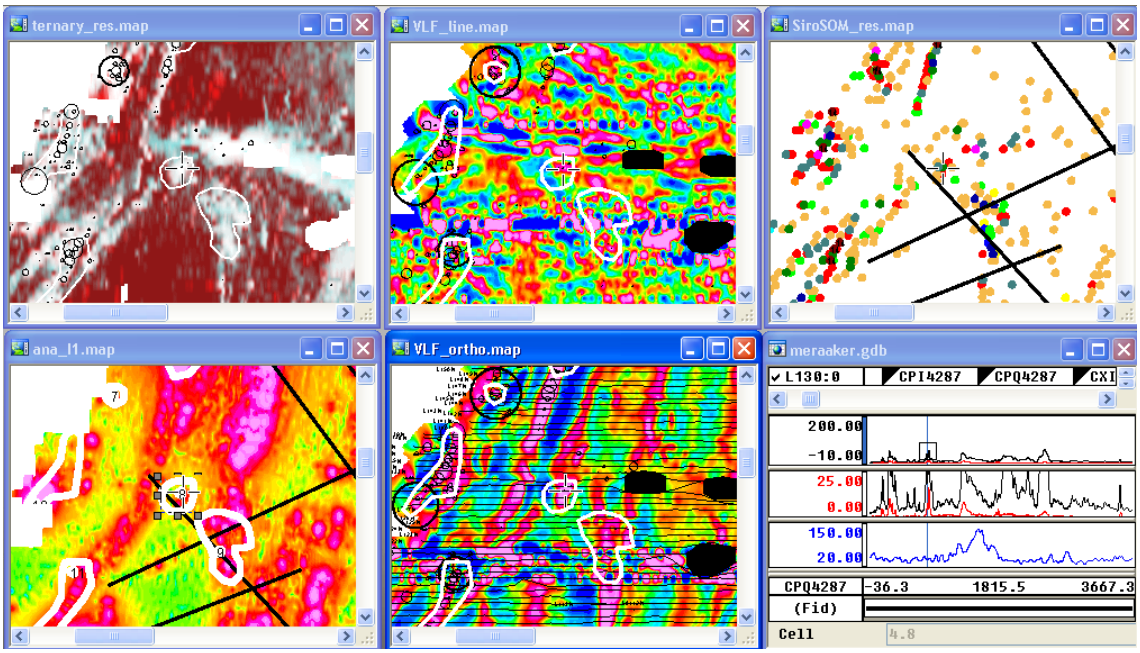
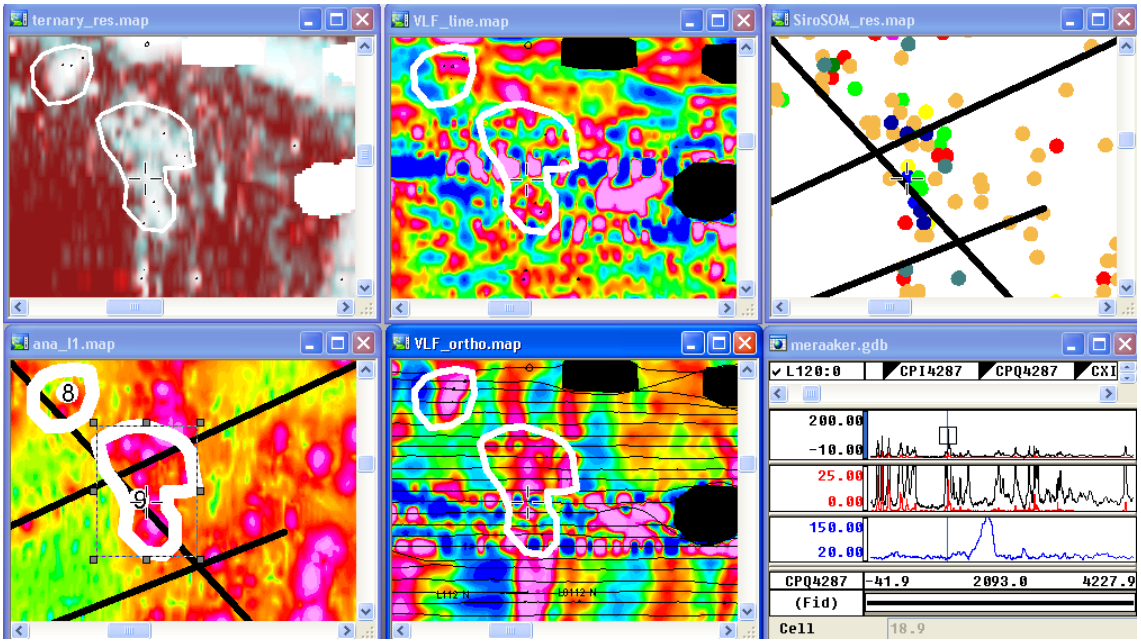


Figure 115. *Meråker target 08; low conductance; medium but clear VLF; medium magnetic- on magnetic break line; priority 2*

(a)



(b)

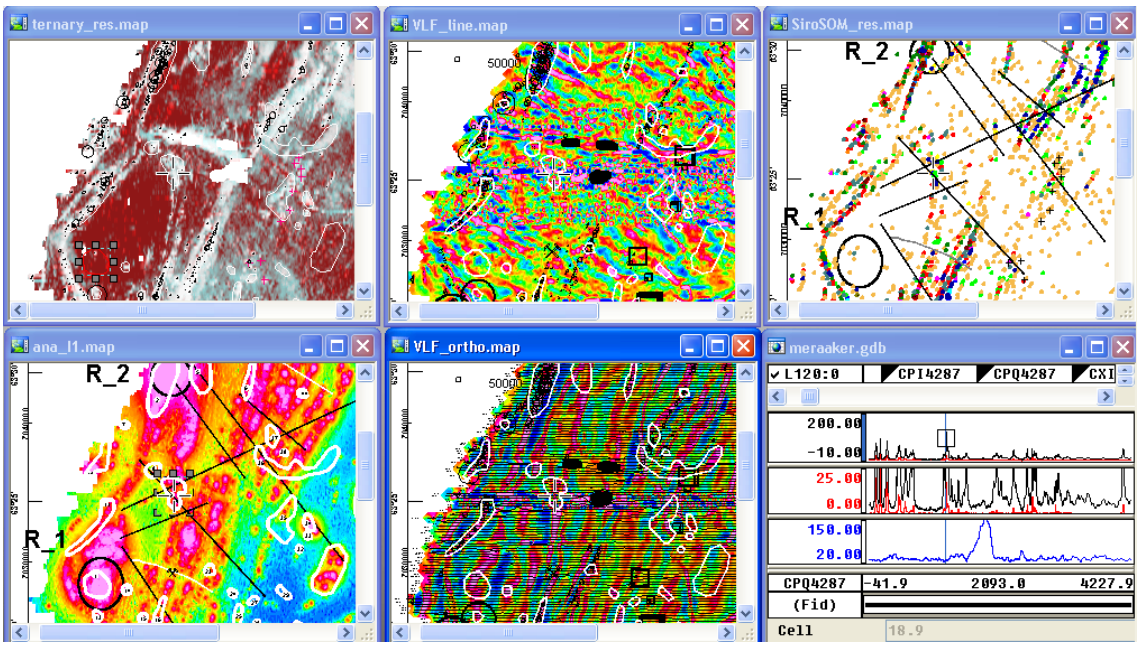
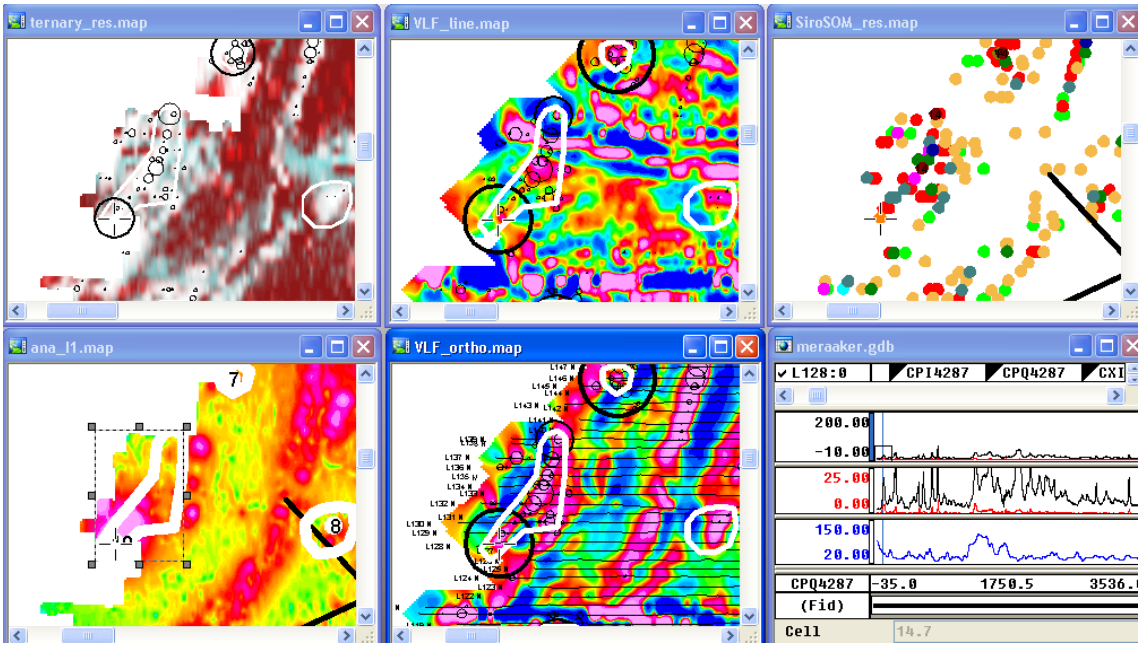


Figure 116. *Meråker target 09; low conductance; VLF noisy; medium magnetic- on two magnetic break line; priority 3*

(a)



(b)

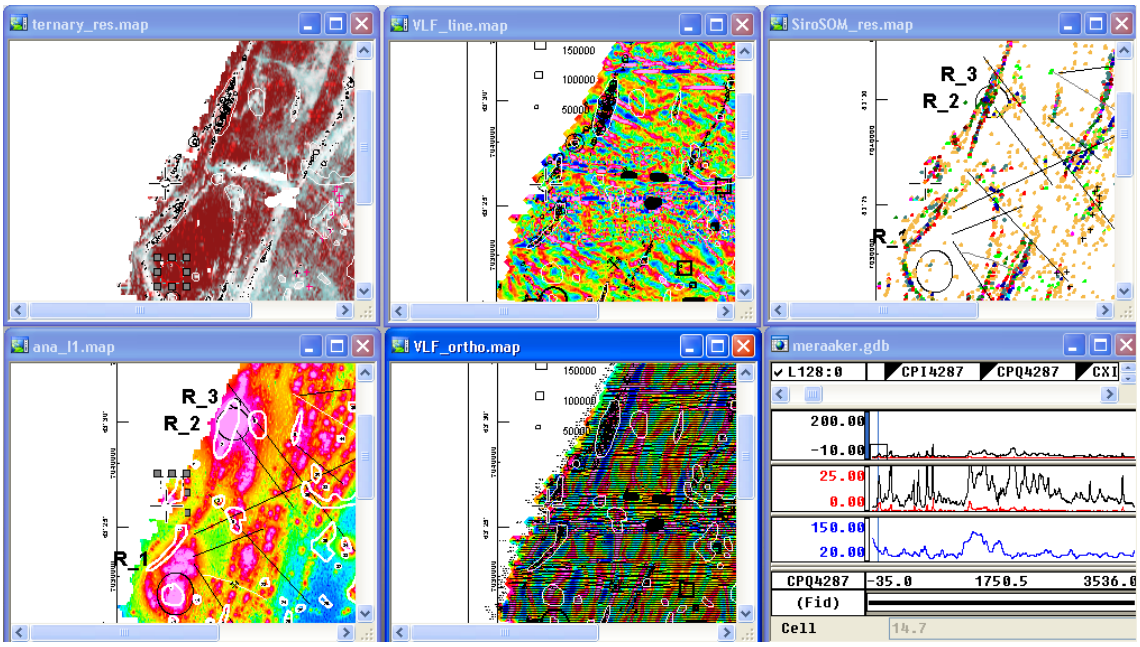
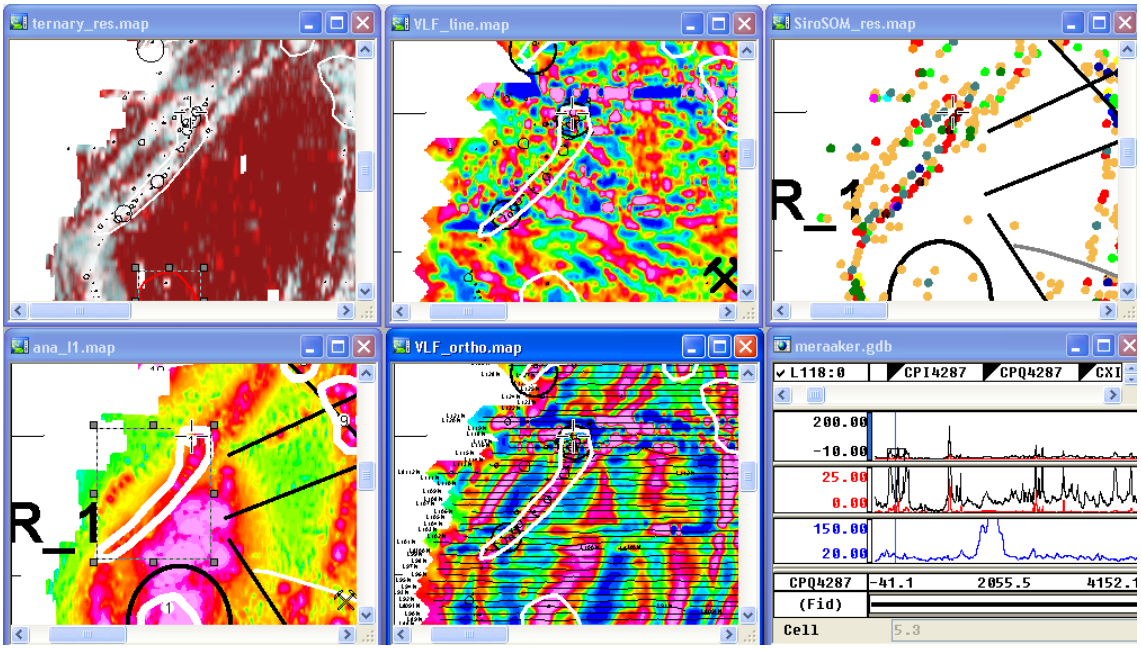


Figure 117. *Meråker target 10; group of medium conductive anomalies; medium but clear VLF; medium short wavelength magnetic anomalies; priority 2*

(a)



(b)

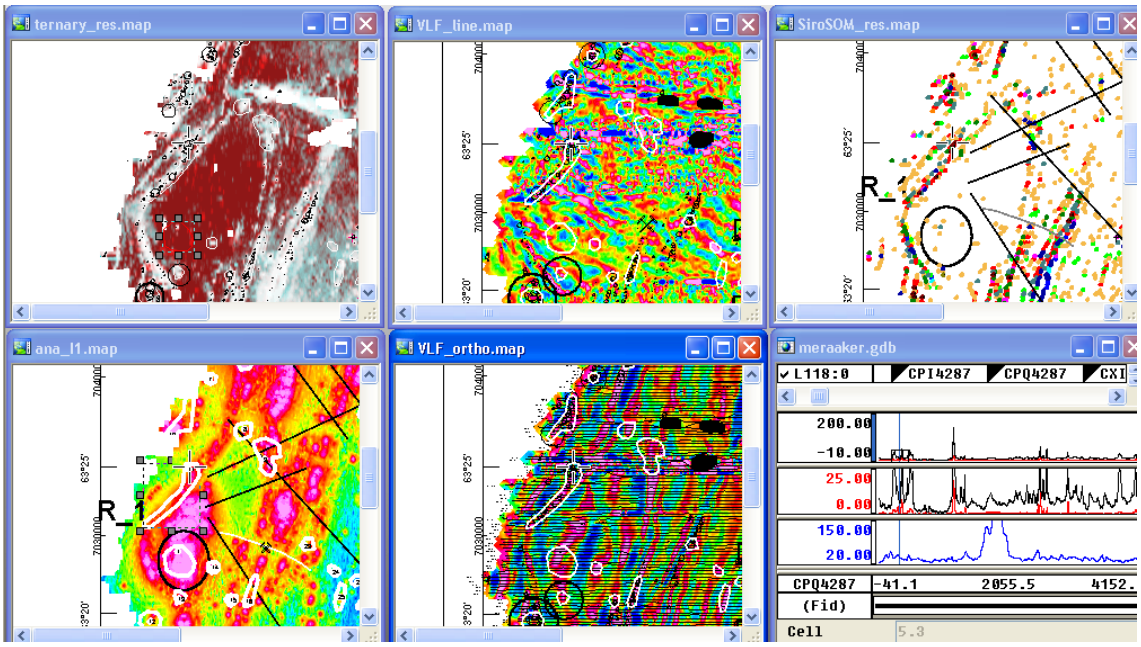
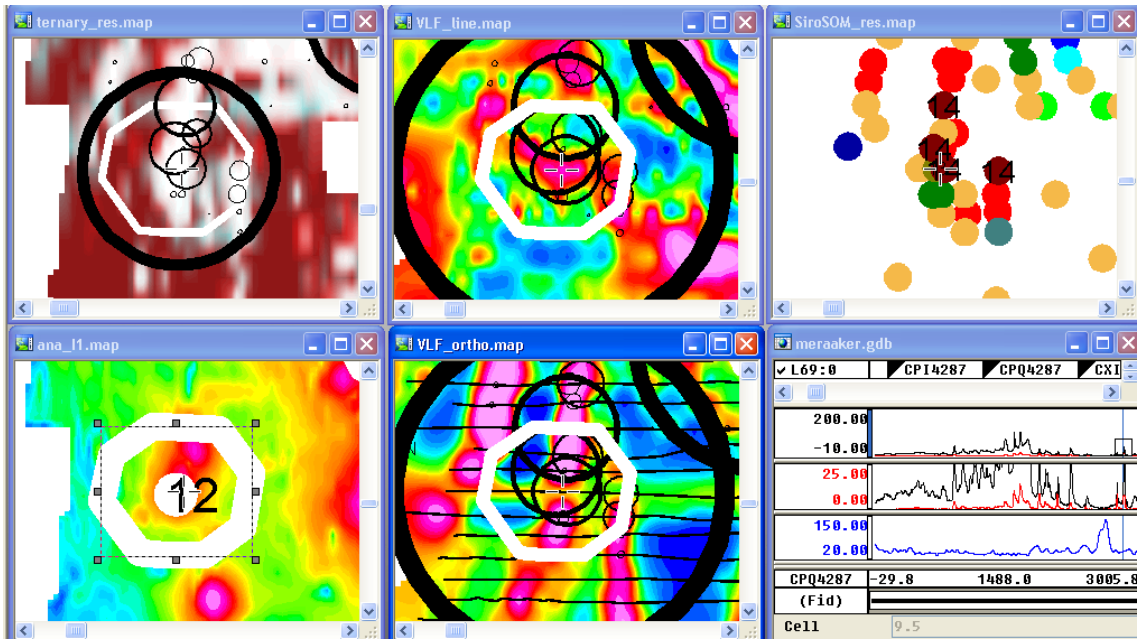


Figure 118. *Meråker target 11; group of medium conductive anomalies; medium but clear VLF; medium magnetic anomalies; priority 2*

(a)



(b)

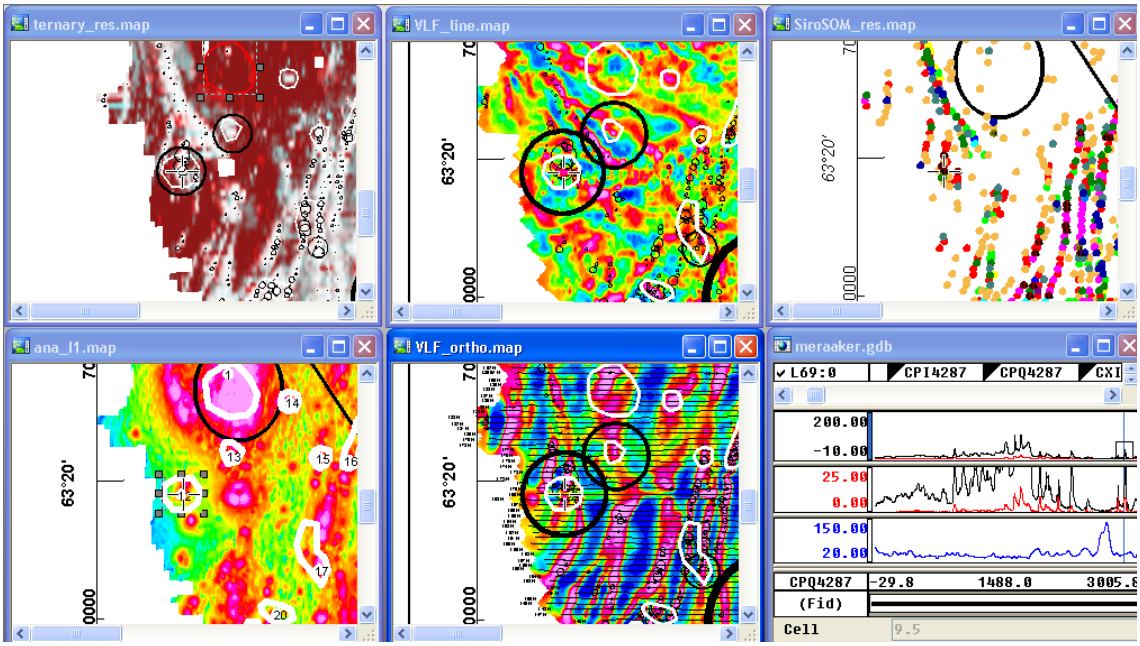
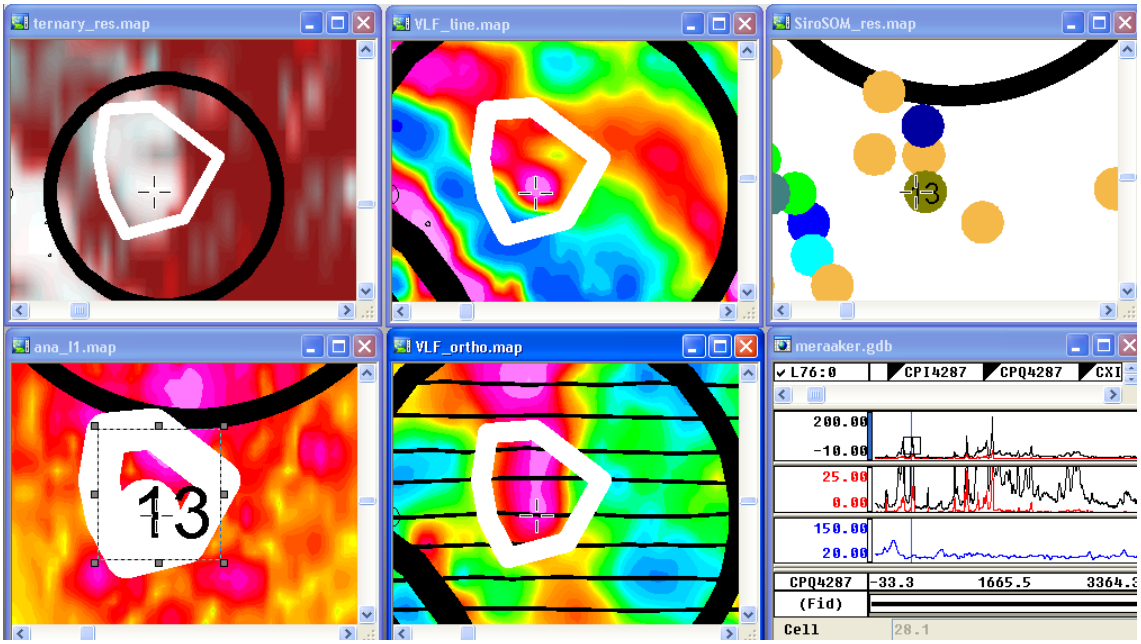


Figure 119. *Meråker target 12; high conductance; variable VLF; short wavelength magnetic anomalies; priority 1*

(a)



(b)

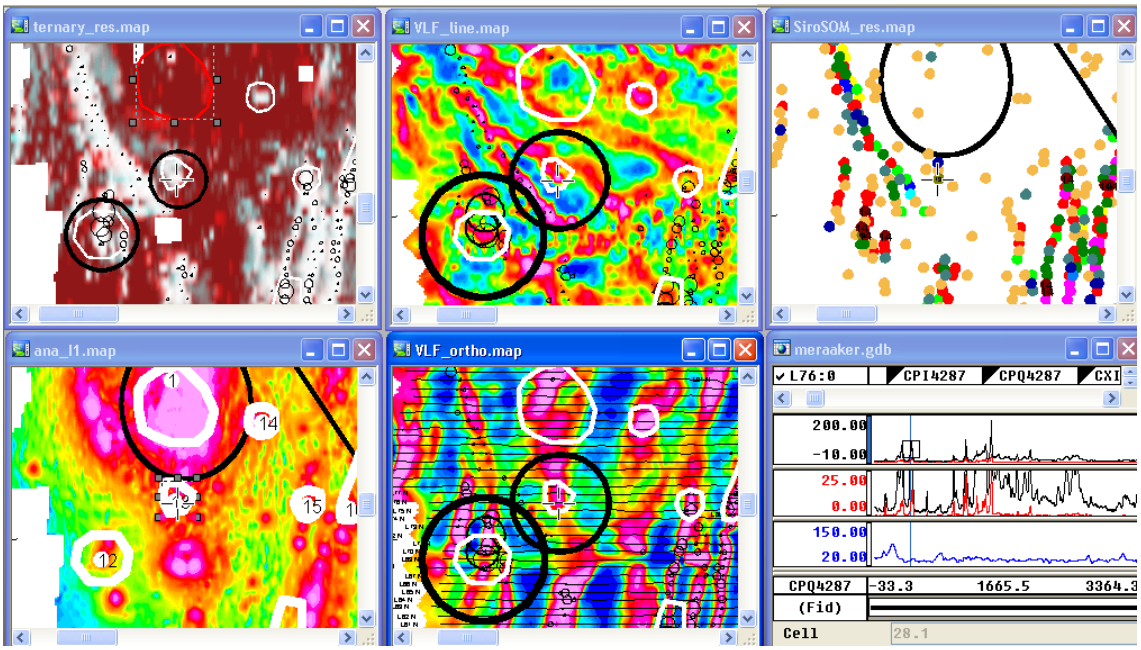
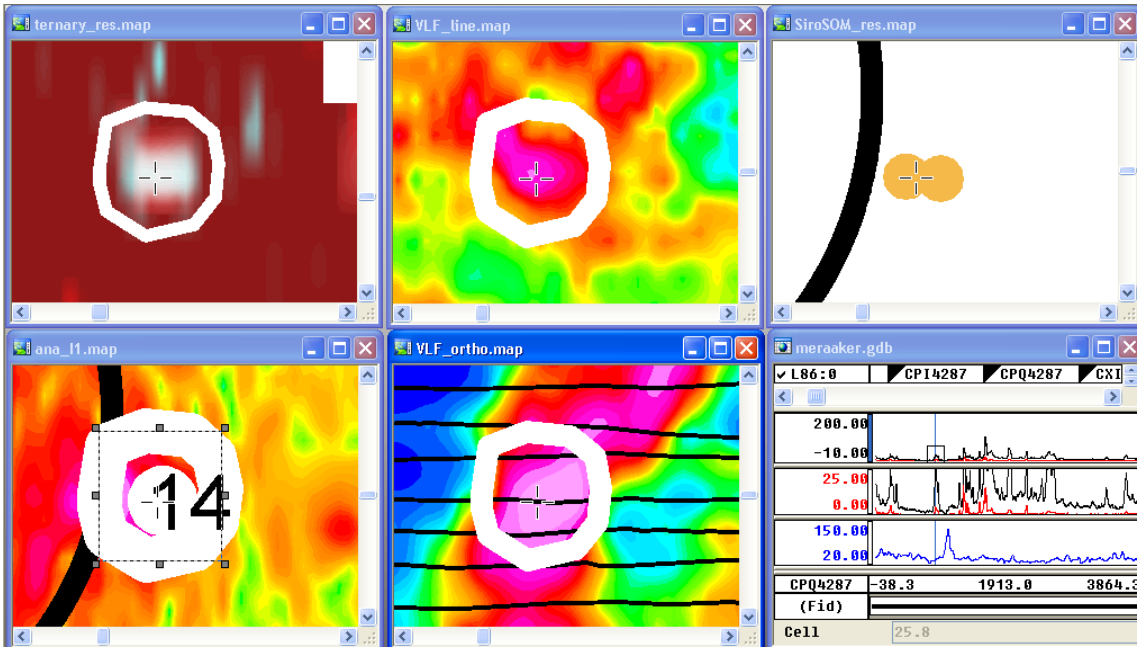


Figure 120. *Meråker target 13; high conductance; high VLF; short wavelength magnetic anomalies; priority 1*

(a)



(b)

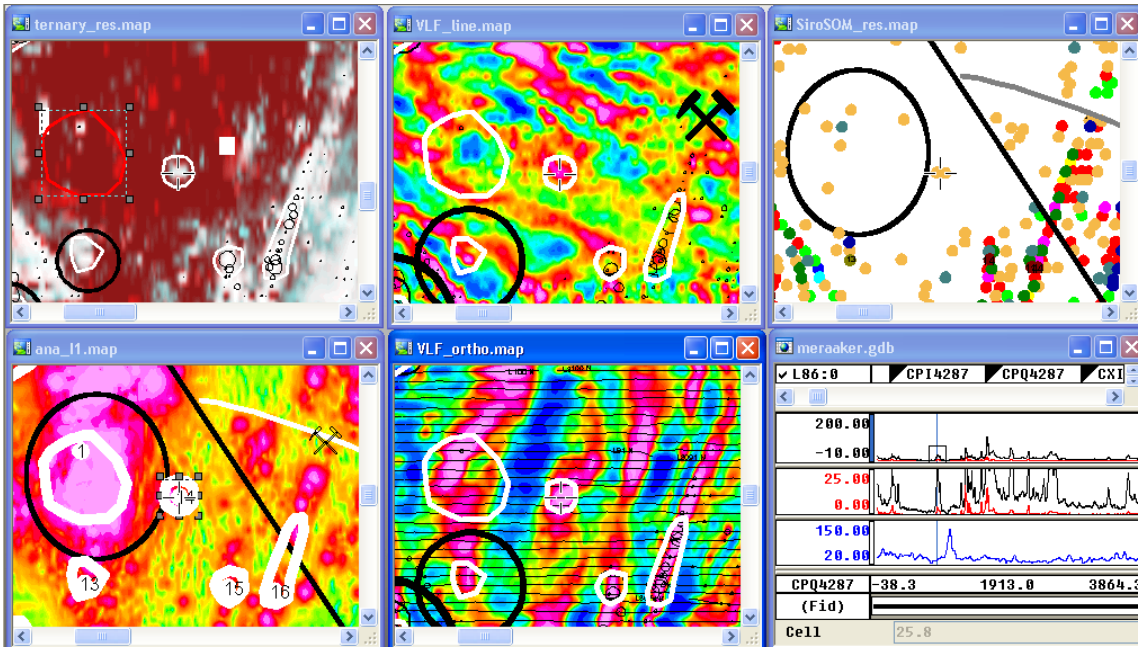
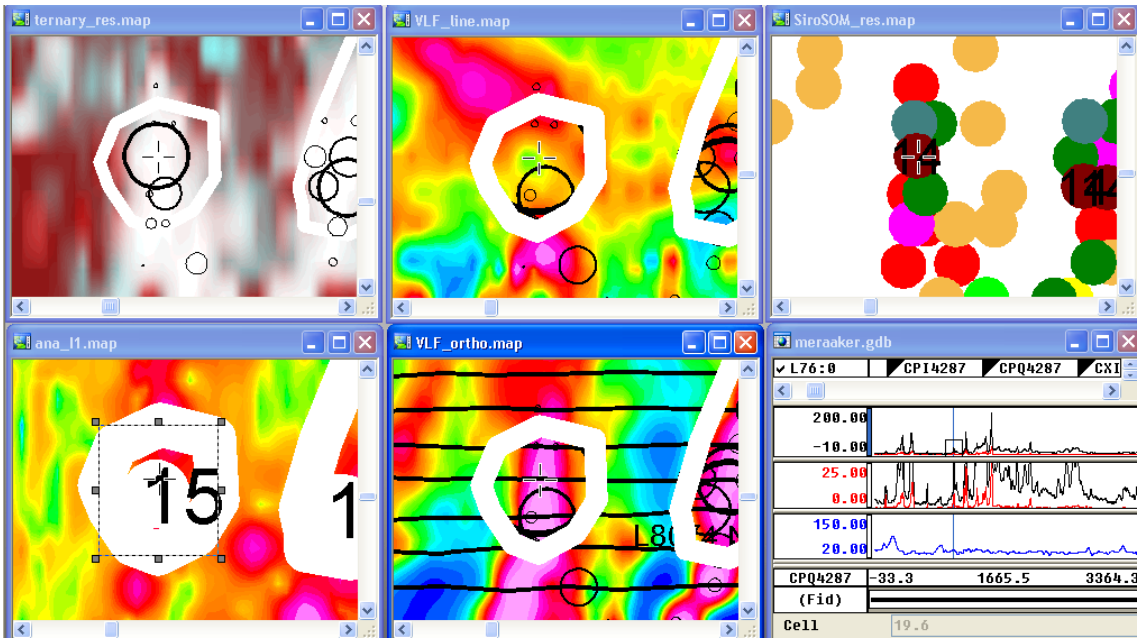


Figure 121. *Meråker target 14; low conductance; clear VLF; short wavelength magnetic anomalies; priority 5*

(a)



(b)

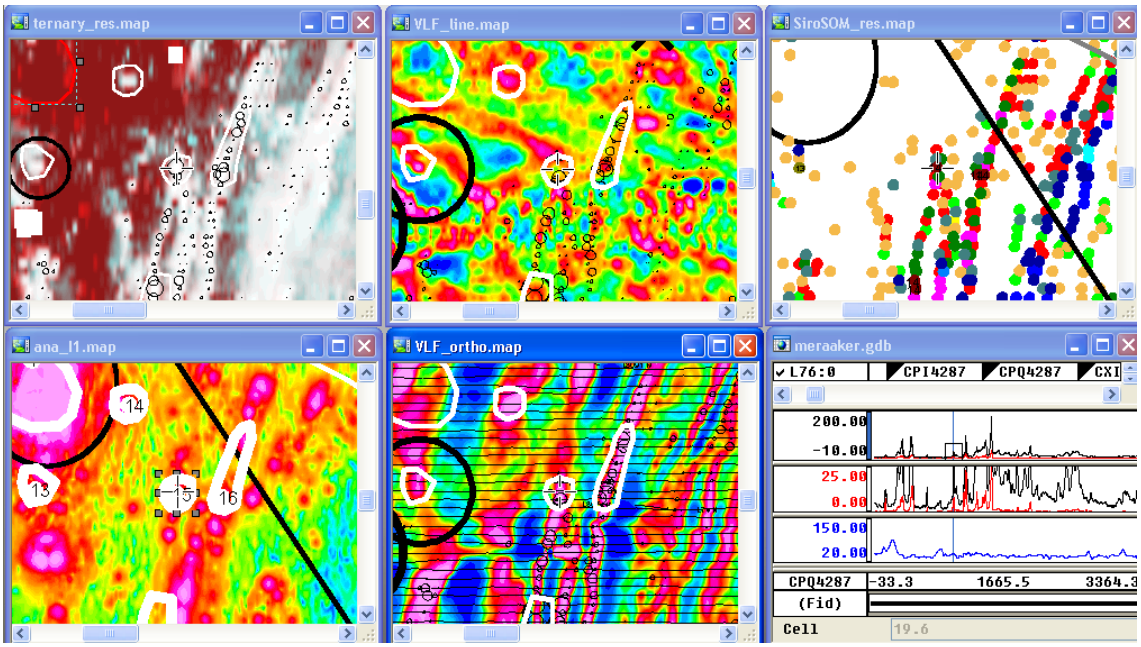
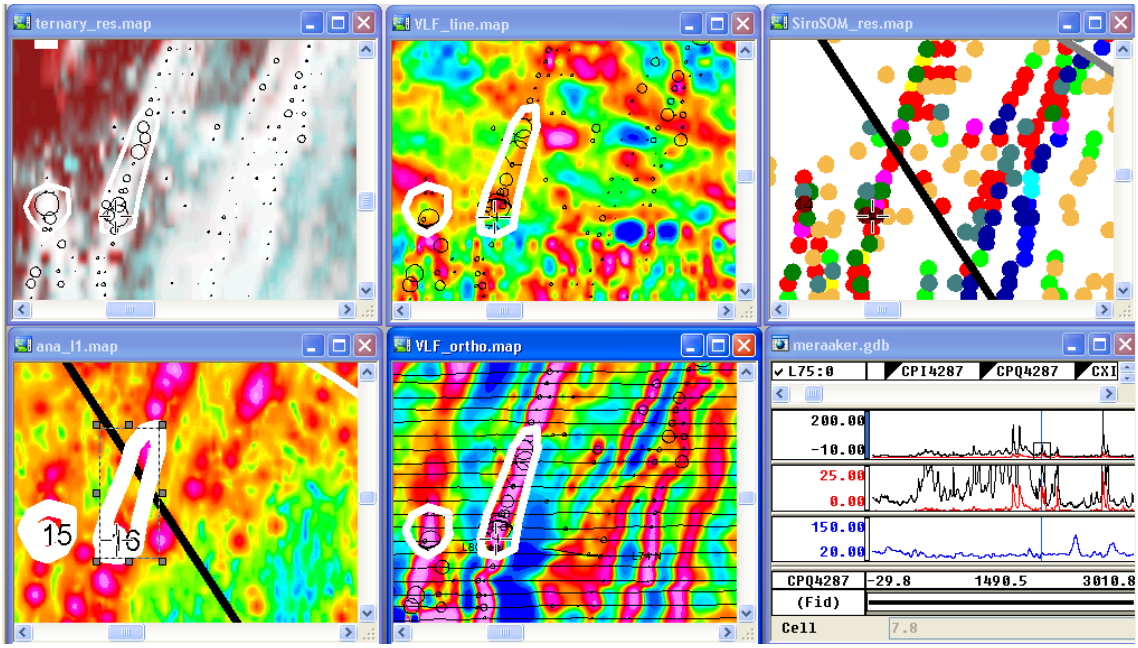


Figure 122. *Meråker target 15; medium conductance; variable VLF; short wavelength magnetic anomalies; priority 4*

(a)



(b)

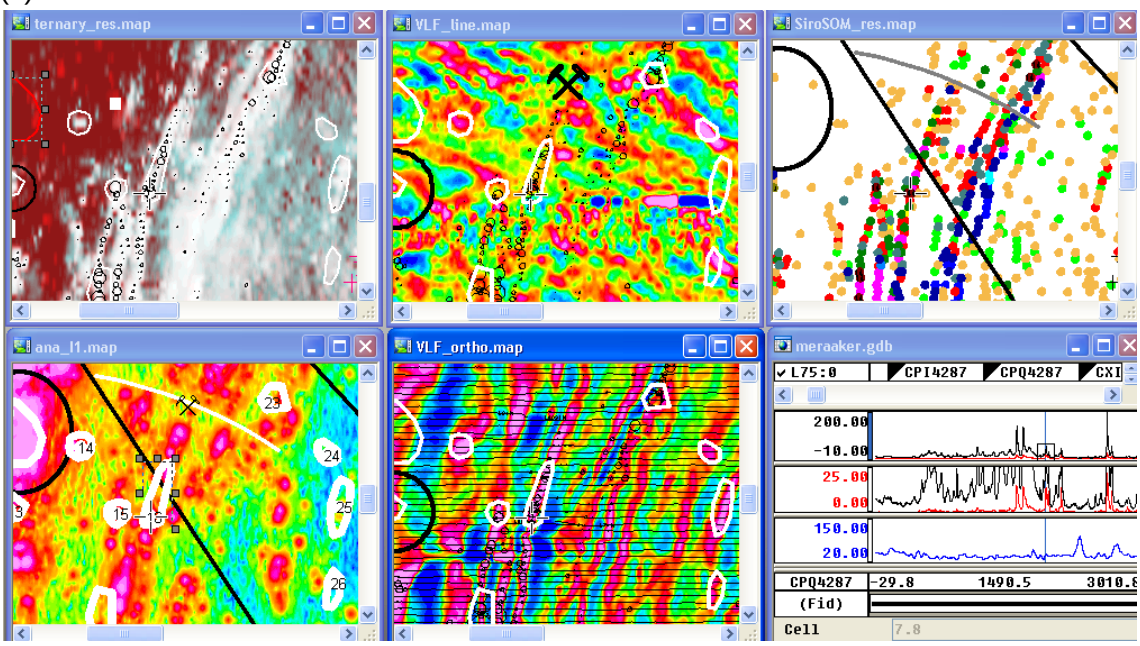
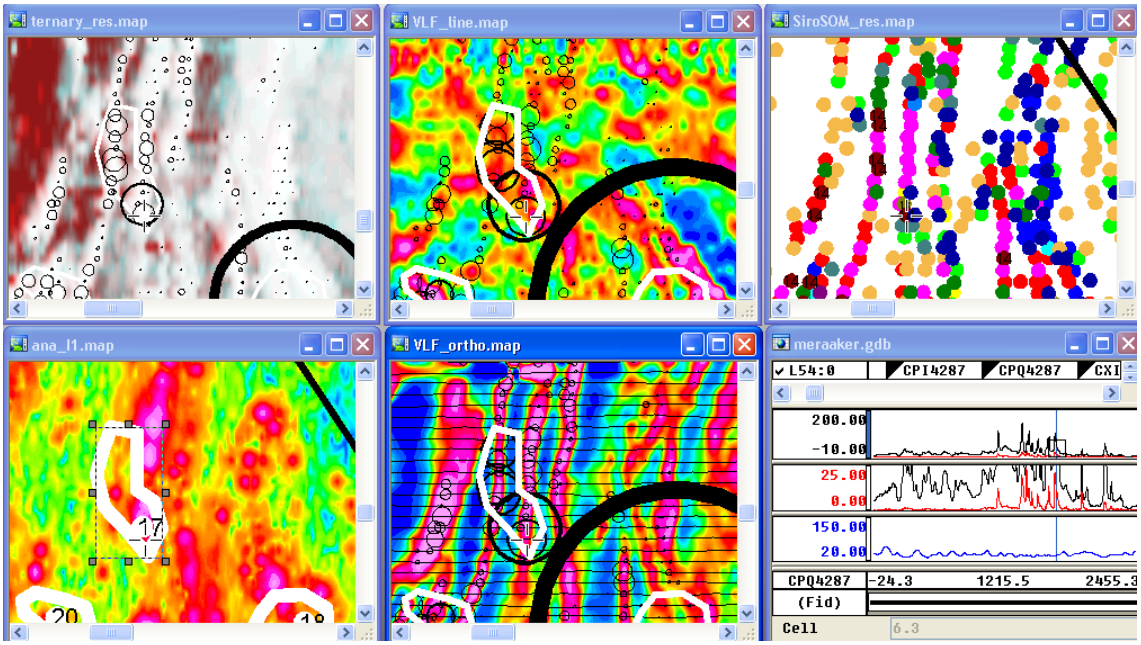


Figure 123. *Meråker target 16; medium conductance; variable VLF; short wavelength magnetic anomalies; priority 3*

(a)



(b)

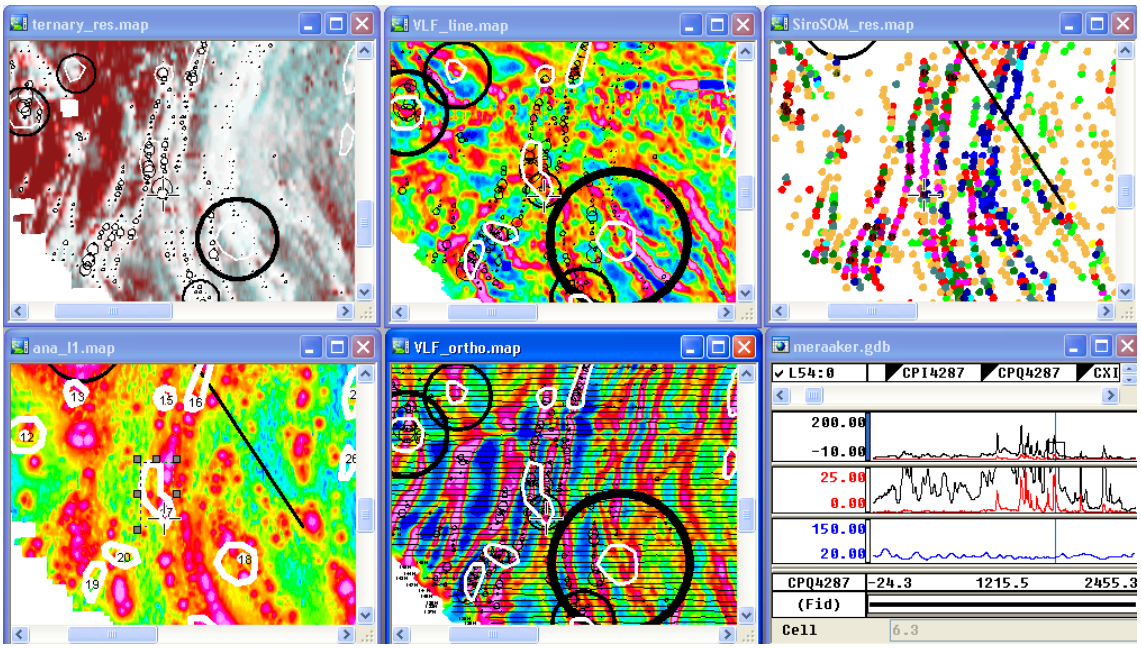
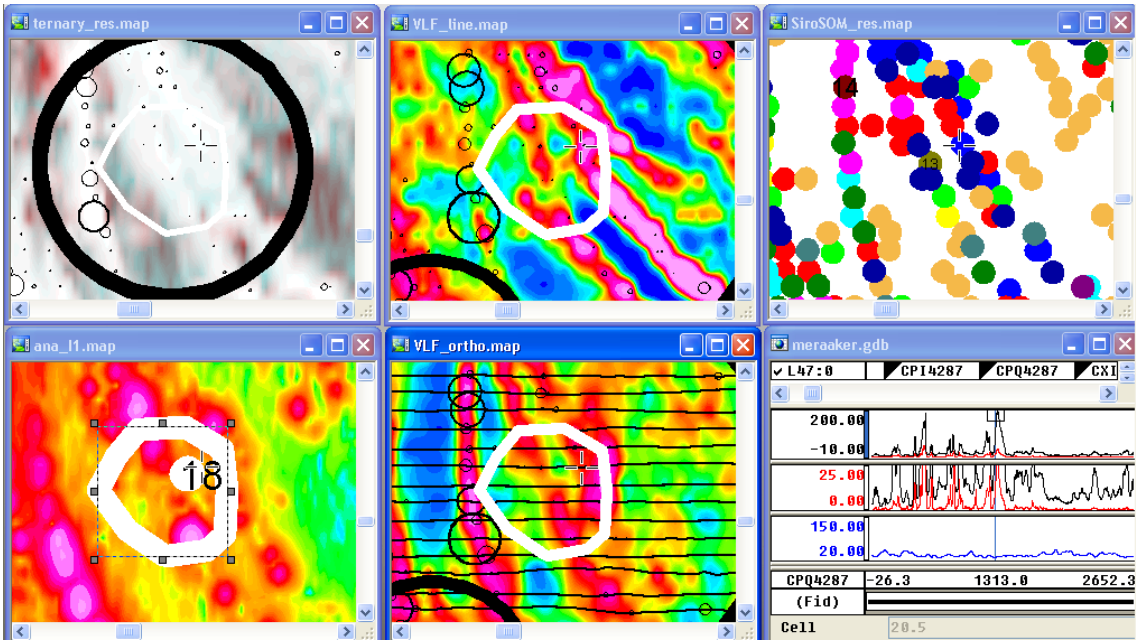


Figure 124. *Meråker target 17; medium conductance; clear VLF; short wavelength magnetic anomalies; priority 3*

(a)



(b)

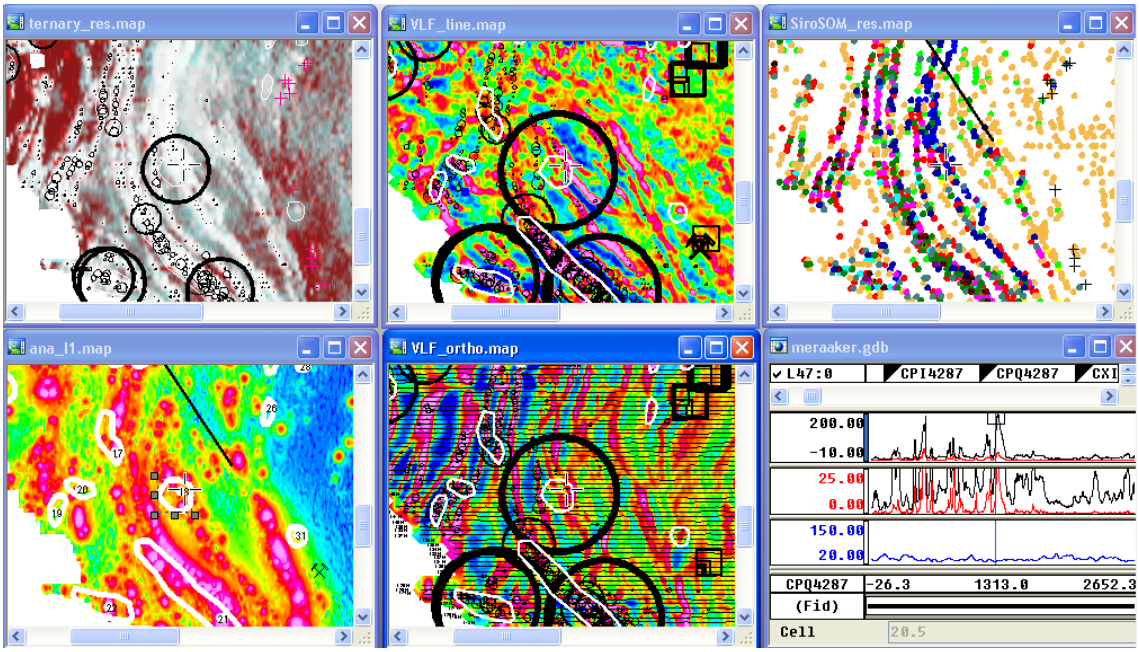
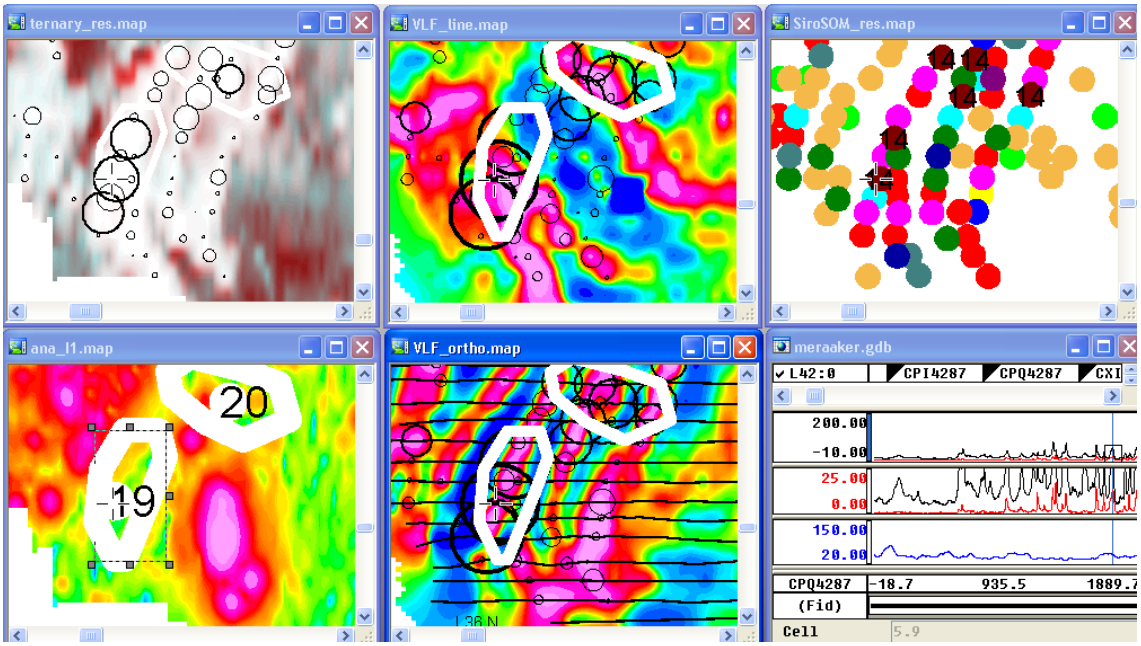


Figure 125. *Meråker target 18; low conductance but clear peak in EM response; clear VLF; short wavelength magnetic anomalies; priority 3*

(a)



(b)

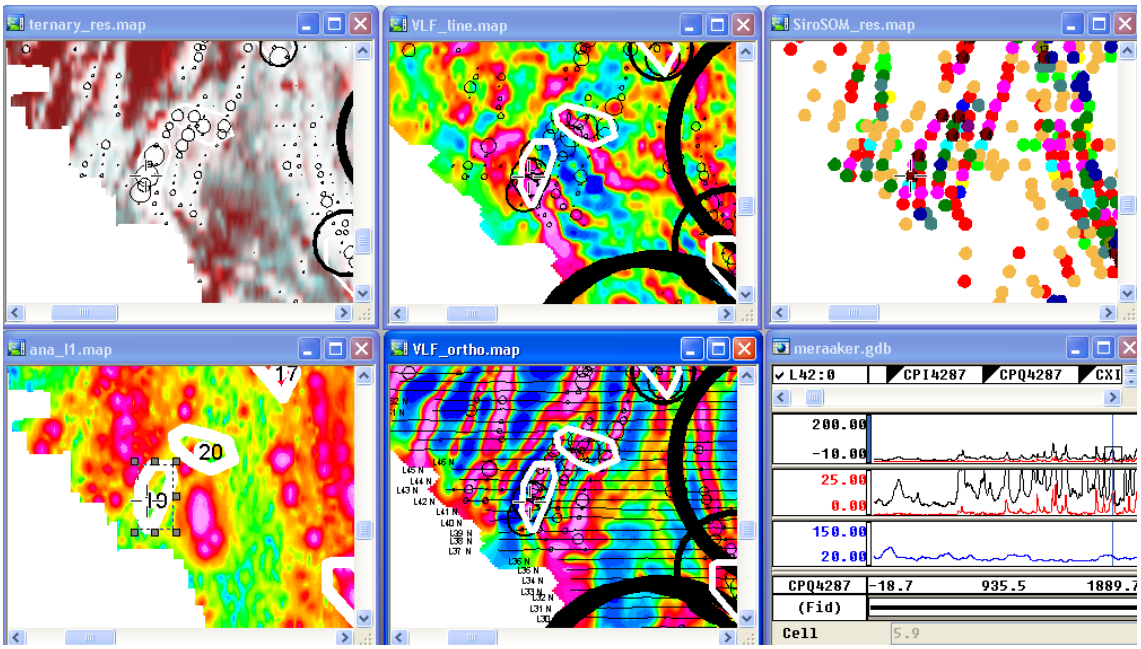
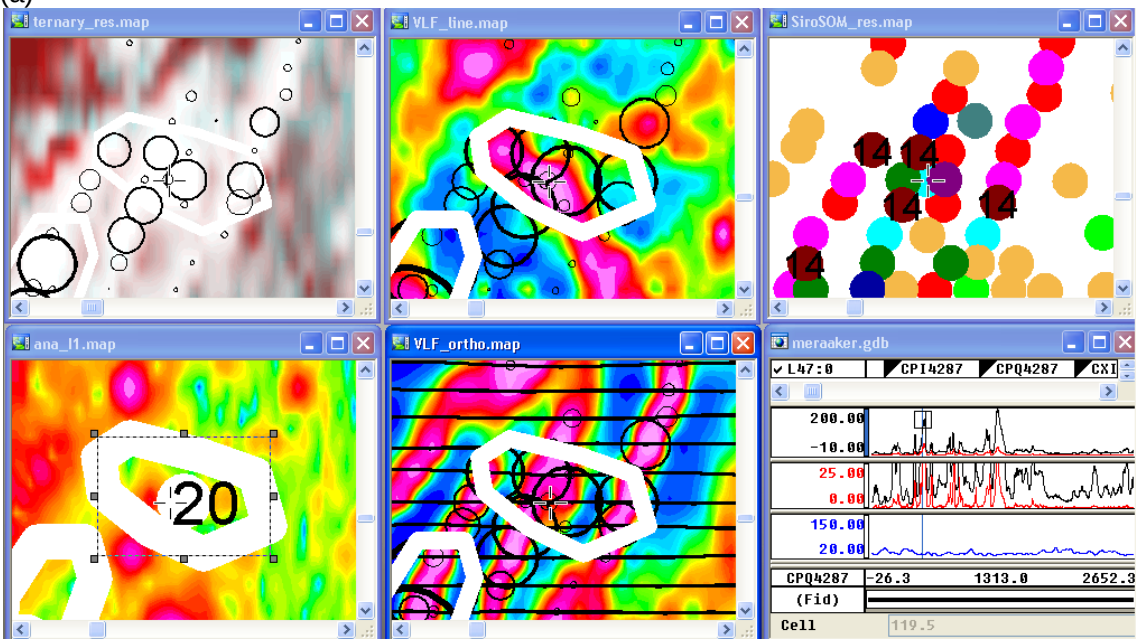


Figure 126. *Meråker target 19; medium conductance; variable VLF; low magnetic field; priority 3*

(a)



(b)

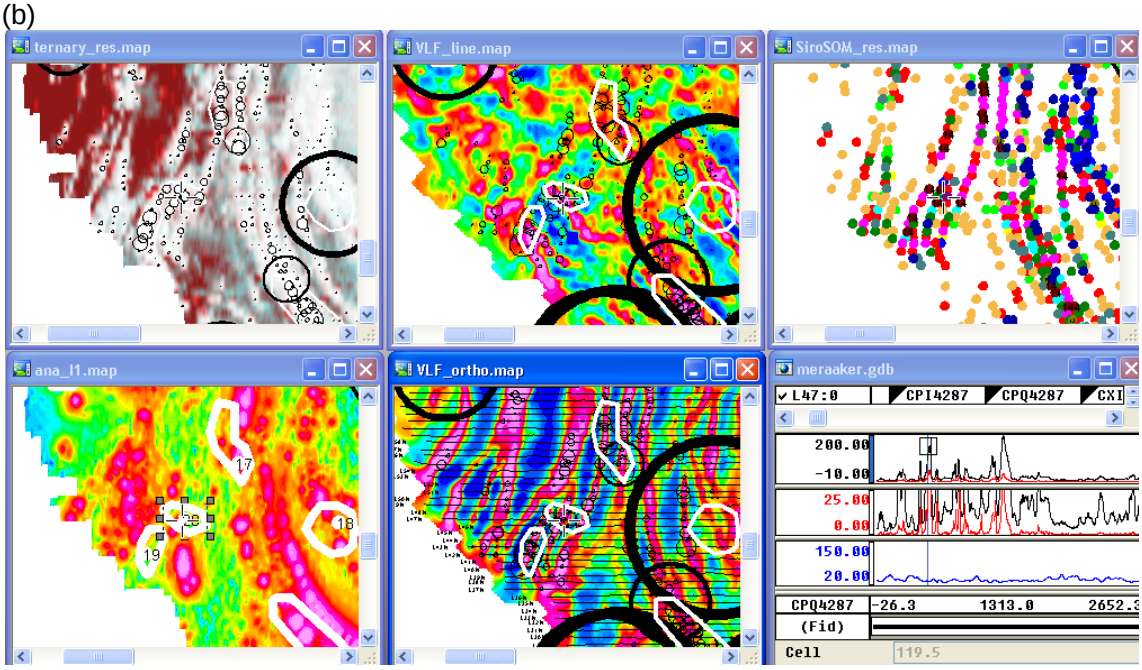
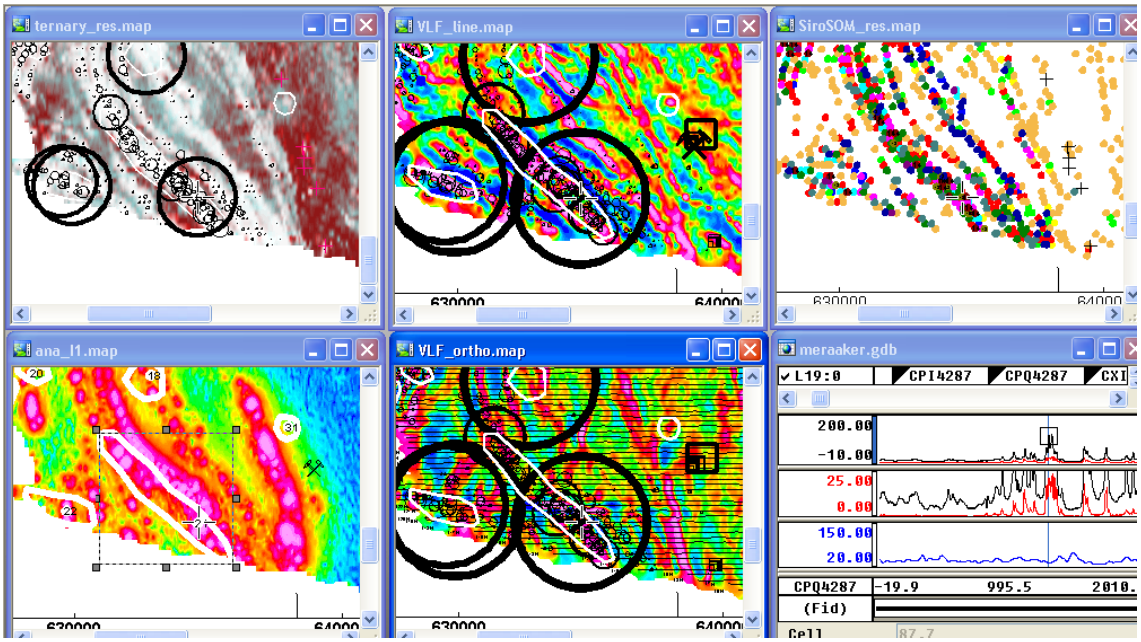


Figure 127. *Meråker target 20; medium conductance; clearVLF; short wavelength magnetic anomalies; priority 3*

(a)



(b)

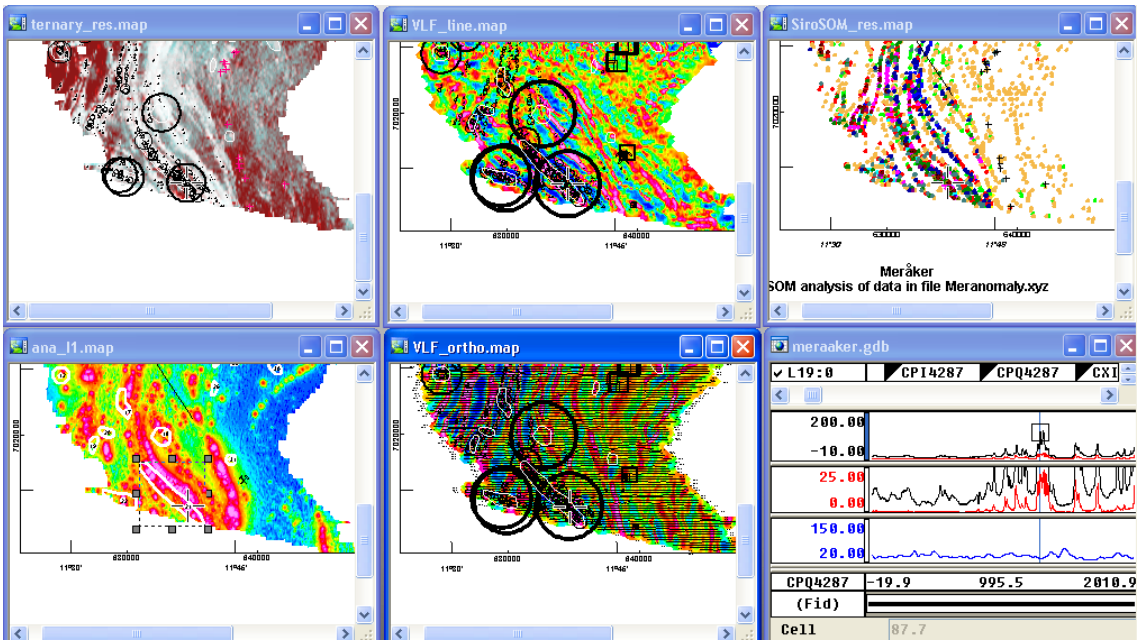
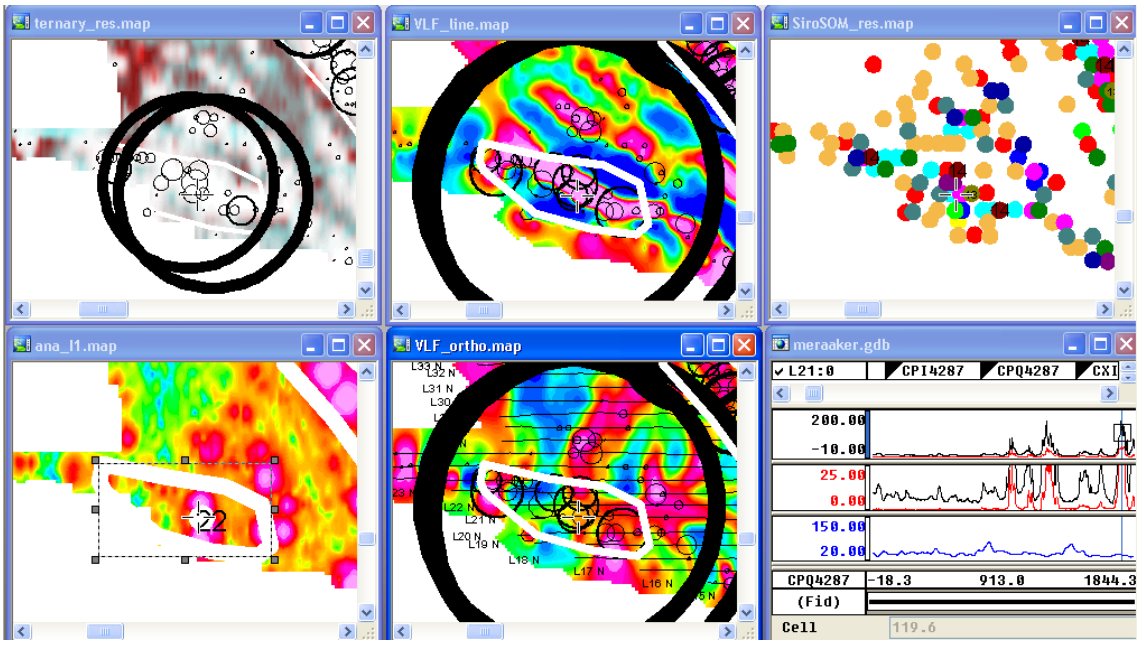


Figure 128. *Meråker target 21; high conductance; strong VLF; short wavelength magnetic anomalies; priority 1*

(a)



(b)

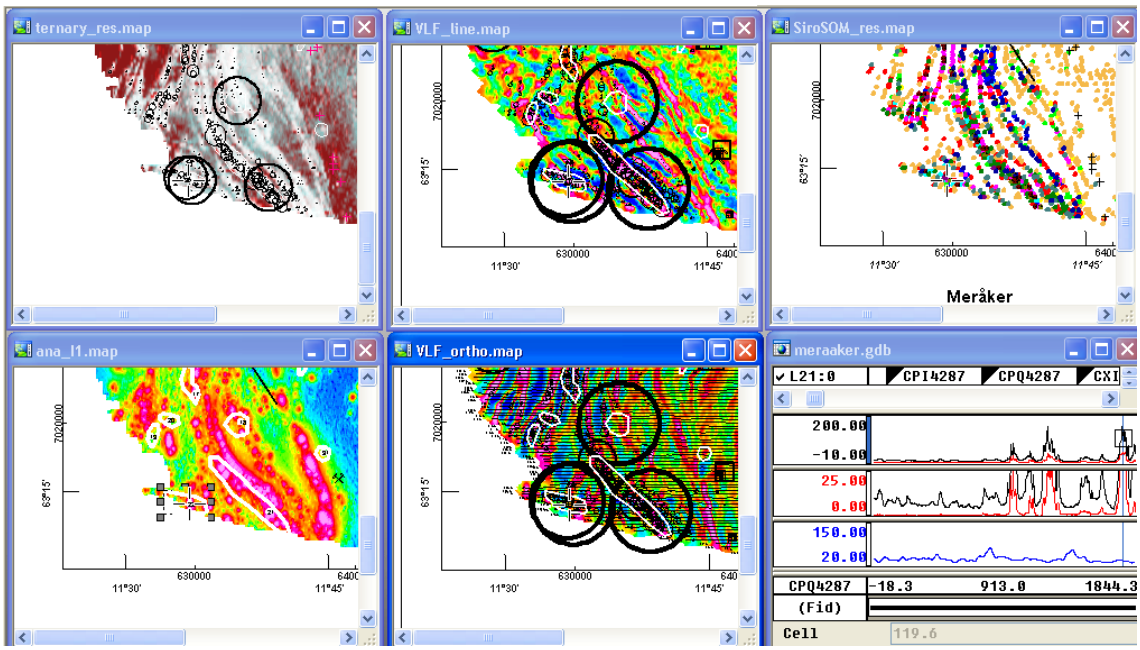
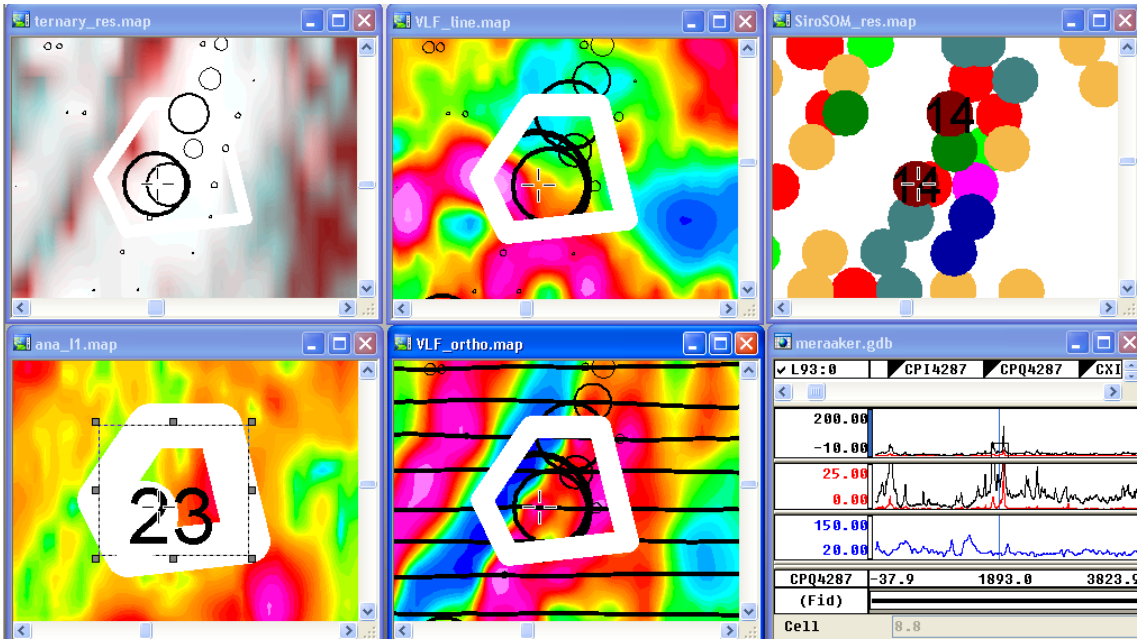


Figure 129. *Meråker target 22; high conductance; strong VLF; short wavelength magnetic anomalies; priority 1*

(a)



(b)

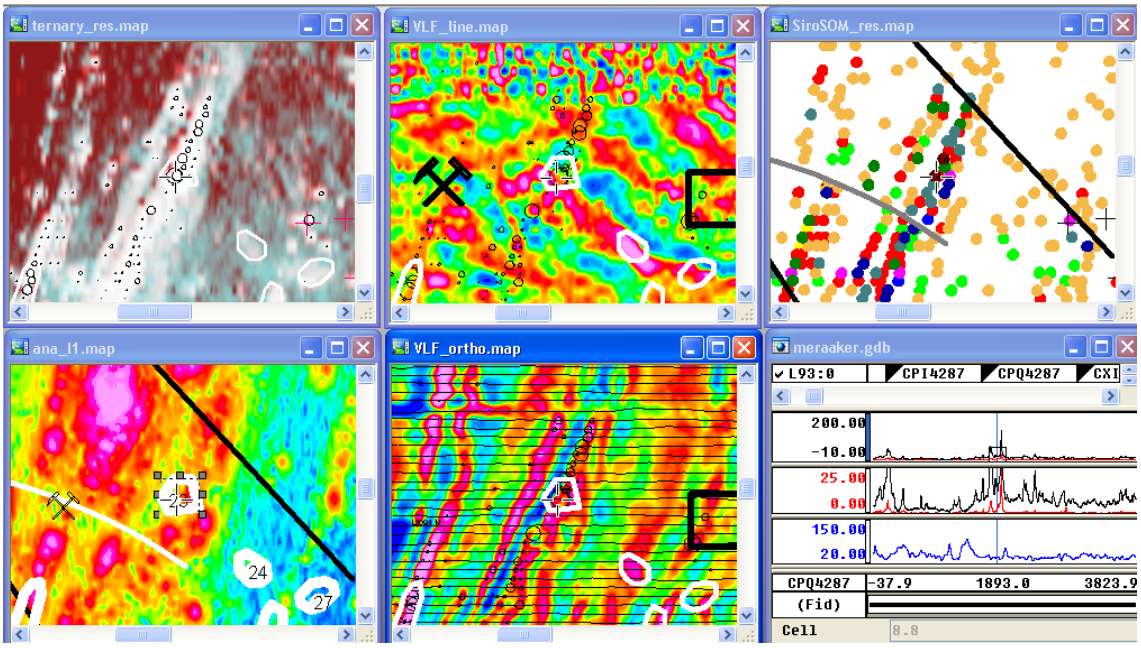
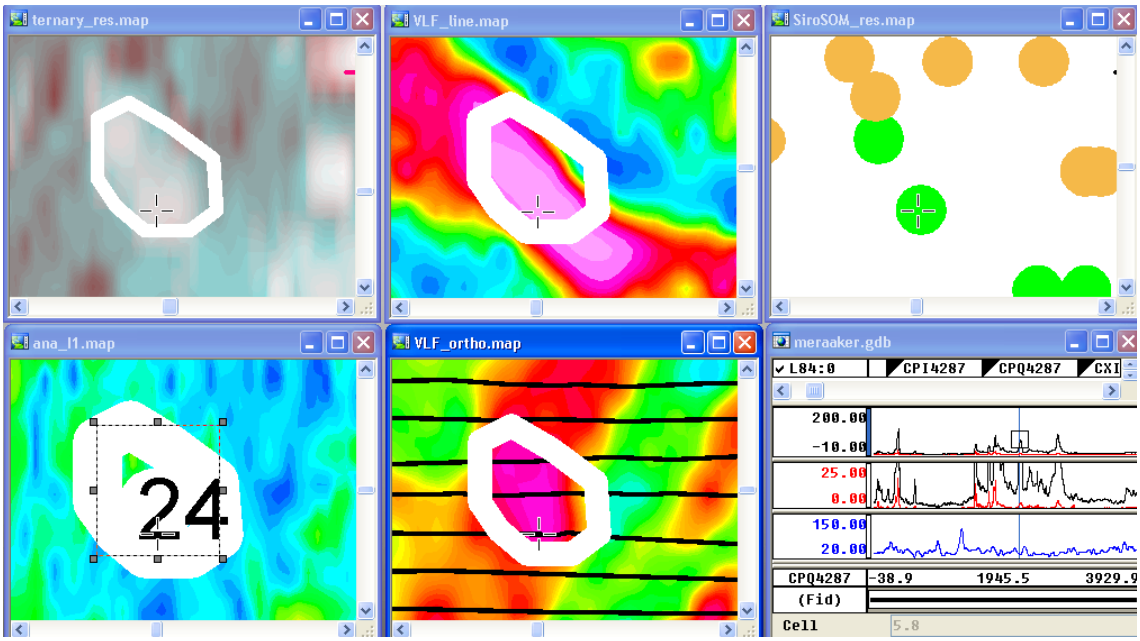


Figure 130. *Meråker target 23; group of medium conductance anomalies close to abandoned mine; clear VLF; short wavelength magnetic anomalies; priority 1*

(a)



(b)

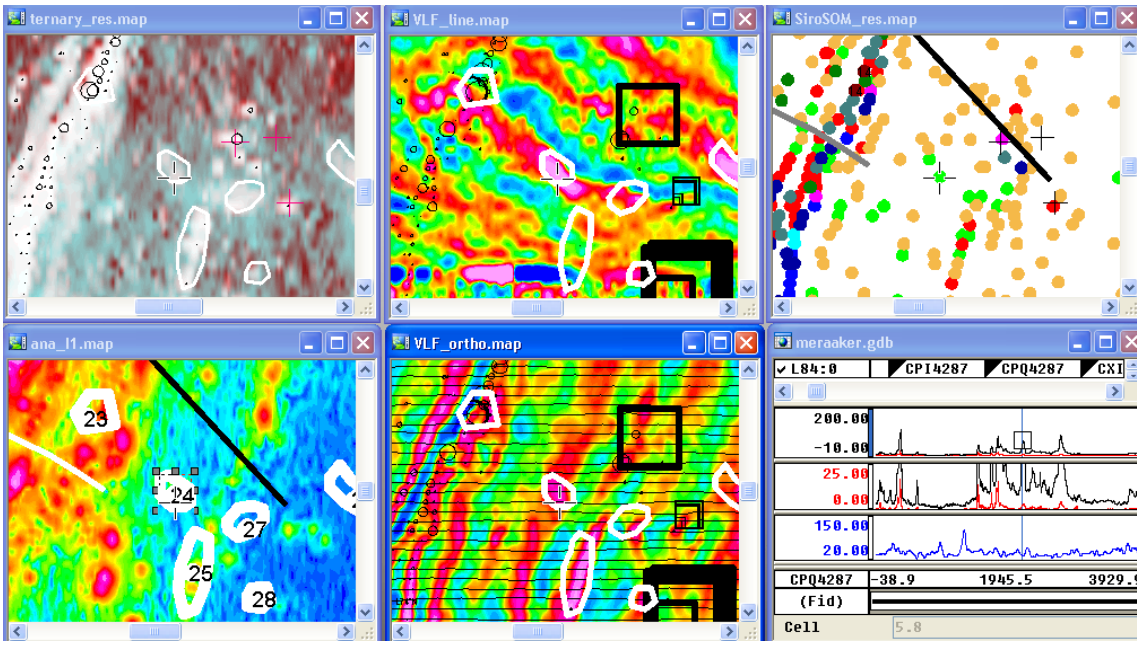
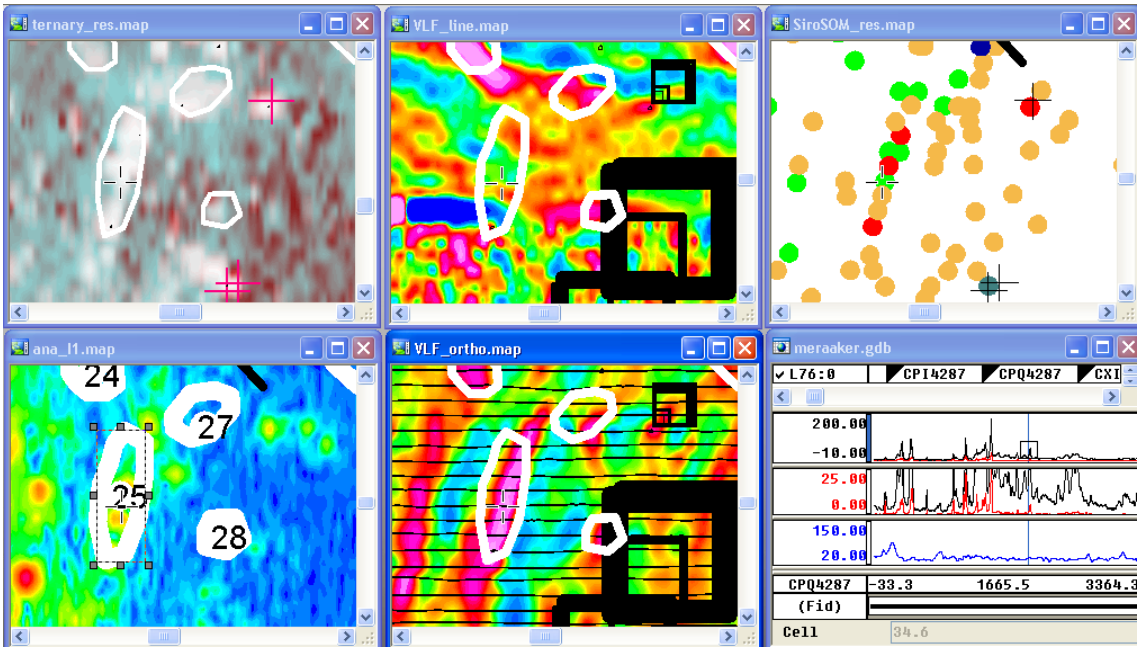


Figure 131. *Meråker target 24; low conductance; clear VLF; low magnetic anomalies; priority 4*

(a)



(b)

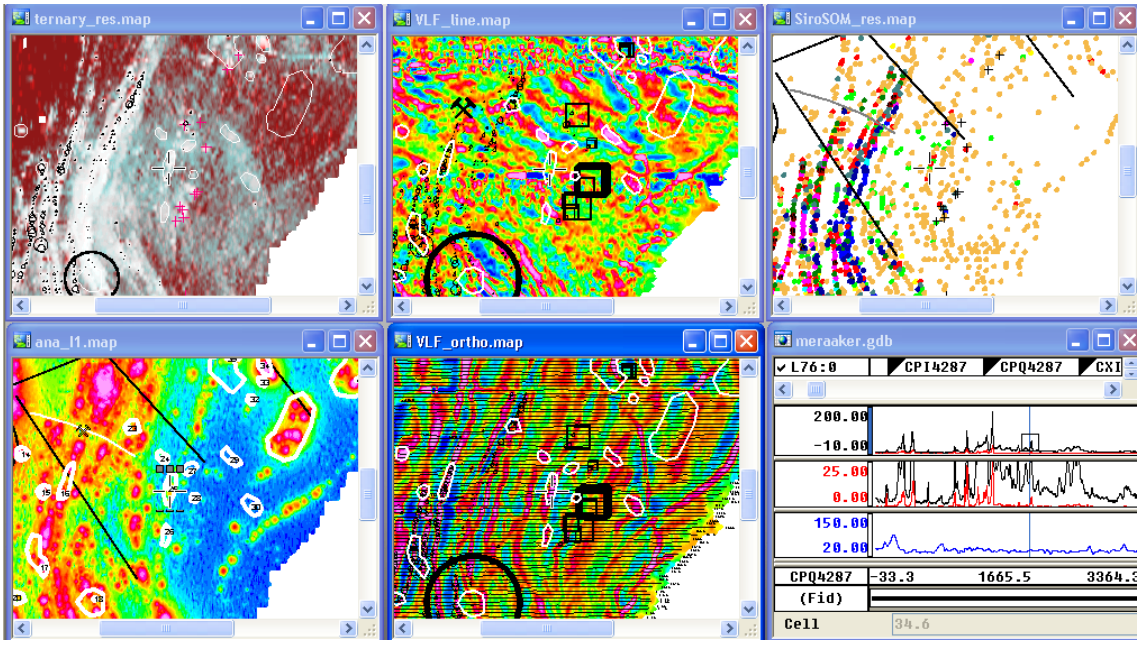
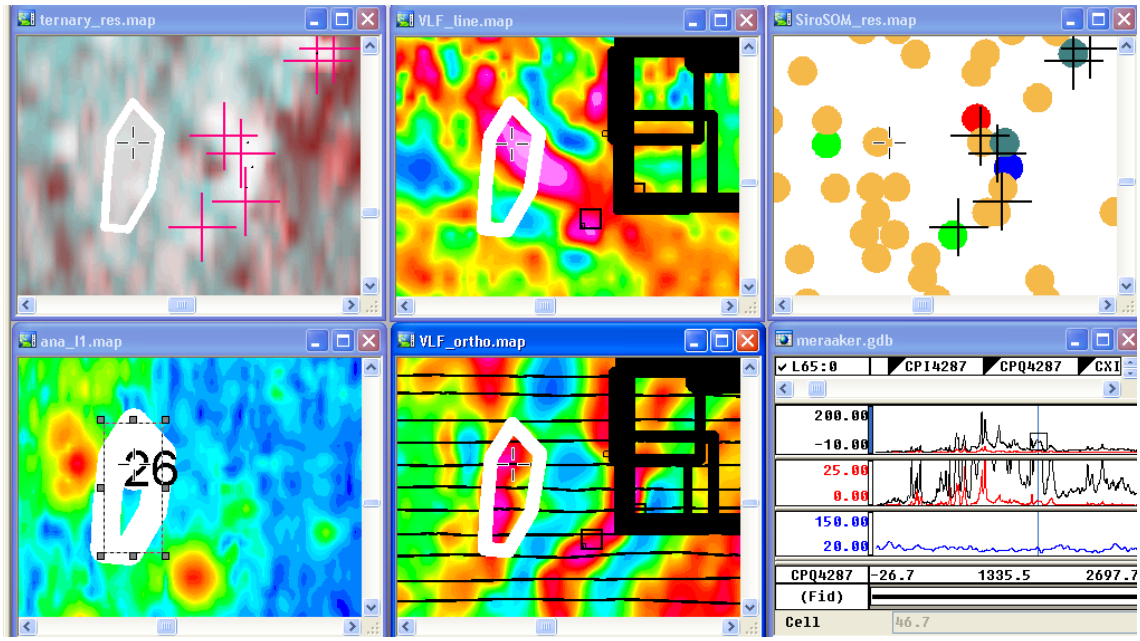


Figure 132. *Meråker target 25; low conductance; clear VLF; short wavelength magnetic anomalies; priority 5*

(a)



(b)

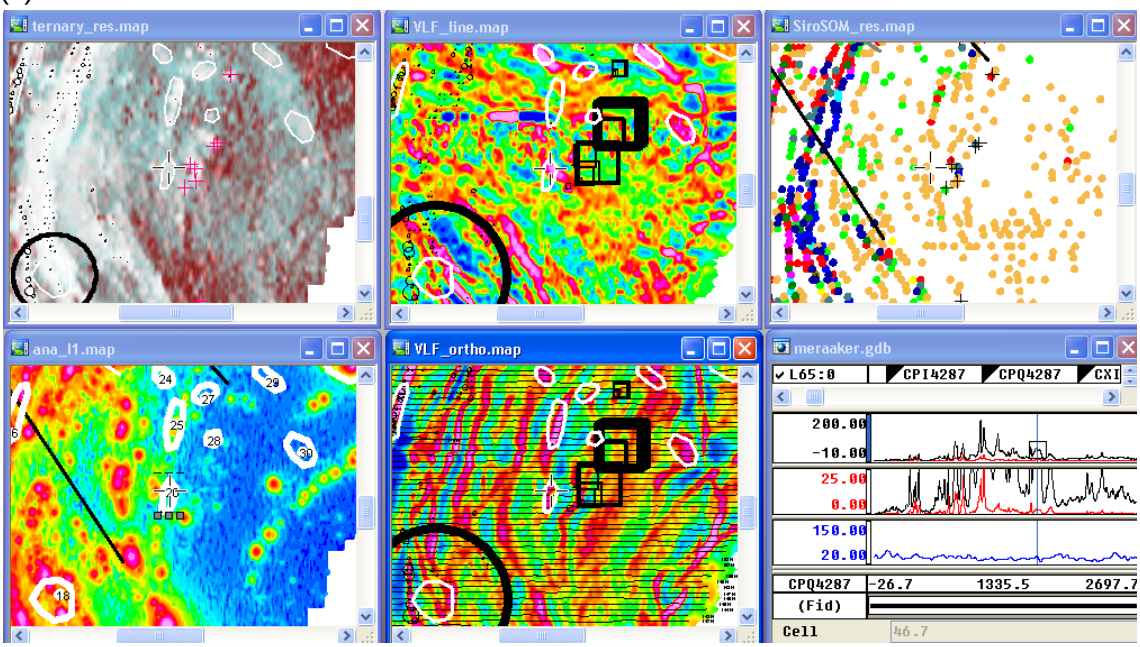
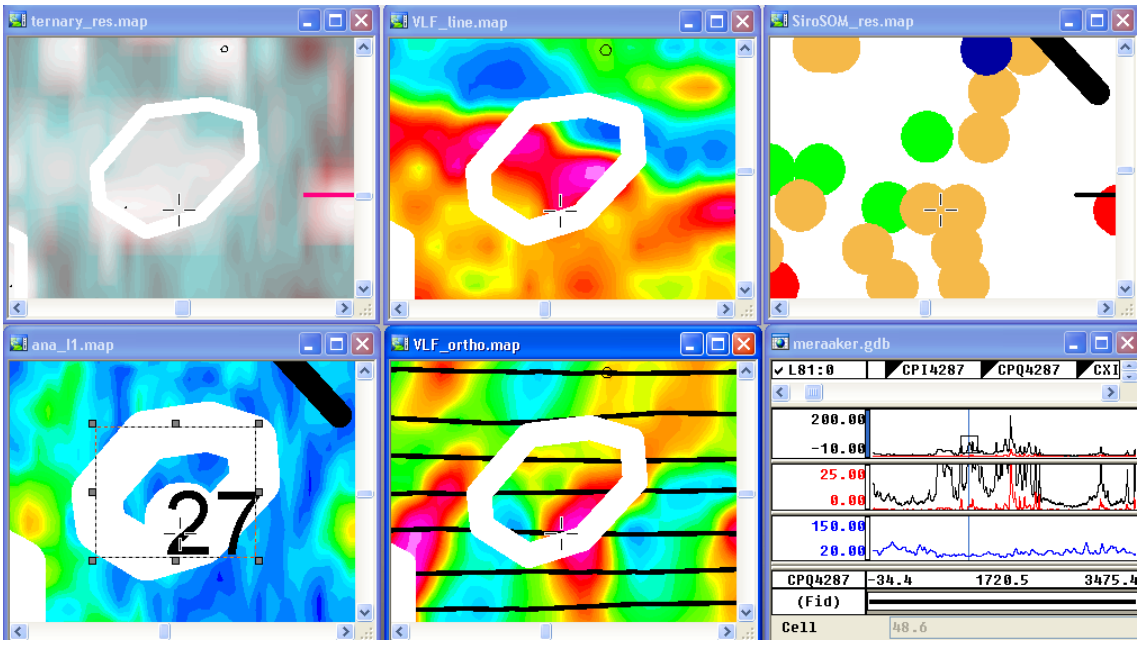


Figure 133. *Meråker target 26; low conductance; clear VLF; short wavelength magnetic anomalies; priority 5*

(a)



(b)

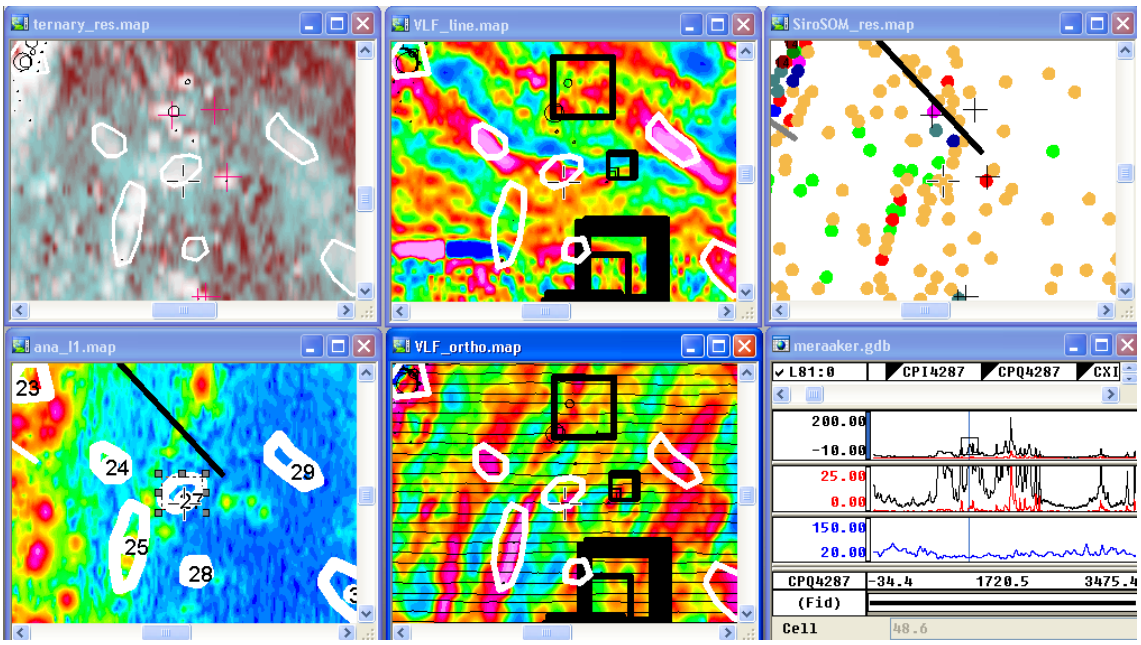
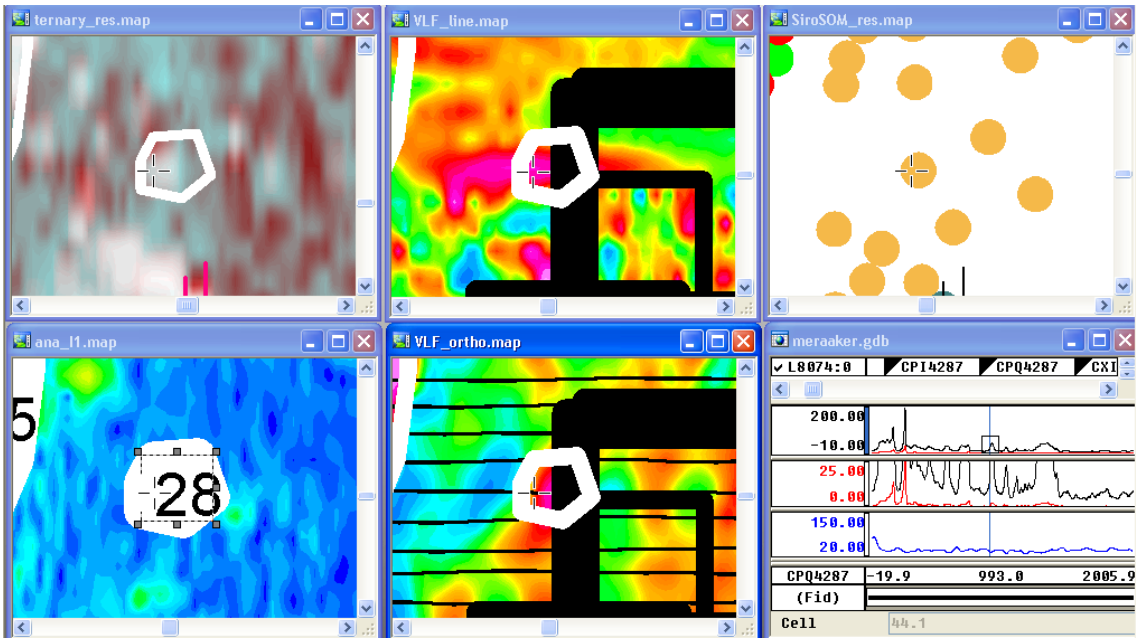


Figure 134. *Meråker target 27; low conductance; variable VLF; short wavelength magnetic anomalies; priority 5*

(a)



(b)

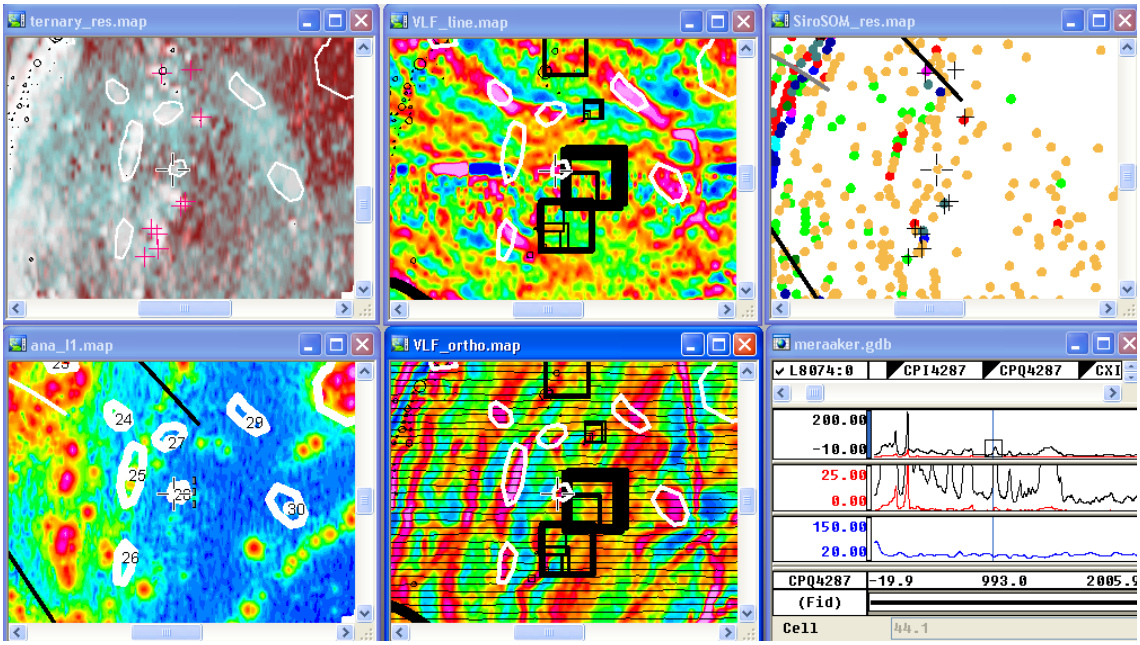
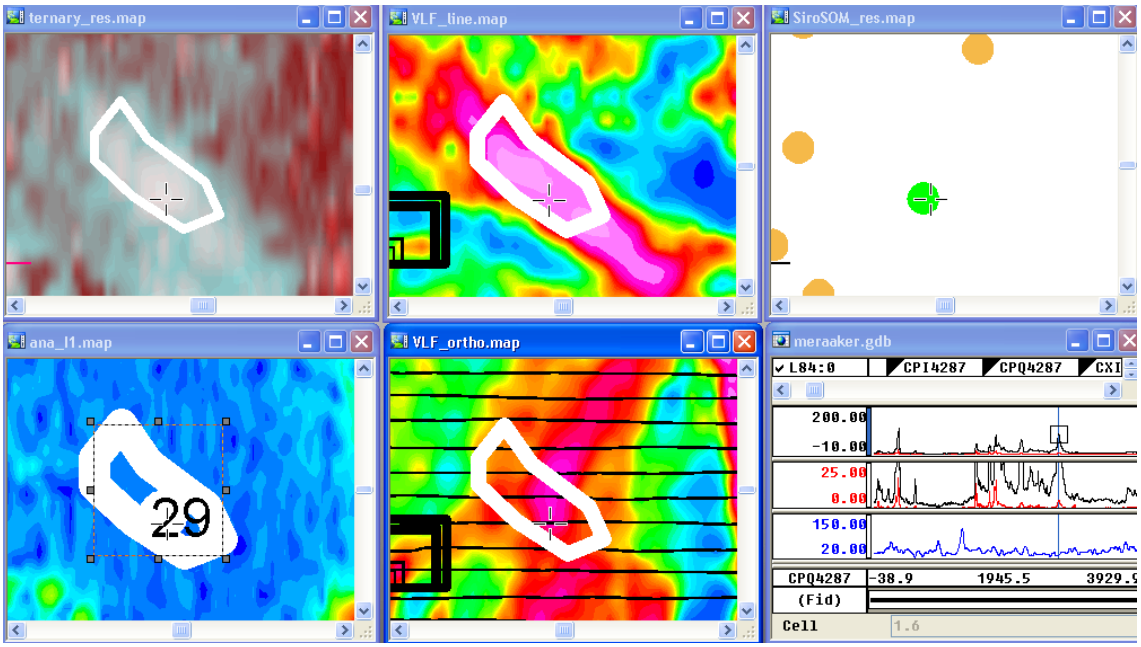


Figure 135. *Meråker target 28; low conductance; clear VLF; low magnetic anomalies; priority 5*

(a)



(b)

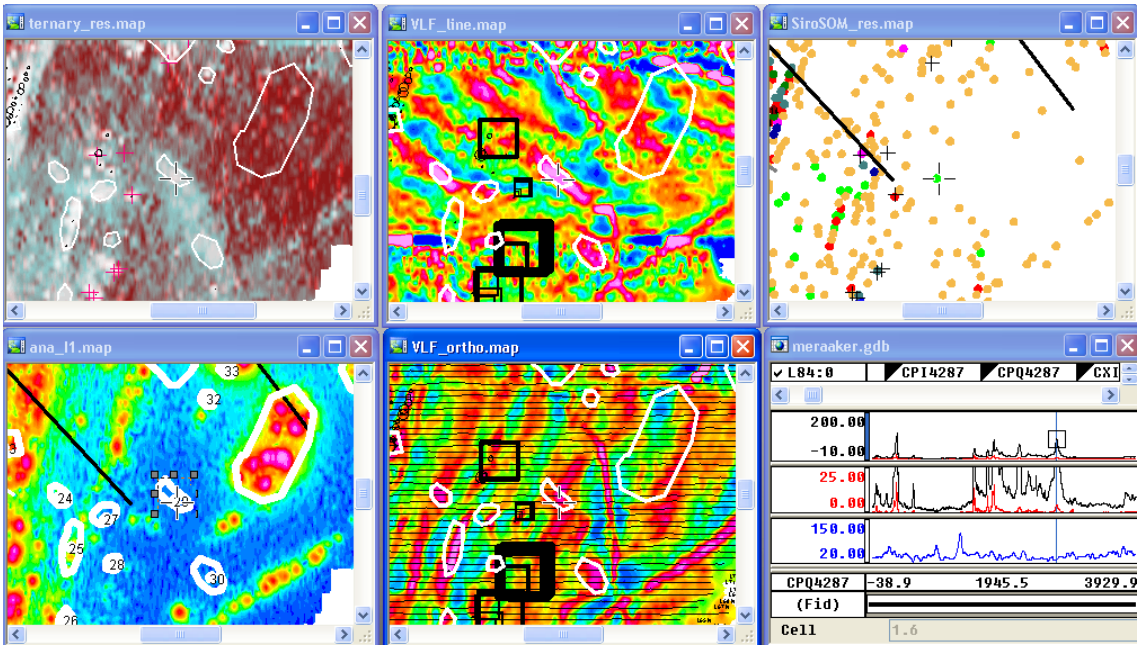
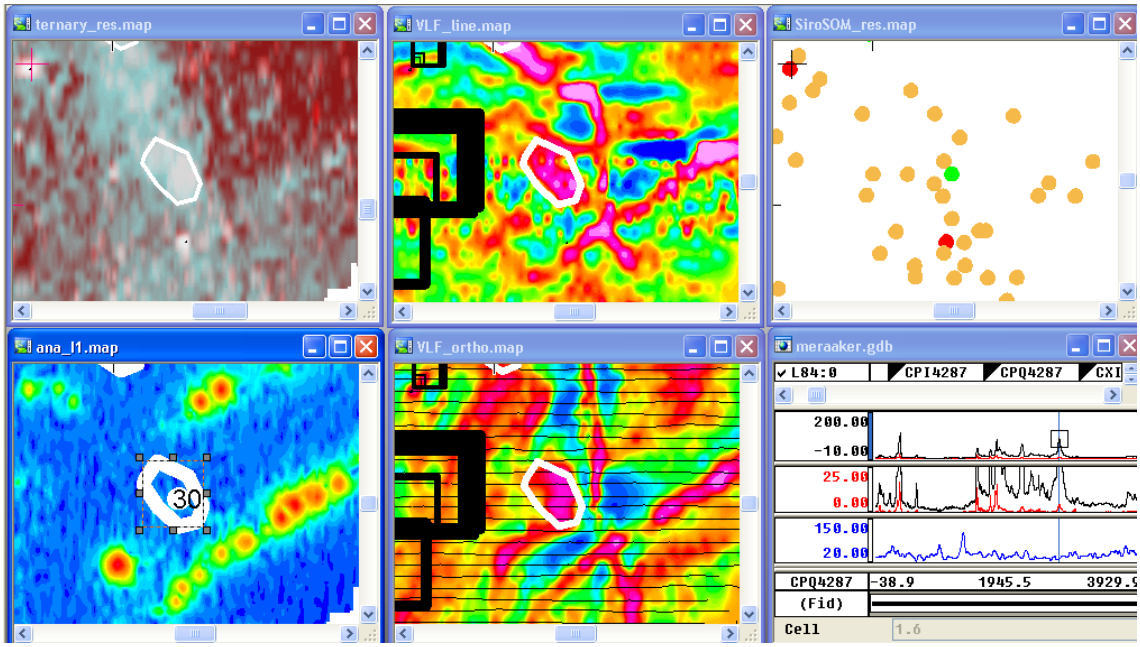


Figure 136. *Meråker target 29; low conductance; clear VLF; close to magnetic break line; priority 4*

(a)



(b)

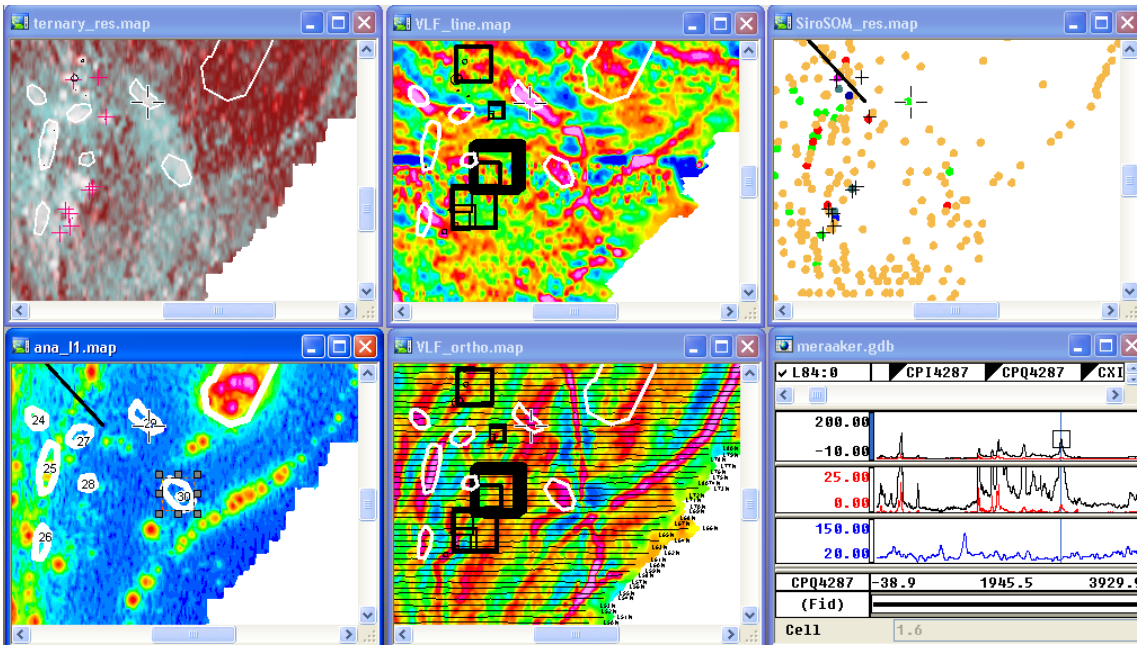
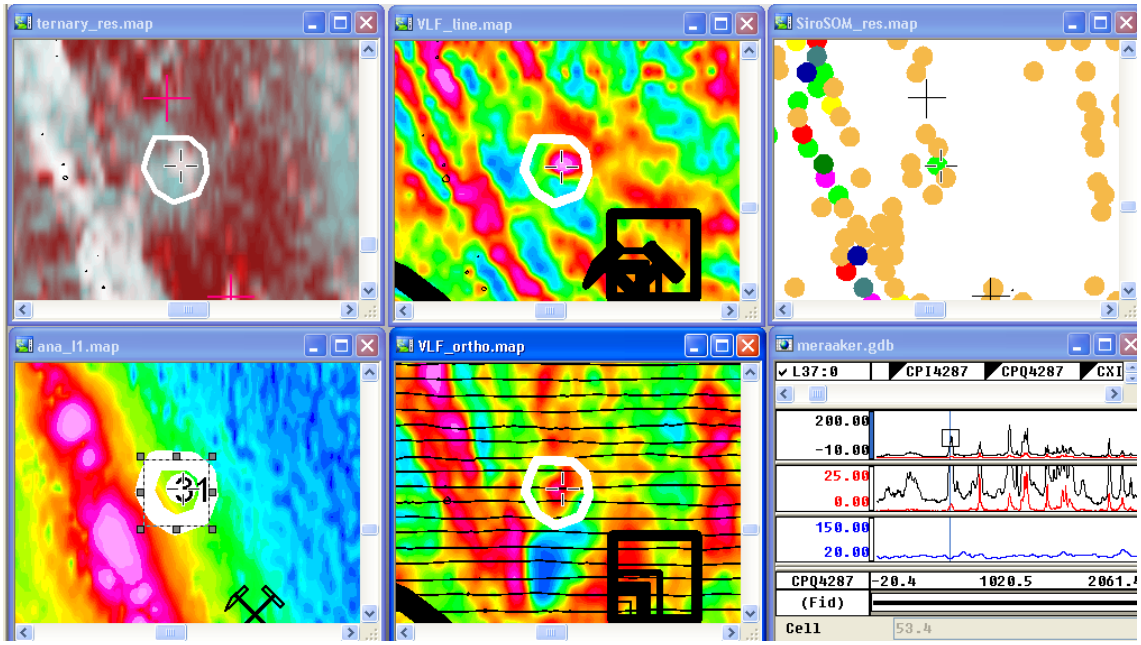


Figure 137. *Meråker target 30; low conductance; clear VLF; low magnetic field; priority 5*

(a)



(b)

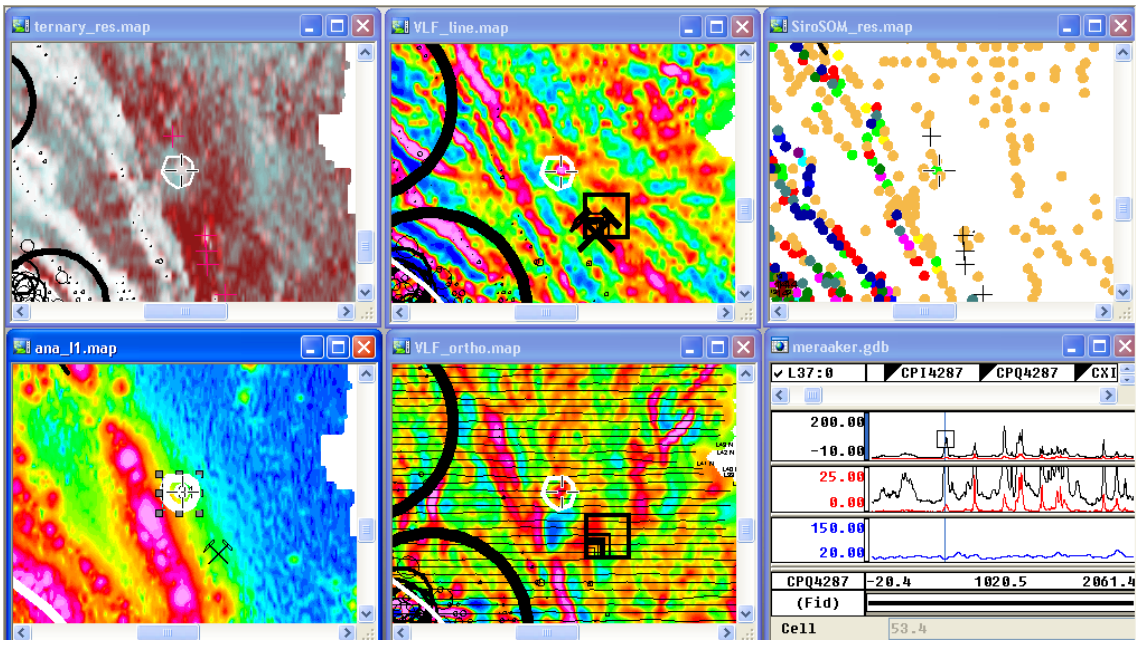
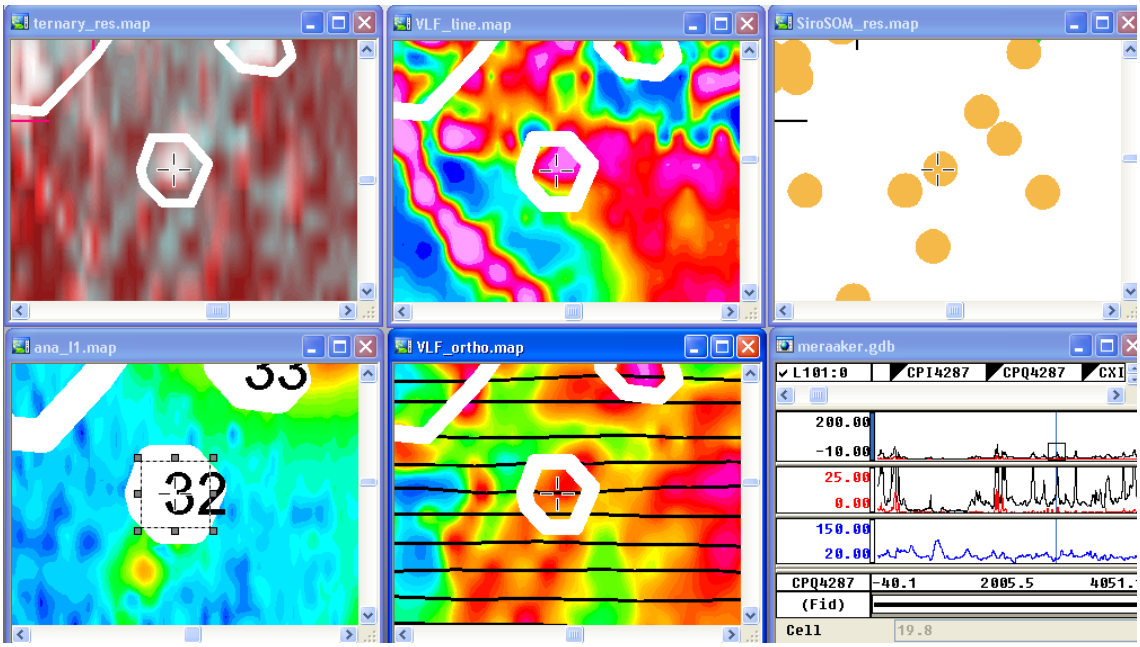


Figure 138. *Meråker target 31; low conductance at location close to abandoned mine – clear peak in 923 Hz quadrature response; clear VLF; same distance to magnetic anomaly as mine; priority 2*

(a)



(b)

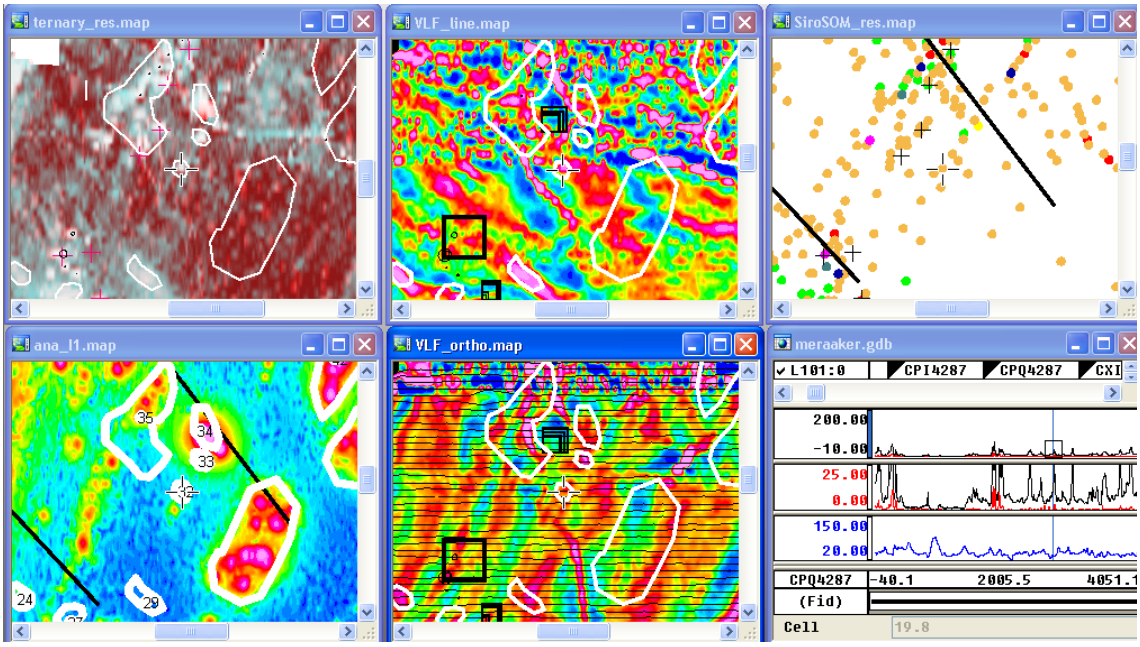
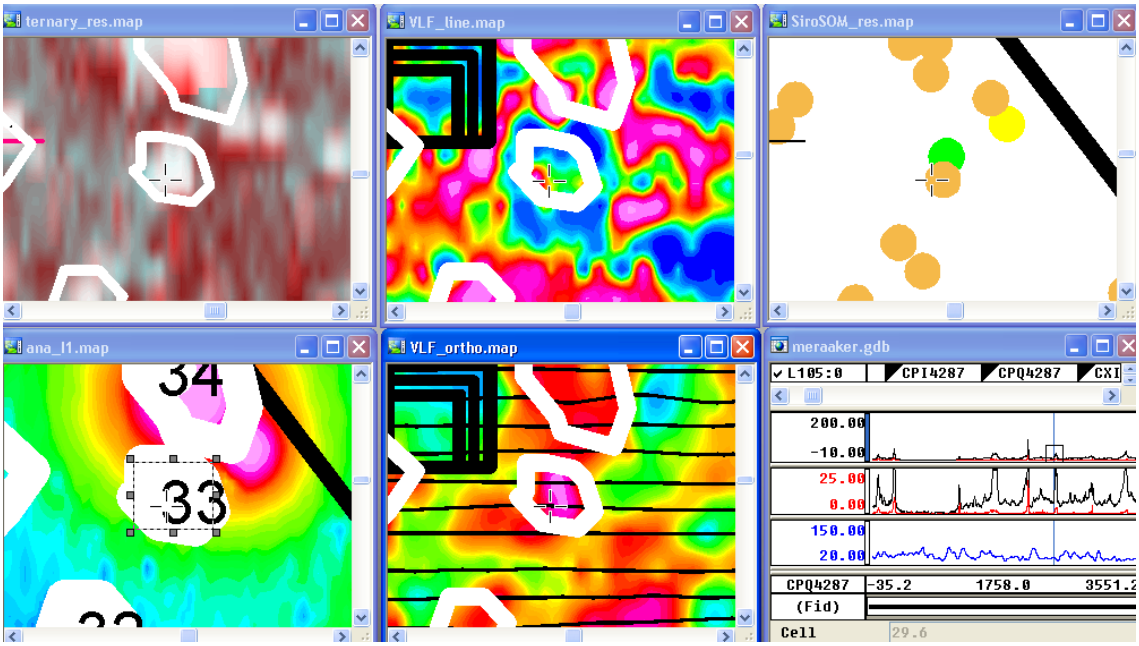


Figure 139. *Meråker target 32; scattered low conductance anomalies; variable VLF; short wavelength magnetic anomalies; priority 4*

(a)



(b)

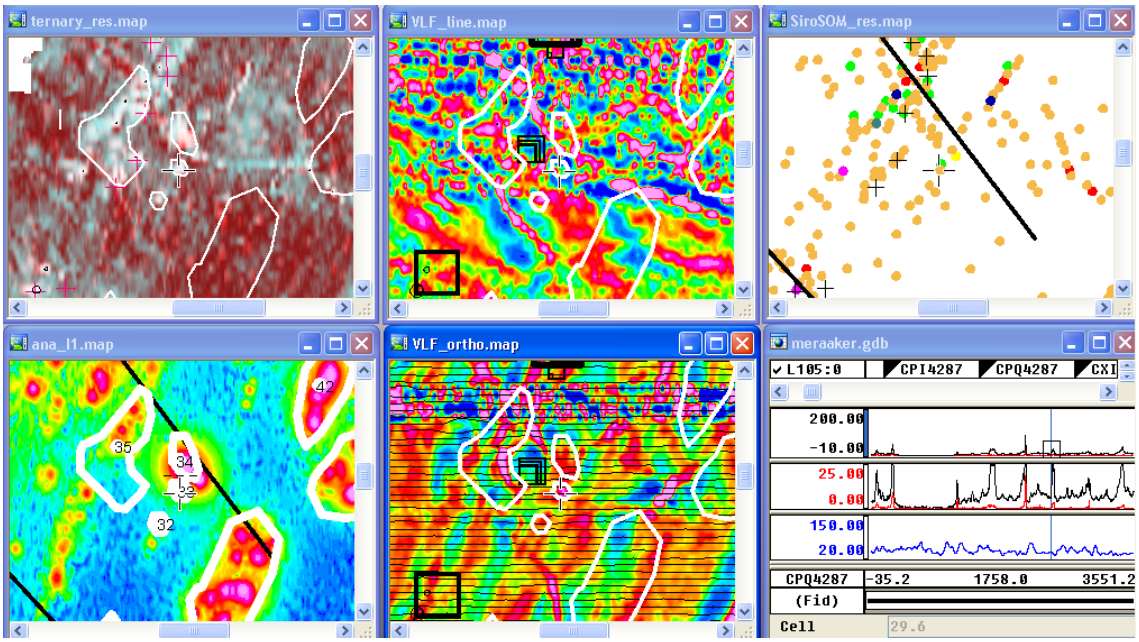
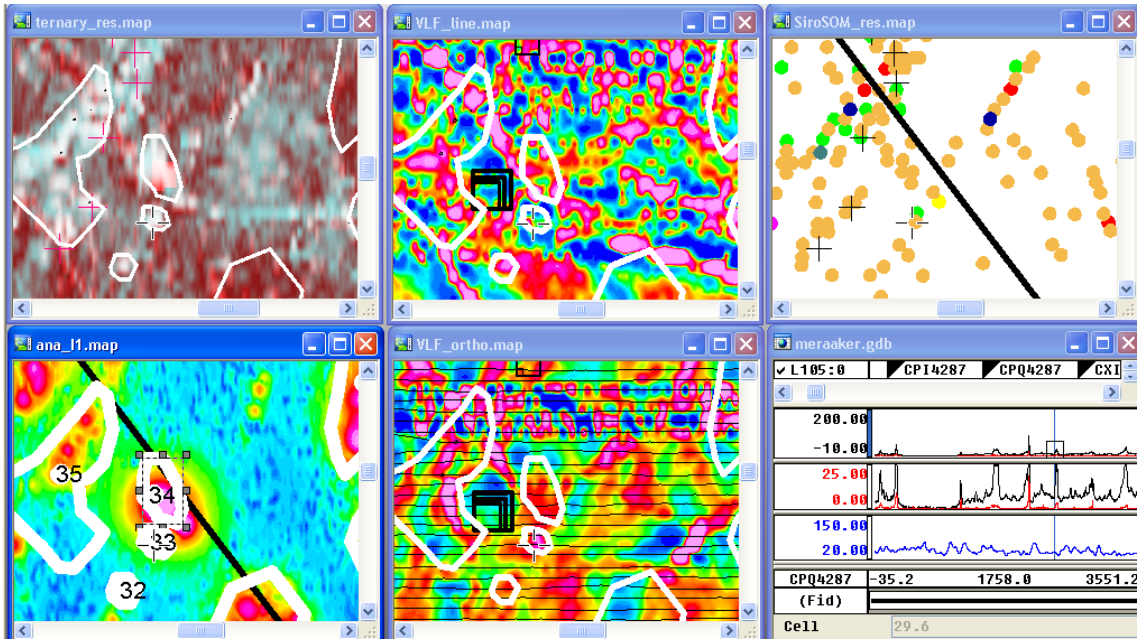


Figure 140. *Meråker target 33; low conductance; variable VLF; short wavelength magnetic anomalies close to magnetic break line; priority 4*

(a)



(b)

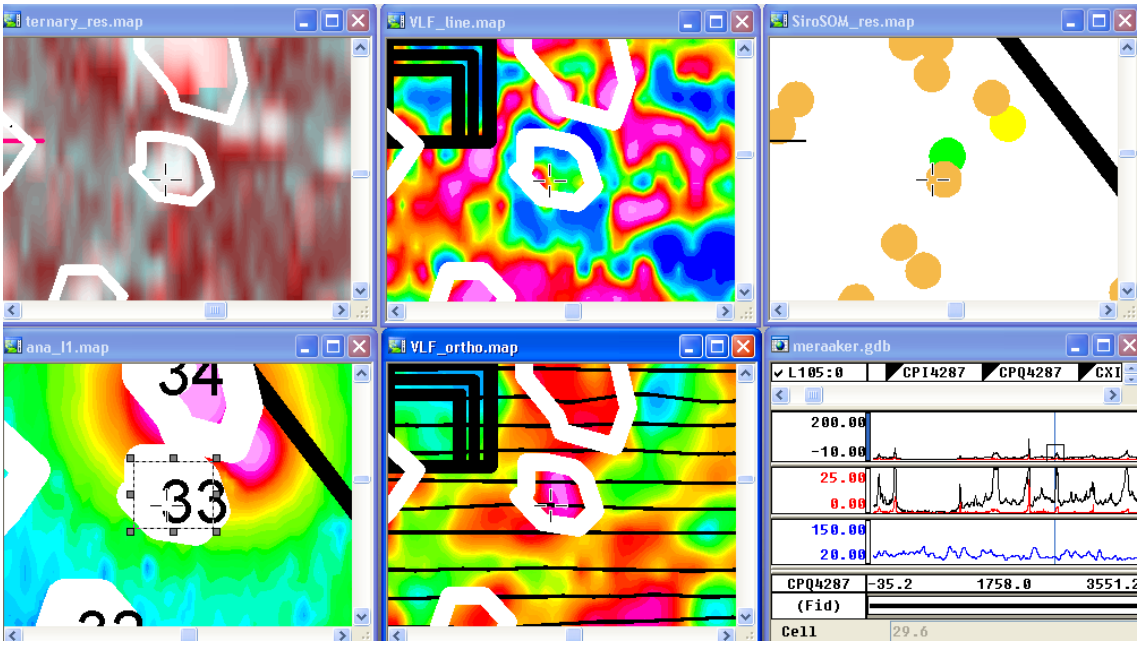
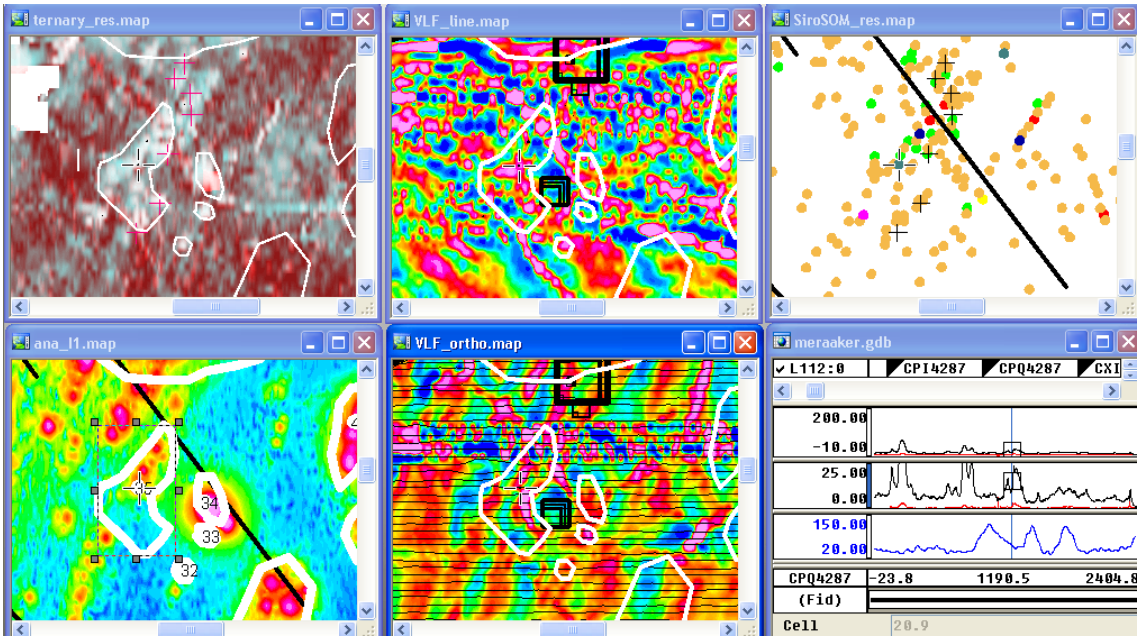


Figure 141. *Meråker target 34; low conductance; variable VLF; short wavelength magnetic anomalies; priority 5*

(a)



(b)

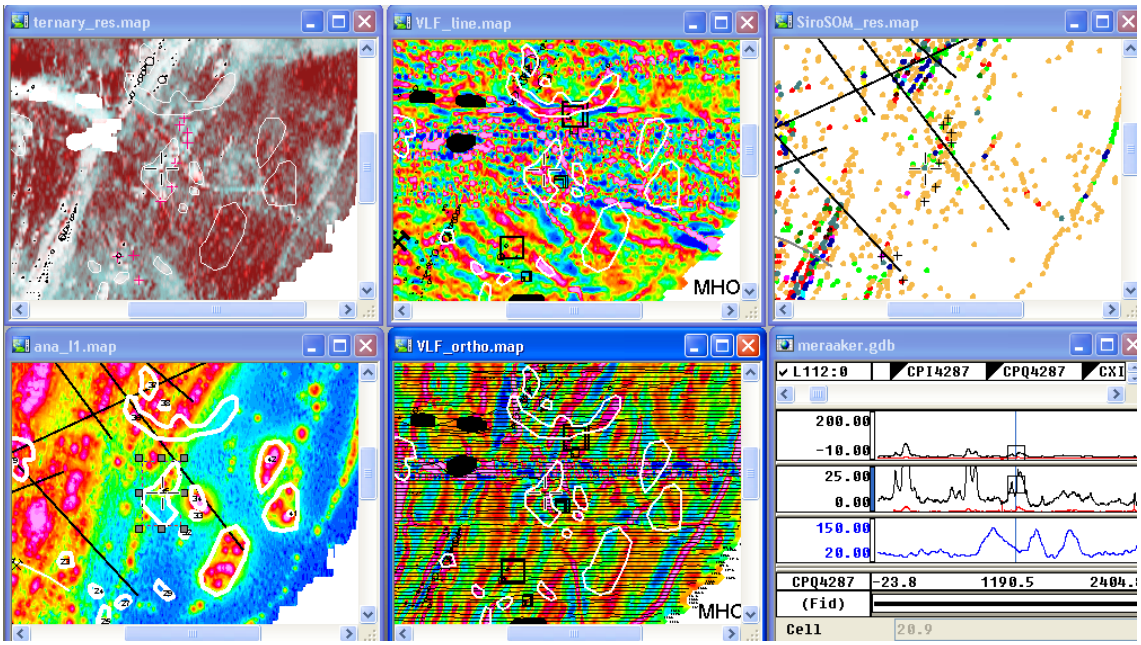
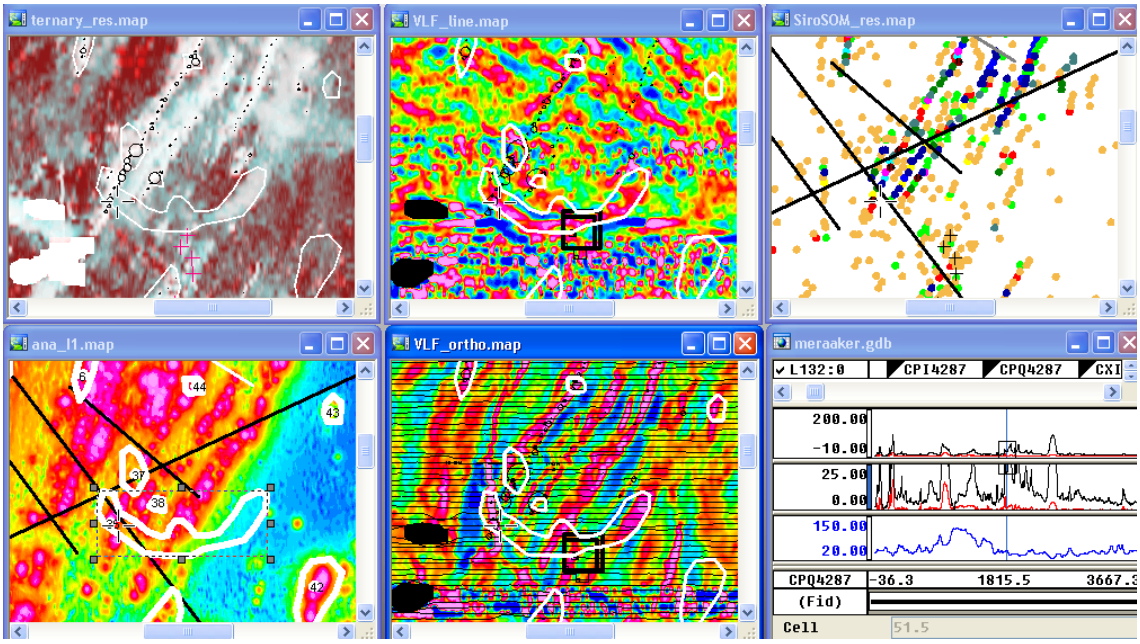


Figure 142. *Meråker target 35; low conductance; variable VLF; short wavelength magnetic anomalies; priority 5*

(a)



(b)

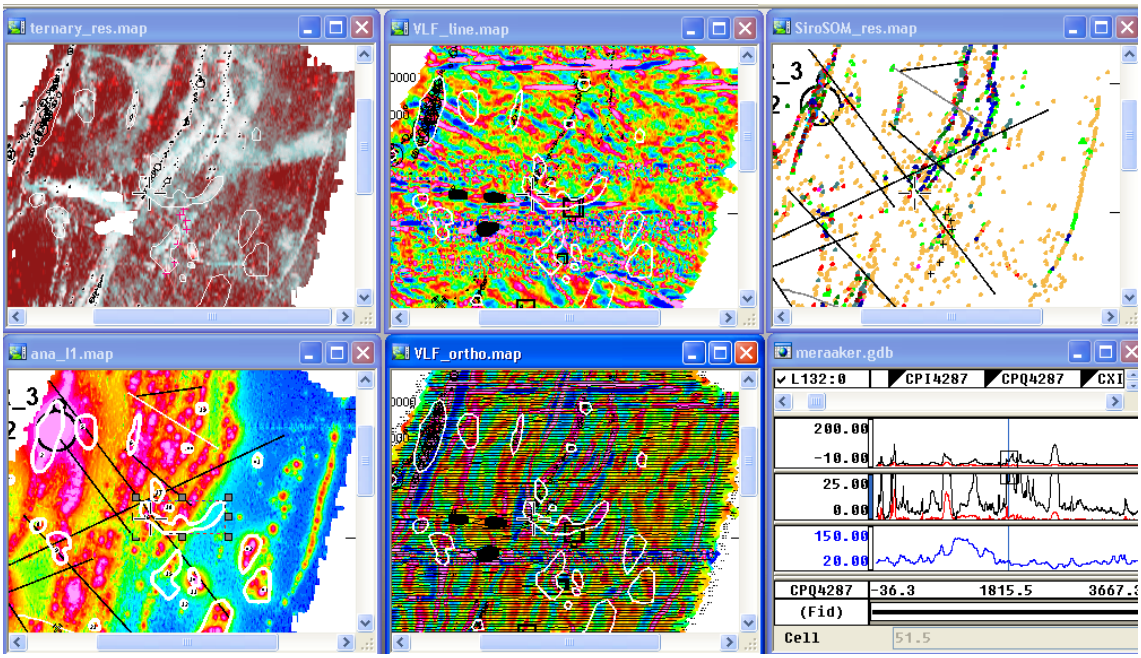
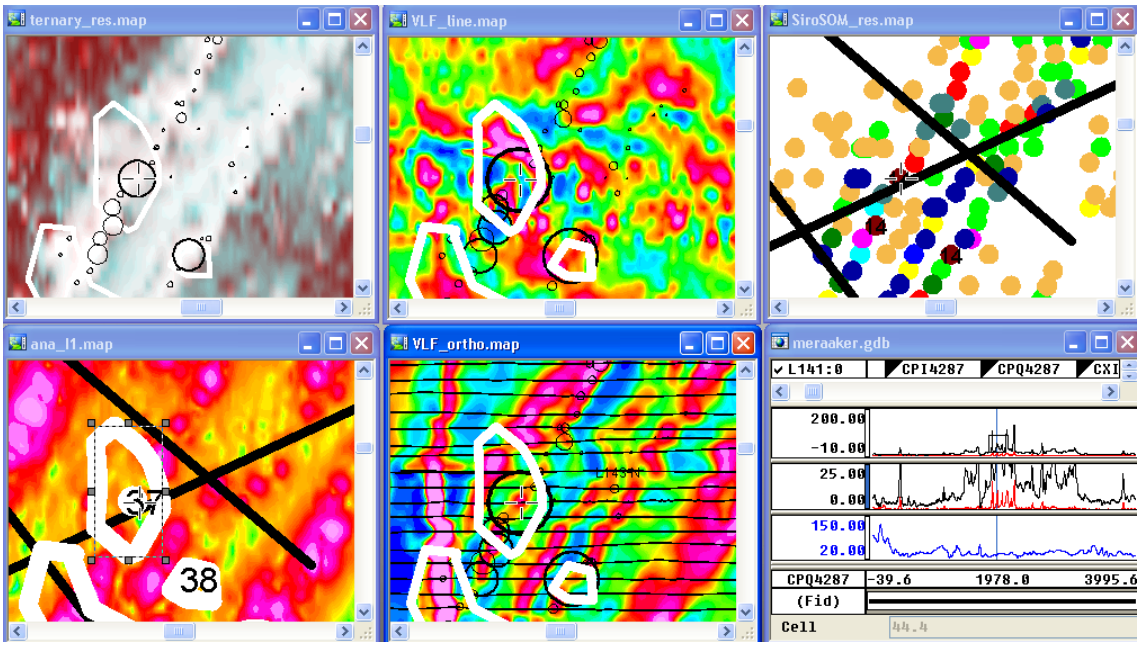


Figure 143. *Meråker target 36; medium (west) to low conductance; variable VLF; short wavelength magnetic anomalies; priority 4*

(a)



(b)

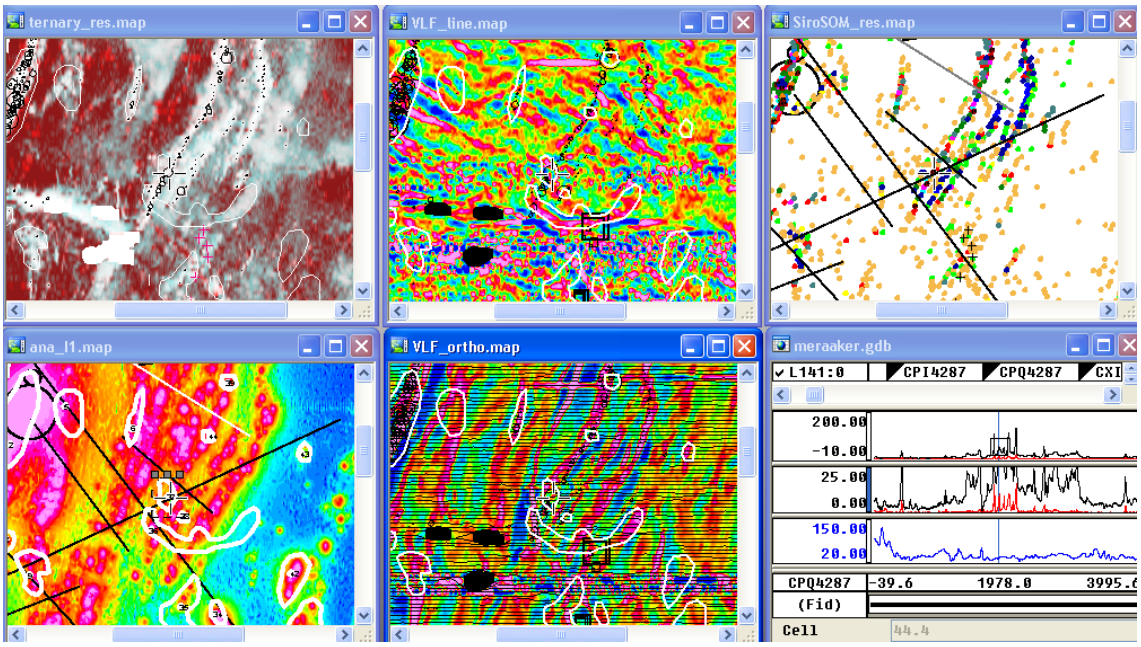
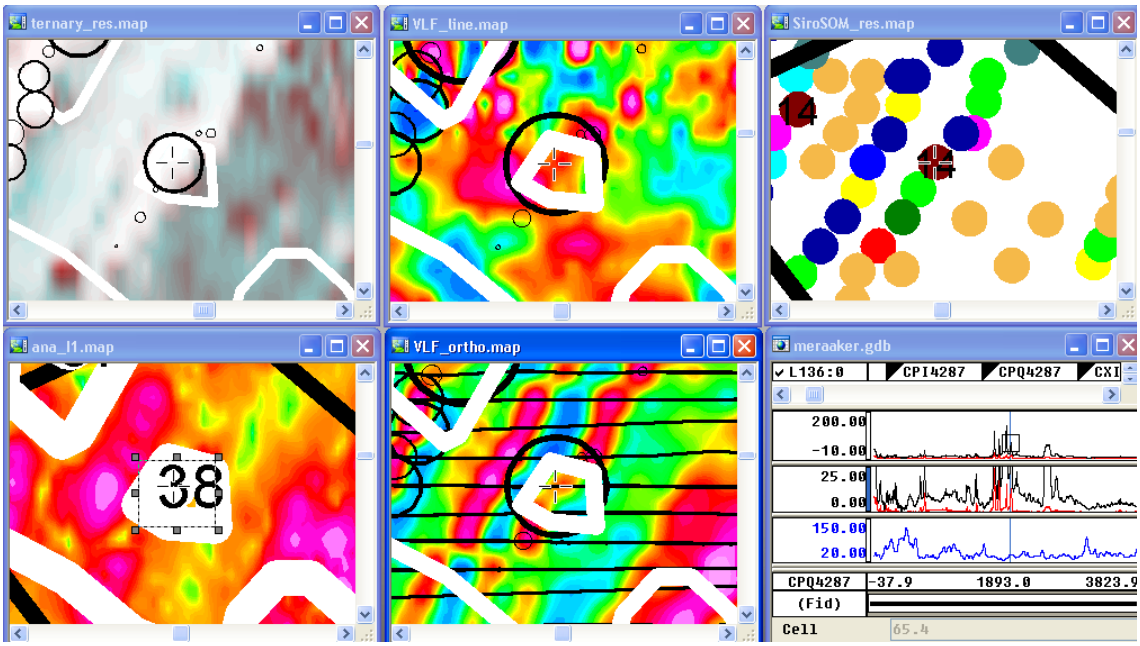


Figure 144. *Meråker target 37; several medium to low conductance anomalies; variable VLF; short wavelength magnetic anomalies and close to magnetic break line; priority 2*

(a)



(b)

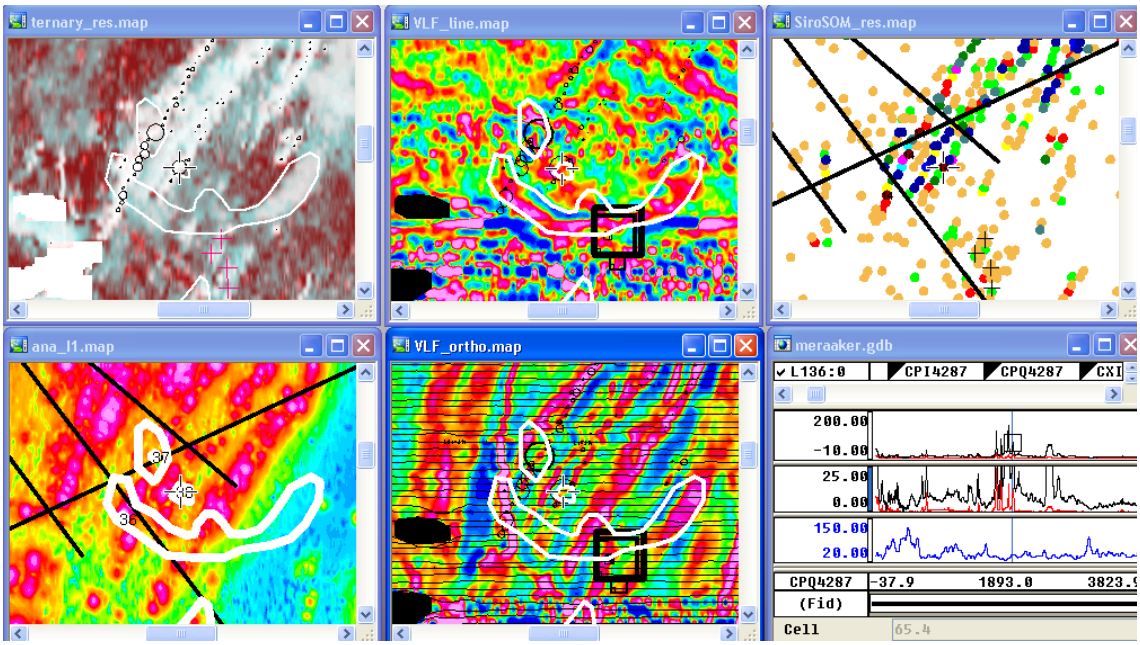
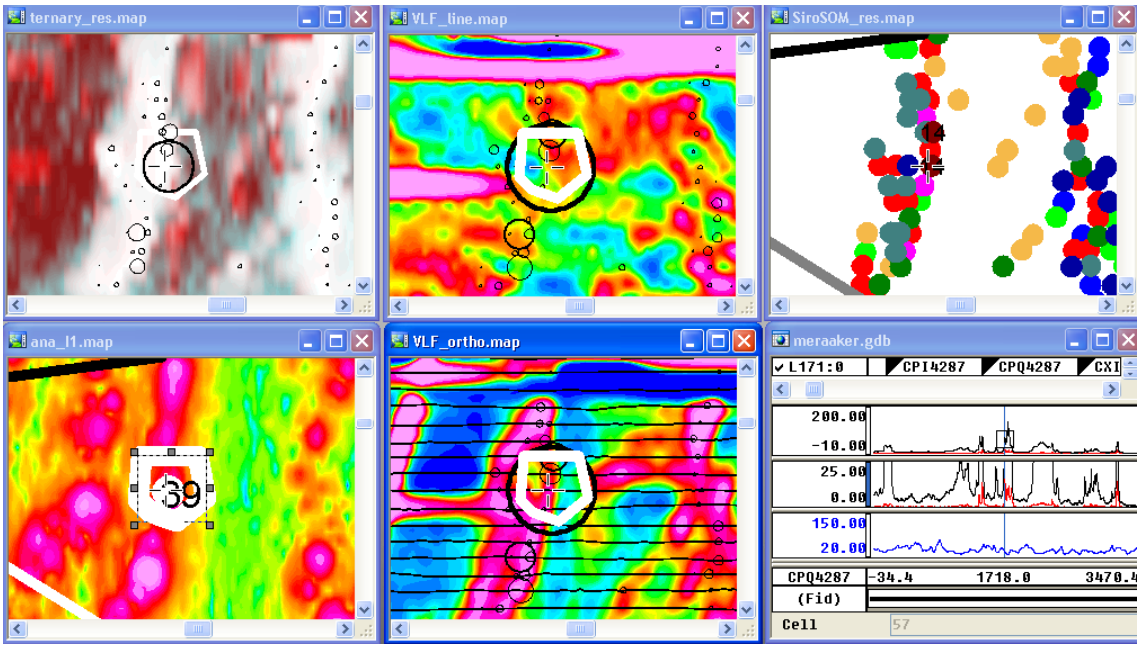


Figure 145. *Meråker target 38; high conductance; clear VLF; short wavelength magnetic anomalies; priority 2*

(a)



(b)

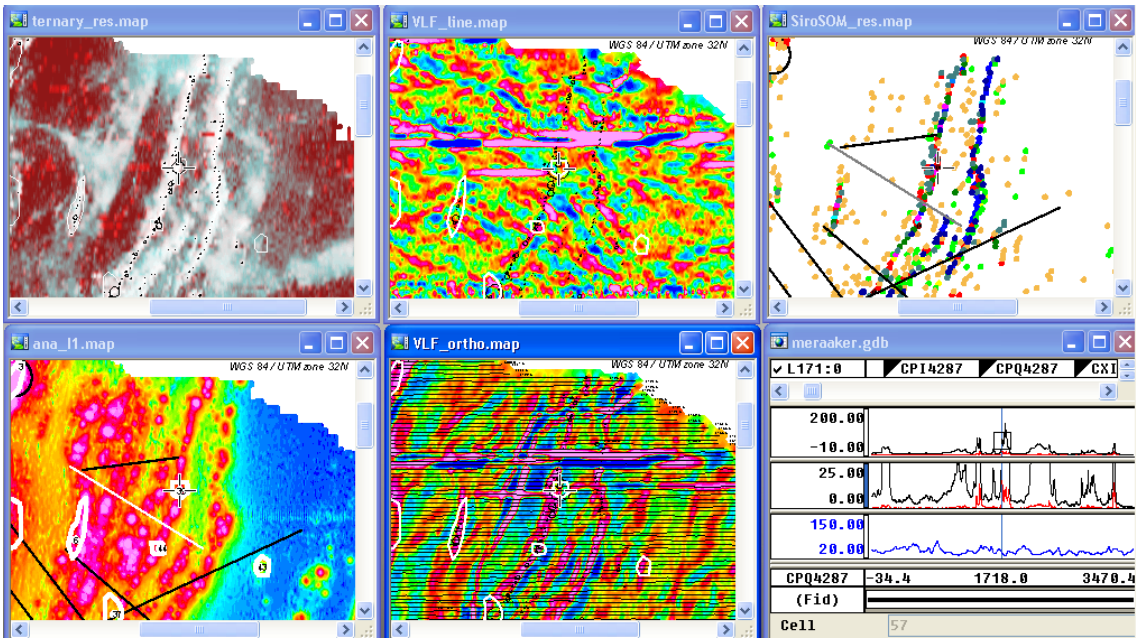
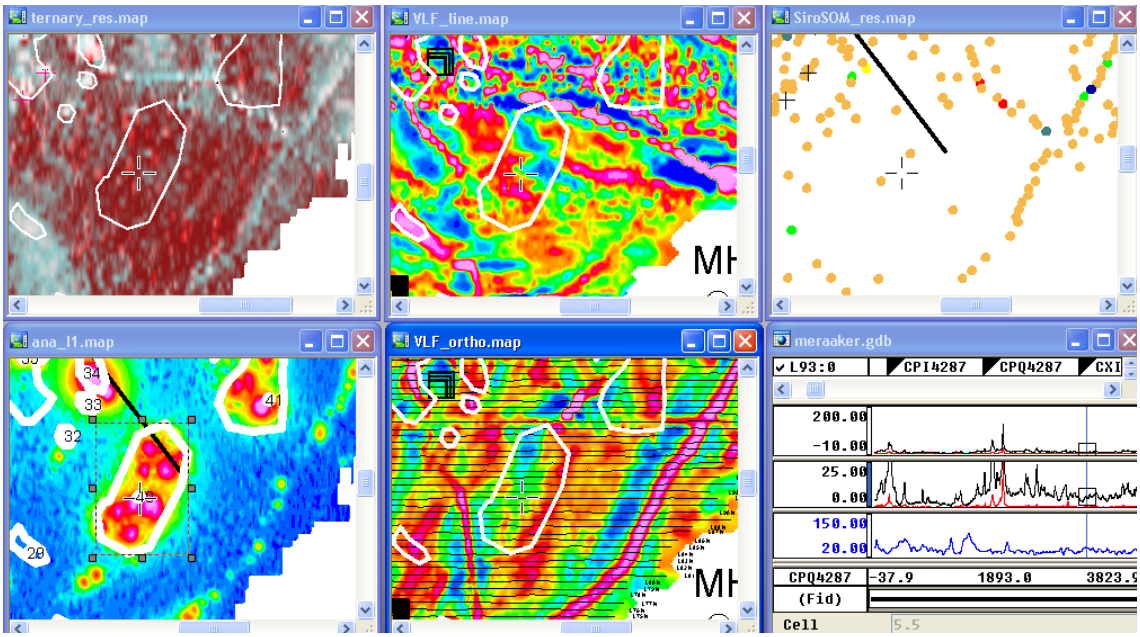


Figure 146. *Meråker target 39; medium conductance; variable VLF; short wavelength magnetic anomalies; priority 3*

(a)



(b)

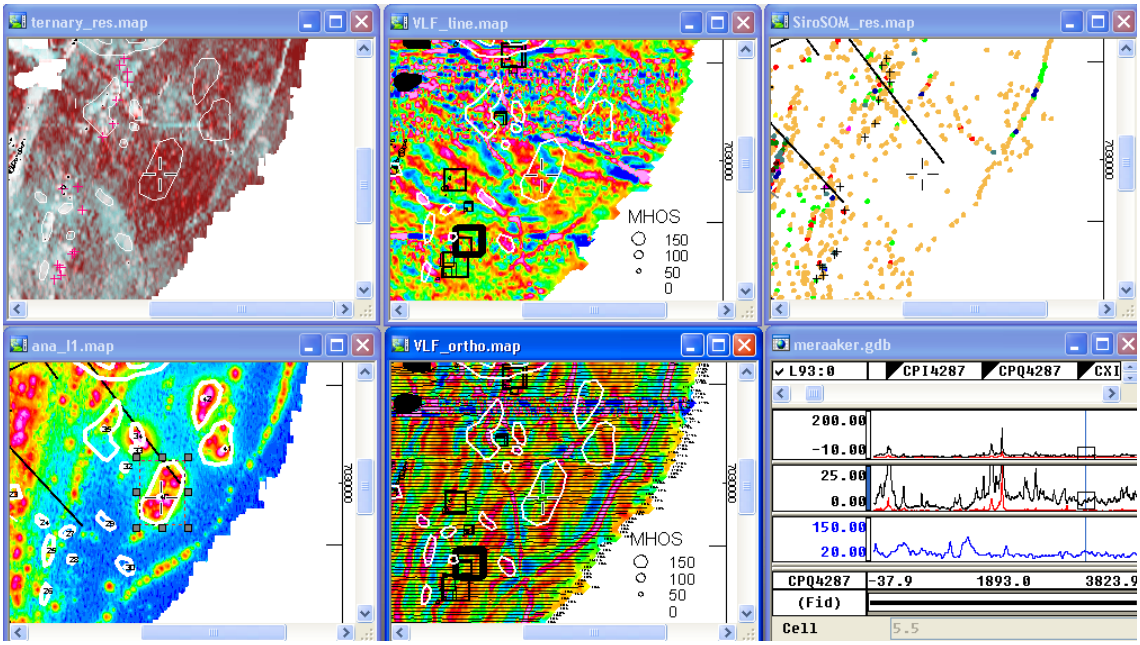
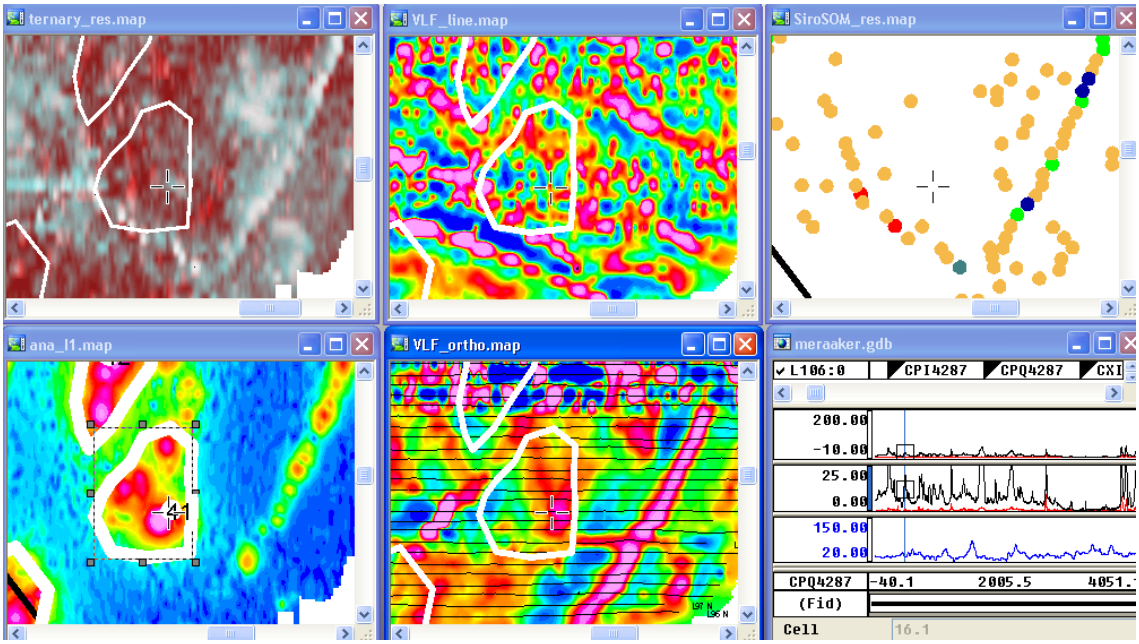


Figure 147. *Meråker target 40; low conductance; variable VLF; several short wavelength magnetic anomalies and magnetic break line; priority 3*

(a)



(b)

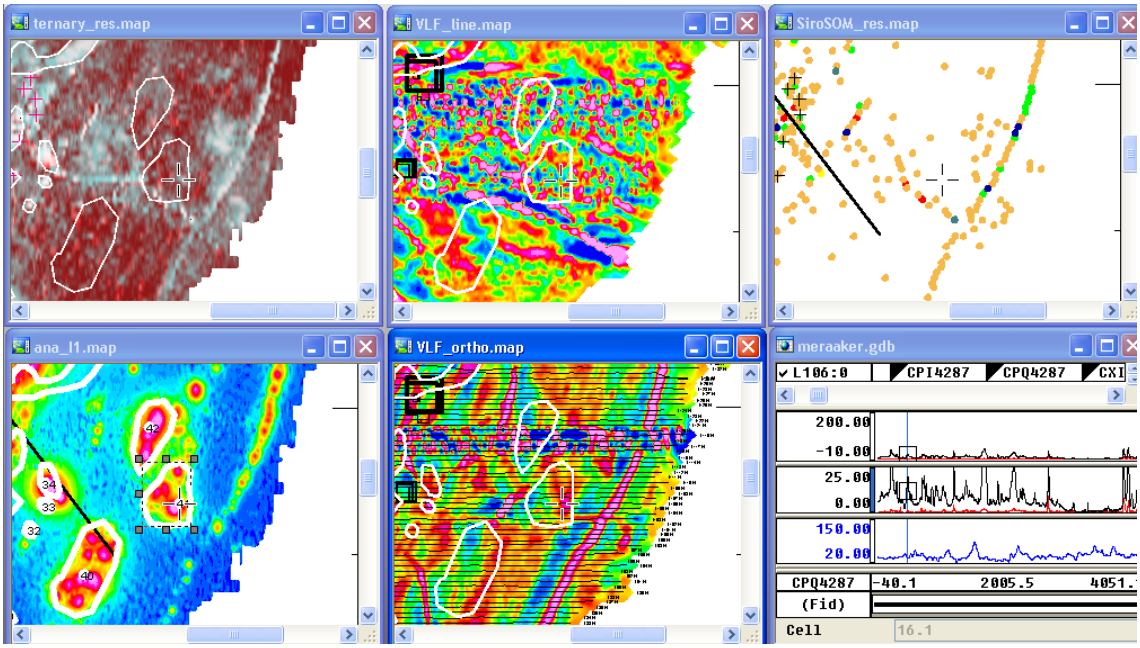
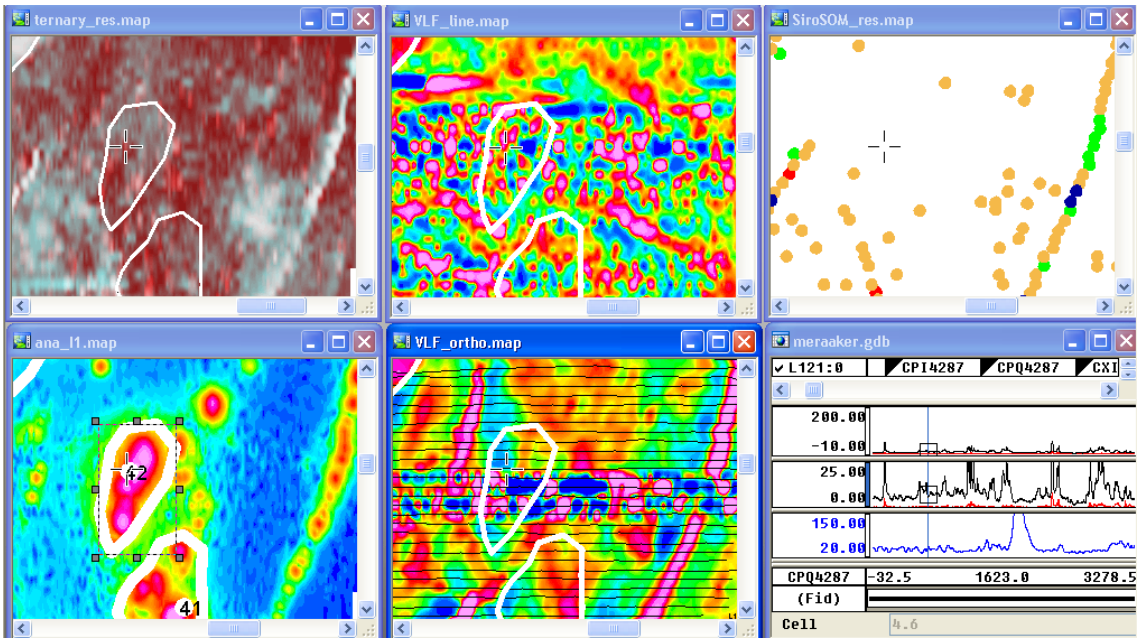


Figure 148. *Meråker target 41; low conductance; variable VLF; several short wavelength magnetic anomalies; priority 4*

(a)



(b)

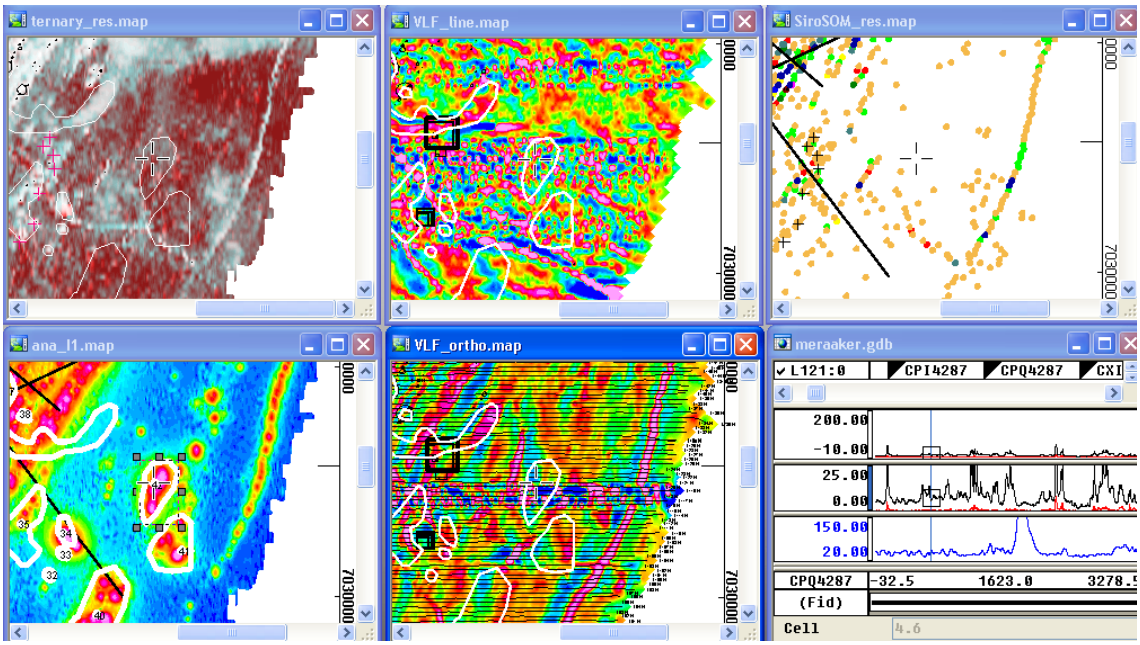
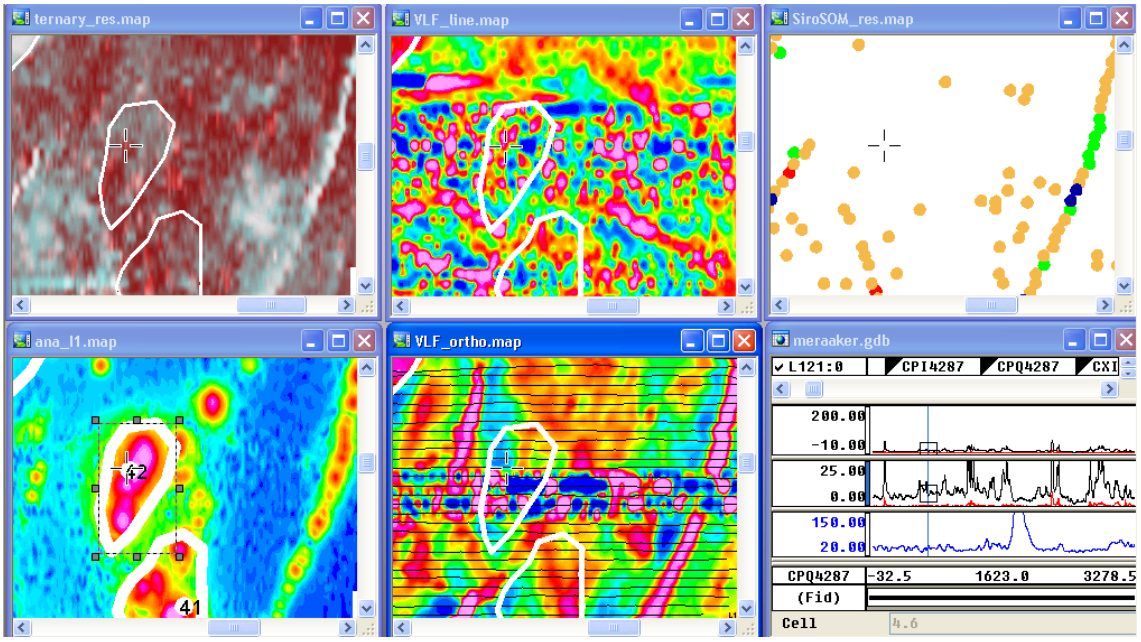


Figure 149. *Meråker target 42; low conductance; noisy VLF; several short wavelength magnetic anomalies; priority 4*

(a)



(b)

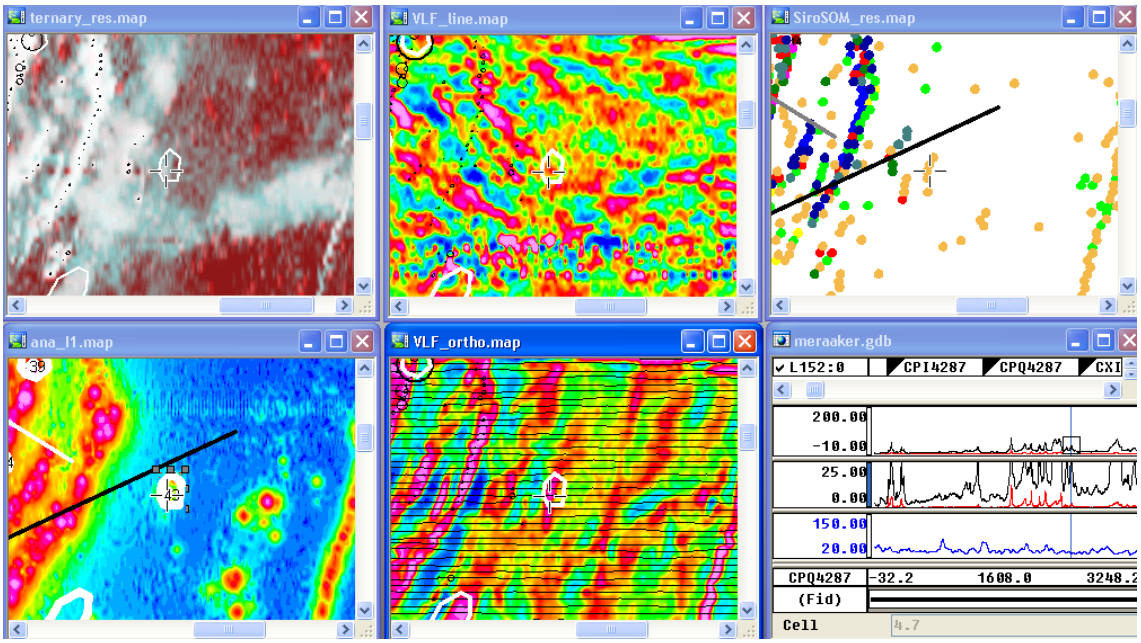
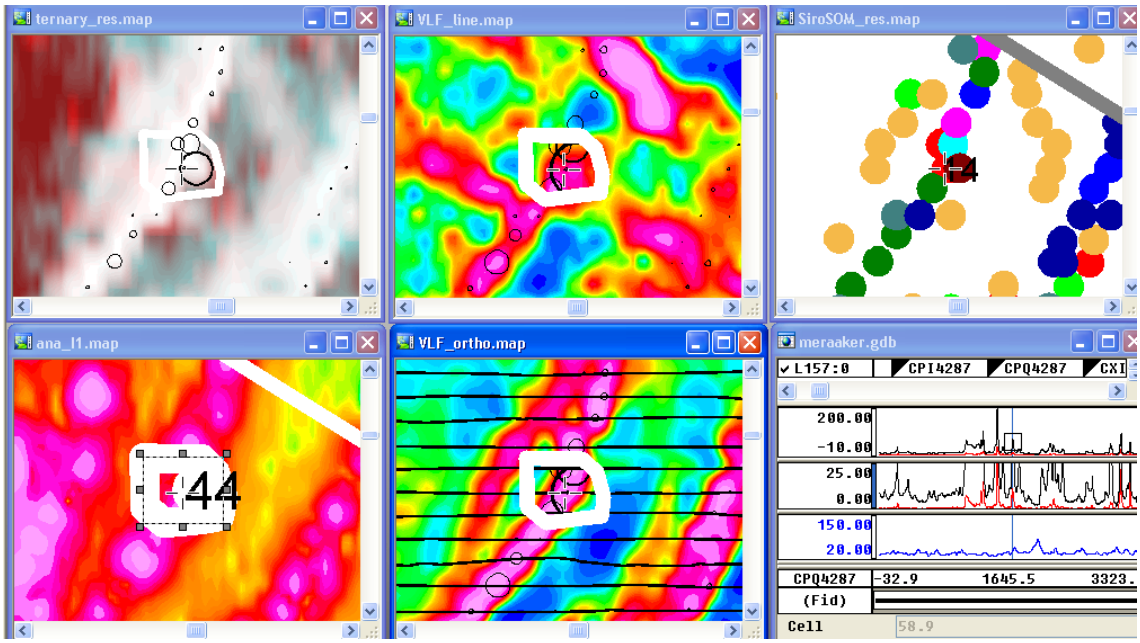


Figure 150. *Meråker target 43; low conductance; variable VLF; magnetic anomaly; priority 5*

(a)



(b)

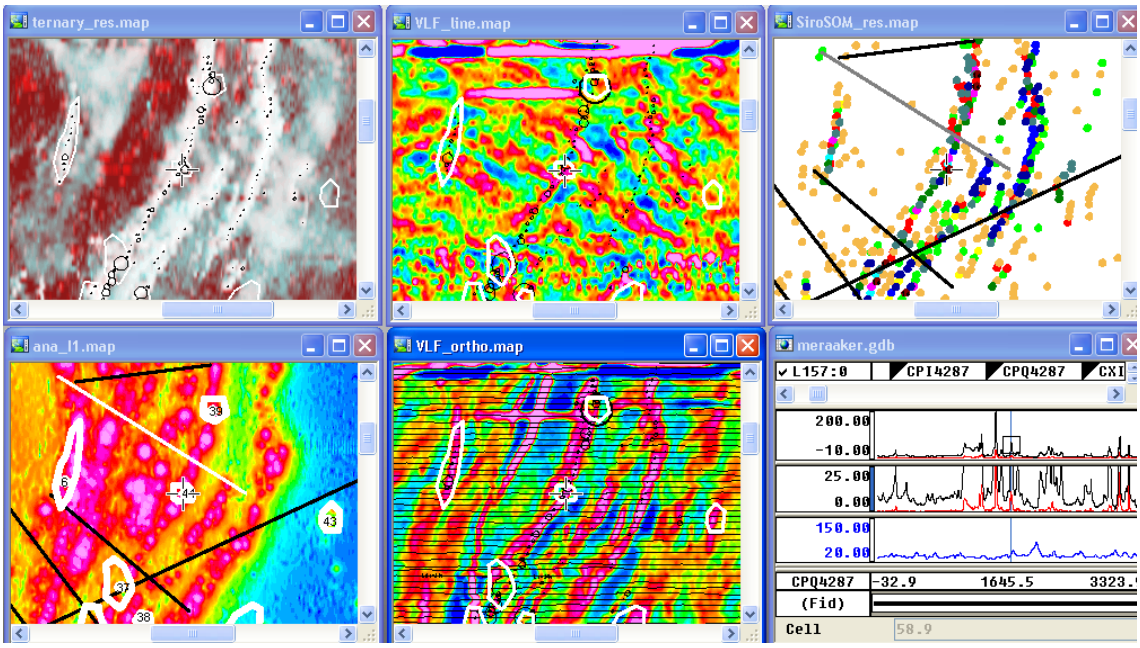


Figure 151. *Meråker target 44; medium conductance; variable VLF; short wavelength magnetic anomalies; priority 3*